Lino Guzzella

Analysis and Synthesis of MIMO Control Systems

"Regelungstechnik II"

April 28, 2021

ETH Zürich

Preface

Prerequisites and Objectives

Students planning to follow this course must have taken the class "Regelungstechnik I" or an equivalent first course on control system design. In particular, they must have a thorough understanding of linear and time-invariant single-input and single-output (SISO) control systems.

The course "Regelungstechnik II" has two main objectives. The first is to introduce some additional methods for the analysis and synthesis of SISO control systems. This is a continuation of the course "Regelungstechnik I" and the material discussed in this part is contained in the corresponding text book [11]. The second objective of "Regelungstechnik II" is to introduce some basic analysis and synthesis tools, which are useful when dealing with multiple-input and multiple-output (MIMO) control systems.

Handouts

There are several excellent books available that can be used as introductory texts to the field of MIMO system analysis and controller design. A list of some recommended monographs is included at the end of this text. The handouts you have in your hands now are not meant to replace such books. Rather they simply collect all the material presented in the lecture and relieve students from the painstaking task of taking notes. Many people have contributed to the preparation of this text, particularly Raffael Hedinger, Christian Küttel and Thomas Bucher. I'd like to acknowledge gratefully that valuable help.

Spring 2021 *Lino Guzzella*

Contents

Part II Time Domain MIMO Controller Design

Part I

MIMO System Analysis

1

MIMO Versus SISO Systems

1.1 Introductory Example: Heat Exchanger

In the first chapter a simple system with multiple inputs and multiple outputs (MIMO) is analyzed with the objective to illustrate some of the most important differences between single-input single-output (SISO) systems and MIMO systems. The system analyzed is a heat exchanger, for which a simple yet informative mathematical model is derived first. This model is used afterwards to illustrate the concept of *cross couplings* and to show the typical difficulties encountered when MIMO systems with strong cross couplings are controlled using SISO controllers.

The plant to be modeled is a counter-flow heat exchanger. One strand of such a system is illustrated in Figure 1.1.

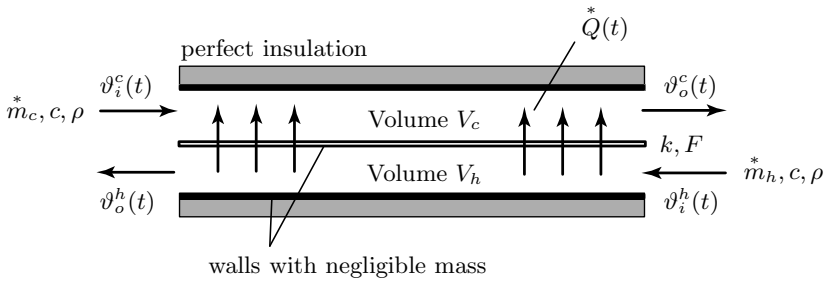

Figure 1.1: Schematic representation of a counter-flow heat exchanger.

A precise mathematical description of such a system is possible only with a set of partial differential equations (PDEs) and includes rather complex heat-transfer laws. For the purposes of this lecture a simplified model, as illustrated

in Figure 1.2, is derived that would not be sufficiently precise for a realistic modeling of a heat exchanger.[1] However, this model will be useful to illustrate the main problems encountered when dealing with strongly-coupled MIMO systems.

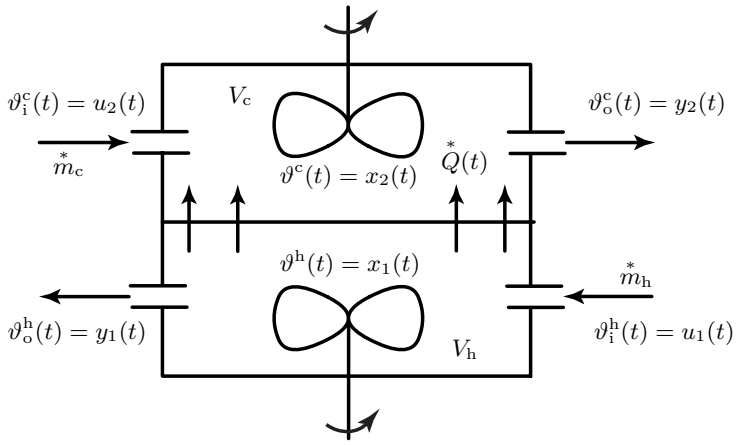

Figure 1.2: Simplified structure of a counter-flow heat exchanger.

The following definitions are adopted:

1. state variables:
   $x_1(t) = \vartheta^{\mathrm{h}}(t)$: temperature of the hot fluid in the heat exchanger
   $x_2(t) = \vartheta^{\mathrm{c}}(t)$: temperature of the cold fluid in the heat exchanger

2. input variables:[2]
   $u_1(t) = \vartheta_{\mathrm{i}}^{\mathrm{h}}(t)$: temperature of the hot fluid entering the heat exchanger
   $u_2(t) = \vartheta_{\mathrm{i}}^{\mathrm{c}}(t)$: temperature of the cold fluid entering the heat exchanger

[1] Stacking several of these modules in a series connection improves the model quality, but it increases the model order.

[2] Of course, choosing the input variables as indicated above is somewhat questionable. It would be more natural to use the mass flows entering the two heat-exchanger strands as control inputs. However, that choice would result in *nonlinear* ordinary differential equations (ODEs) describing the system dynamics. Since the main point of this example is to show the importance of the MIMO cross couplings, the simpler approach indicated above that yields *linear* ODEs has been chosen here.

3. output variables:
   $y_1(t) = \vartheta_{\mathrm{o}}^{\mathrm{h}}(t)$: temperature of the exiting hot fluid
   $y_2(t) = \vartheta_{\mathrm{o}}^{\mathrm{c}}(t)$: temperature of the exiting cold fluid

The model is derived using the following simplifications:

1. no mass storage in the heat exchanger (incompressible fluid, e.g., water, with constant density ρ);
2. perfect insulation and, therefore, no heat losses to the environment;
3. very thin pipe and heat exchanger walls and, therefore, no heat stored in these parts;
4. perfect mixing inside the heat exchanger, i.e., $\vartheta_{\mathrm{o}}^{\mathrm{h/c}}(t) = \vartheta^{\mathrm{h/c}}(t)$; and
5. constant fluid mass flows $\overset{*}{m}_{\mathrm{c}}$ and $\overset{*}{m}_{\mathrm{h}}$, specific heat capacity c, and heat transfer coefficient k.

Moreover, in this section it will be assumed that $\overset{*}{m}_{\mathrm{c}} = \overset{*}{m}_{\mathrm{h}} = \overset{*}{m}$ and that $V_{\mathrm{c}} = V_{\mathrm{h}} = V$. This simplification, which is adopted to streamline notation, will be dropped later.

The first principle of thermodynamics yields the two coupled differential equations

$$\frac{\mathrm{d}}{\mathrm{d}t}U^{\mathrm{h}}(t) = \overset{*}{H}_{\mathrm{i}}^{\mathrm{h}}(t) - \overset{*}{H}_{\mathrm{o}}^{\mathrm{h}}(t) - \overset{*}{Q}(t) \tag{1.1}$$

$$\frac{\mathrm{d}}{\mathrm{d}t}U^{\mathrm{c}}(t) = \overset{*}{H}_{\mathrm{i}}^{\mathrm{c}}(t) - \overset{*}{H}_{\mathrm{o}}^{\mathrm{c}}(t) + \overset{*}{Q}(t) \tag{1.2}$$

that describe the dynamics of the simplified heat exchanger cell shown in Figure 1.2.

In Equations (1.1) and (1.2) the variable $\overset{*}{H}$ represents enthalpy flow, the variable $\overset{*}{Q}$ heat flow, and the variable U internal energy. Using the definitions adopted above, the caloric equations

$$U^{\mathrm{h/c}}(t) = \rho \cdot V \cdot c \cdot \vartheta^{\mathrm{h/c}}(t) \tag{1.3}$$

$$\overset{*}{H}_{\mathrm{i/o}}^{\mathrm{h/c}}(t) = \overset{*}{m} \cdot c \cdot \vartheta_{\mathrm{i/o}}^{\mathrm{h/c}}(t) \tag{1.4}$$

and the heat transfer law

$$\overset{*}{Q}(t) = k \cdot F \cdot \left(\vartheta^{\mathrm{h}}(t) - \vartheta^{\mathrm{c}}(t)\right) \tag{1.5}$$

where F is the contact area between the hot and the cold strand of the heat exchanger, the ODEs in Equations (1.1) and (1.2) can be stated as

$$\rho \cdot V \cdot c \cdot \frac{\mathrm{d}}{\mathrm{d}t}x_1(t) = \overset{*}{m} \cdot c \cdot (u_1(t) - x_1(t)) - k \cdot F \cdot (x_1(t) - x_2(t)) \tag{1.6}$$

$$\rho \cdot V \cdot c \cdot \frac{\mathrm{d}}{\mathrm{d}t}x_2(t) = \overset{*}{m} \cdot c \cdot (u_2(t) - x_2(t)) + k \cdot F \cdot (x_1(t) - x_2(t)) \tag{1.7}$$

where $x_1(t) = \vartheta^h(t)$ and $x_2(t) = \vartheta^c(t)$.

Using the definitions

$$\tau = \frac{\rho \cdot V \cdot c}{\overset{*}{m} \cdot c + k \cdot F} \ , \ \sigma = \frac{k \cdot F}{\overset{*}{m} \cdot c + k \cdot F} \ , \ \beta = \frac{\overset{*}{m} \cdot c}{\overset{*}{m} \cdot c + k \cdot F} \tag{1.8}$$

the following control-oriented form of the equations describing the system dynamics is obtained

$$\tau \cdot \frac{\mathrm{d}}{\mathrm{d}t} x_1(t) = -x_1(t) + \sigma \cdot x_2(t) + \beta \cdot u_1(t) \tag{1.9}$$

$$\tau \cdot \frac{\mathrm{d}}{\mathrm{d}t} x_2(t) = -x_2(t) + \sigma \cdot x_1(t) + \beta \cdot u_2(t) \tag{1.10}$$

All physical parameters are greater than 0. Accordingly, the control-oriented parameters satisfy the conditions

$$0 < \tau, \quad 0 < \sigma < 1, \quad 0 < \beta < 1 \quad \text{and} \quad \sigma + \beta = 1 \tag{1.11}$$

These results will later be shown to have interesting system-theoretic consequences.

1.1.1 System Properties

In this section some of the most important properties of the heat exchanger system are analyzed. To facilitate such an analysis, a state-space form of the heat-exchanger model is derived first

$$\begin{aligned} \tfrac{\mathrm{d}}{\mathrm{d}t} x(t) &= A \cdot x(t) + B \cdot u(t) \\ y(t) &= C \cdot x(t) + D \cdot u(t) \end{aligned} \tag{1.12}$$

where

$$A = \begin{bmatrix} -1/\tau & \sigma/\tau \\ \sigma/\tau & -1/\tau \end{bmatrix}, \quad B = \begin{bmatrix} \beta/\tau & 0 \\ 0 & \beta/\tau \end{bmatrix} \tag{1.13}$$

$$C = \begin{bmatrix} 1 & 0 \\ 0 & 1 \end{bmatrix}, \quad D = \begin{bmatrix} 0 & 0 \\ 0 & 0 \end{bmatrix} \tag{1.14}$$

The number of state variables is $n = 2$, and the system is "square," i.e., the number of inputs $m = 2$ is equal to the number of outputs $p = 2$. Since B and C are both rank-two matrices, the system is completely controllable and observable.

The eigenvalues of A are computed to analyze the system stability. The eigenvalues are the solutions of the characteristic equation

$$\det(s \cdot I - A) = 0 \tag{1.15}$$

where

$$\det(s \cdot I - A) = (s + 1/\tau)^2 - (\sigma/\tau)^2 \tag{1.16}$$

The roots of this polynomial are

$$\lambda_{1,2} = \frac{-2 \cdot \tau \pm \sqrt{4 \cdot \tau^2 - 4 \cdot \tau^2 \cdot (1 - \sigma^2)}}{2 \cdot \tau^2} = \frac{-1 \pm \sigma}{\tau} \tag{1.17}$$

Using the inequalities in Equation (1.11) it is easy to see that for all physically meaningful parameter values, the system is asymptotically stable and has two real ("non-oscillatory") eigenvalues.

The transfer function of the system

$$P(s) = C \cdot (s \cdot I - A)^{-1} \cdot B + D \tag{1.18}$$

will be useful to analyze in more detail the system dynamics. Inserting $\{A, B, C, D\}$ defined in Equation (1.13) yields

$$P(s) = \begin{bmatrix} s + 1/\tau & -\sigma/\tau \\ -\sigma/\tau & s + 1/\tau \end{bmatrix}^{-1} \cdot \frac{\beta}{\tau} \tag{1.19}$$

The inversion is computed using Cramer's rule

$$M^{-1} = \frac{1}{\det(M)} \cdot \mathrm{Adj}\,(M) \tag{1.20}$$

yielding

$$P(s) = \begin{bmatrix} \dfrac{\beta \cdot (\tau \cdot s + 1)}{\tau^2 \cdot s^2 + 2 \cdot \tau \cdot s + (1 - \sigma^2)} & \dfrac{\beta \cdot \sigma}{\tau^2 \cdot s^2 + 2 \cdot \tau \cdot s + (1 - \sigma^2)} \\ \dfrac{\beta \cdot \sigma}{\tau^2 \cdot s^2 + 2 \cdot \tau \cdot s + (1 - \sigma^2)} & \dfrac{\beta \cdot (\tau \cdot s + 1)}{\tau^2 \cdot s^2 + 2 \cdot \tau \cdot s + (1 - \sigma^2)} \end{bmatrix} \tag{1.21}$$

The static gain[3] of this transfer function is

$$P(0) = \begin{bmatrix} \dfrac{\beta}{1 - \sigma^2} & \dfrac{\beta \cdot \sigma}{1 - \sigma^2} \\ \dfrac{\beta \cdot \sigma}{1 - \sigma^2} & \dfrac{\beta}{1 - \sigma^2} \end{bmatrix} = \begin{bmatrix} \dfrac{1 - \sigma}{1 - \sigma^2} & \dfrac{(1 - \sigma) \cdot \sigma}{1 - \sigma^2} \\ \dfrac{(1 - \sigma) \cdot \sigma}{1 - \sigma^2} & \dfrac{1 - \sigma}{1 - \sigma^2} \end{bmatrix} \tag{1.22}$$

[3] In the lecture "Regelungstechnik 1" also referred to as DC gain.

In the two extreme cases $\sigma = 0$ (no heat exchange) and $\sigma = 1$ (complete heat exchange) the following two limit cases arise

$$P(0)_{\sigma=0} = \begin{bmatrix} 1 & 0 \\ 0 & 1 \end{bmatrix}, \quad P(0)_{\sigma=1} = \begin{bmatrix} 0.5 & 0.5 \\ 0.5 & 0.5 \end{bmatrix} \tag{1.23}$$

As expected, in the first case in each channel the output temperatures are the same as the corresponding input temperatures; in the second case the output temperatures of both channels are identical and equal to the average of the two input temperatures.

Quick Check 1.1.1: Using physical arguments, explain why this must be the case. ⌟

The input/output (IO) representation in Equation (1.21) of the system could have been experimentally obtained by identifying each of the four channels $u_{1,2} \to y_{1,2}$ individually. Such an approach has some problems because looking at the four SISO transfer functions in Equation (1.21) one might believe that:

1. the system has 8 poles (but it is known to only have two eigenvalues); and
2. the system has 2 minimumphase zeros $\zeta_{1,2} = -1/\tau$ (but it is not clear if these zeros are active in a MIMO sense).

The first problem shows that it is not possible to find a *minimal* realization $\{A, B, C, D\}$ of a MIMO plant in a straightforward way. Realizing these four transfer functions using a naive approach, which would use eight state variables, would yield a system $\{\widetilde{A}, \widetilde{B}, \widetilde{C}, \widetilde{D}\}$ that has some non-controllable and/or some non-observable modes.[4]

The second question can be answered using the definition of the zeros of a MIMO system[5] as the solution of the equation

$$\det \begin{bmatrix} (\zeta \cdot I - A) & -B \\ C & D \end{bmatrix} = 0 \tag{1.24}$$

Since the determinant of Equation (1.24) is the non-zero constant β^2/τ^2, it is clear that the MIMO heat exchanger model in Equation (1.13) has no finite zeros.

To obtain a better understanding of the system dynamics, the step responses and the frequency responses of the open-loop plant are analyzed below.

[4] This is just another example that clarifies why models that have been obtained using physical first principles are more useful than those obtained by interpolation of measured data.

[5] These *transmission zeros* will be discussed in detail in Section 1.5.

Of course, to be able to compute these step responses numerical values have to be assigned to the system parameters. Reasonable values are

$$\overset{*}{m} = 0.5\,\mathrm{kg/s},\ \rho = 1000\,\mathrm{kg/m^3},\ c = 4200\,\mathrm{J/(kg\,K)},$$

$$F = 2\,\mathrm{m^2},\ V = 0.01\,\mathrm{m^3},\ k = 100\,\mathrm{W/(m^2\,K)}$$

With these values the control-oriented parameters can be computed to be

$$\tau \approx 18.26\ \mathrm{s},\quad \sigma \approx 0.087,\quad \beta \approx 0.913$$

and the eigenvalues of the open-loop plant have the numerical values

$$\lambda_1 \approx -0.0500\ \mathrm{rad/s},\ \lambda_2 \approx -0.0595\ \mathrm{rad/s}$$

The step responses of the open-loop plant are shown in Figure 1.3. A two-by-two MIMO plant has, in general, four step responses (from u_1 and u_2 to y_1 and y_2). However, in this special example, the step responses $u_1 \to y_1$ and $u_2 \to y_2$ coincide as can be seen in Equation (1.21); this is true also for $u_1 \to y_2$ and $u_2 \to y_1$, such that in Figure 1.3 only two curves are discernible.

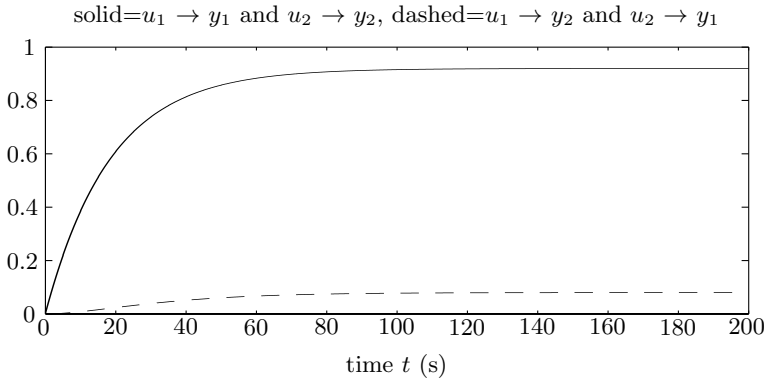

Figure 1.3: Step responses from u_i to y_j with $i, j \in \{1, 2\}$. Note that in this and in all subsequent figures in this section showing time-domain trajectories, the inputs and outputs are the deviations form the corresponding equilibrium points. Since the heat exchanger system is linear, a step magnitude equal 1 is chosen, without loss of generality.

The physical interpretation of these curves is that the gain of the two control channels $u_1 \to y_1$ and $u_2 \to y_2$ is approximately ten times "stronger" than the cross couplings $u_1 \to y_2$ and $u_2 \to y_1$. The same fact can be observed in the magnitude plot of the Bode diagram shown in Figure 1.4 revealing that this separation effect becomes even more pronounced at higher frequencies (for the reasons mentioned above, instead of four only two curves are visible in the magnitude and phase plots).

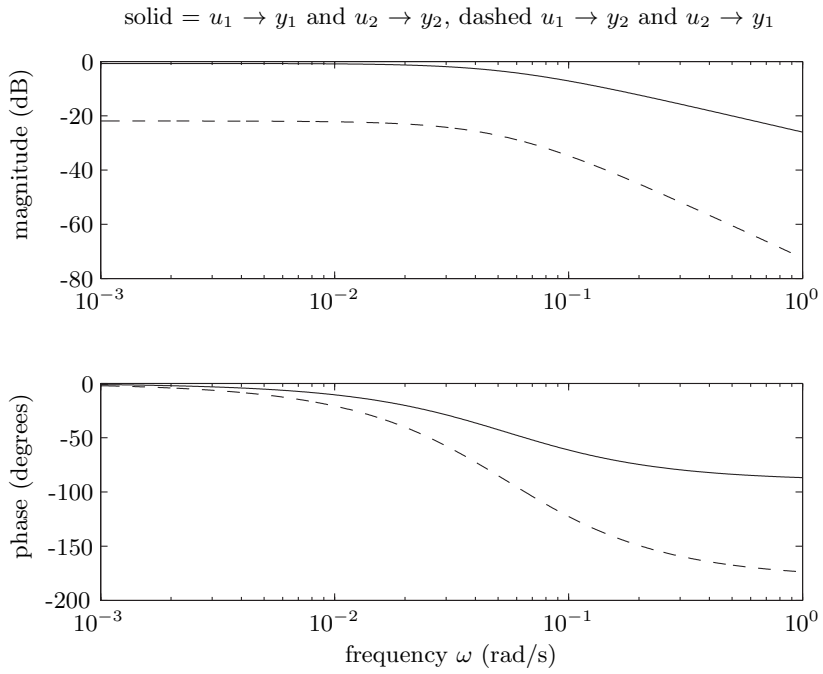

Figure 1.4: Bode plots u_i to y_j with $i, j \in \{1, 2\}$. Case: $k = 100\,\mathrm{W/(m^2\,K)}$.

1.1.2 SISO/MIMO Control System Design

Systems with a weak coupling between the different channels are often referred to as *diagonally dominant*. These systems are "almost SISO," and *breaking one loop at a time*, i.e., designing independent SISO controllers for each control channel neglecting the rest of the system, is expected to yield satisfactory results. Figure 1.5[6] shows the setup that is used when such a one-loop-at-a-time SISO controller is to be designed for the first control channel (the structure is similar for the second channel).

For the heat exchanger analyzed in this chapter a SISO PI controller with a roll-off part

$$C_{\mathrm{SISO}}(s) = k_p \cdot \left(1 + \frac{1}{T_i \cdot s}\right) \cdot \frac{1}{\frac{T_i}{10} \cdot s + 1} \tag{1.25}$$

with parameters $k_p = 3$ and $T_i = 7s$ yields the SISO closed-loop reference step response shown in Figure 1.6 (the dashed curve is the step response of the open-loop control channel $u_1 \to y_1$ as shown in Figure 1.3).

[6] Unlike for SISO systems, for MIMO systems the matrix multiplication is not commutative. Therefore for better readability it is common in signal flow charts for MIMO systems to place the outputs on the left and the inputs on the right.

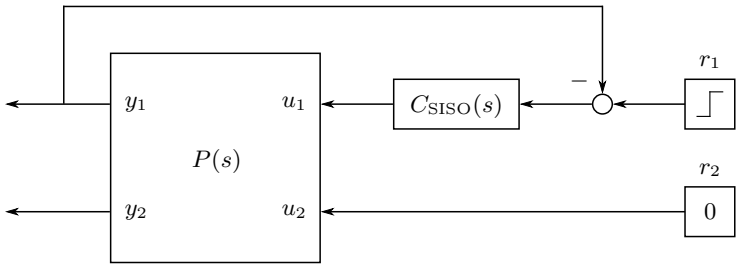

Figure 1.5: System structure of one "one-loop-at-a-time" SISO control loop.

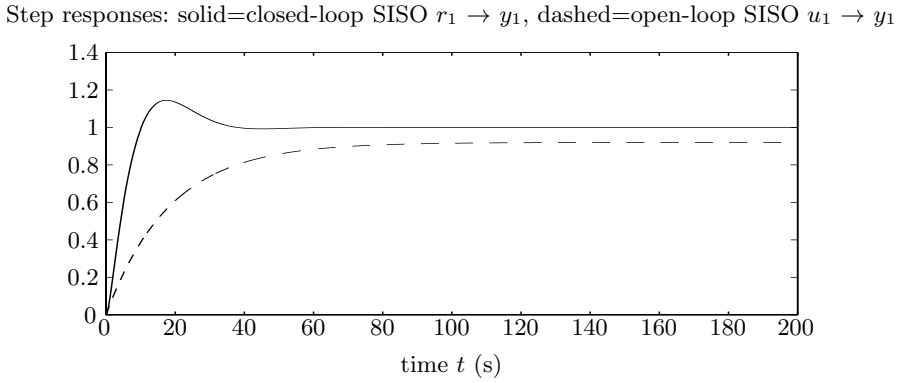

Figure 1.6: Closed-loop step response of the channel $r_1 \to y_1$ with a "one-loop-at-a-time" SISO control system as shown in Figure 1.5 (solid curve). Also shown for reference purposes: open-loop step response of the same channel (dashed curve). Case: $k = 100\,\mathrm{W/(m^2\,K)}$.

Two identical[7] copies of the controller in Equation (1.25) are now used to control the full MIMO heat exchanger plant using the "one-loop-at-a-time" control structure shown in Figure 1.7.

Figure 1.8 shows the step response of the system illustrated in Figure 1.7. As expected, the behavior of the first control channel y_1 (solid curve) does not substantially deviate from the response of the SISO loop (see Figure 1.6). Moreover, the second output y_2 (solid curve) is kept close to its reference value of $r_2 = 0$ (dashed line). The deviations from the expected behavior, as defined by the SISO design, are quite small, and for this special example there seems to be no need to develop truly MIMO control systems.

[7] Since both control channels $u_1 \to y_1$ and $u_2 \to y_2$ have the same dynamics, the same controller can be used in this special case.

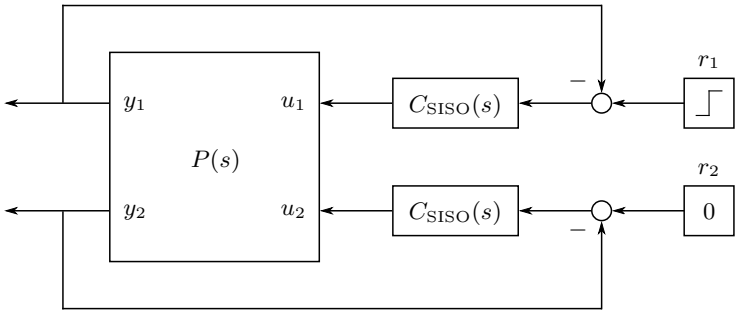

Figure 1.7: System structure of two "one-loop-at-a-time" SISO control loops used to control a MIMO plant.

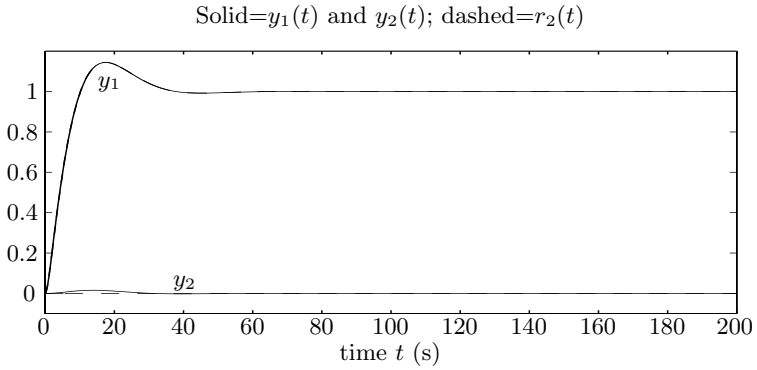

Figure 1.8: Closed-loop step response $r_1(t) = h(t)$, $r_2(t) = 0$ with two "one-loop-at-a-time" control systems as shown in Figure 1.7. Case: $k = 100\,\mathrm{W/(m^2\,K)}$.

Of course this is only true because the plant is diagonally dominant. Increasing the heat transfer coefficient to $k = 10^4\,\mathrm{W/(m^2\,K)}$ completely changes this picture.[8] In fact, as the Bode diagrams shown in Figure 1.9 indicate, in this case the MIMO plant no longer is diagonally dominant (the control channels and the cross-coupling channels have almost the same gain up to 0.1 rad/s). Accordingly, using the same[9] PI controller in Equation (1.25) to control the MIMO plant using the "one-loop-at-a-time" structure shown in Figure 1.7 is not likely to yield a satisfactory closed-loop system behavior.

[8] This value is not realistic; it is only chosen to exemplify well the problems caused by strong cross couplings.

[9] The controller in Equation (1.25) is robust and is able to tolerate the change in the heat-transfer coefficient k without a substantial degradation of the closed-loop SISO performance.

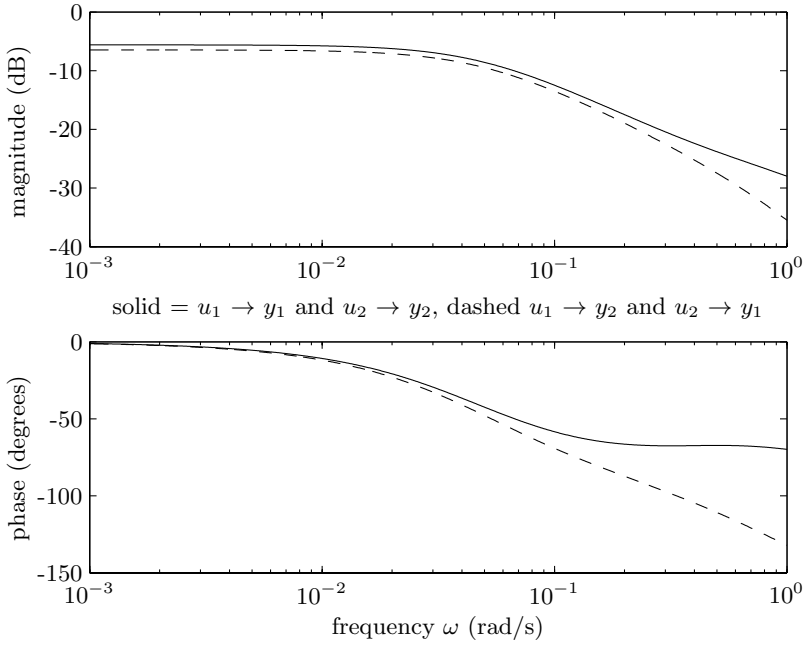

Figure 1.9: Bode plots u_i to y_j with $i, j \in \{1, 2\}$. Case: $k = 10000\,\mathrm{W/(m^2\,K)}$.

This is indeed the case, as Figure 1.10 shows. The step response of the closed-loop system, which has to be compared with the one depicted in Figure 1.8, shows that the output y_1 of the MIMO control loop (solid curve) does not follow well the output that is observed in the SISO case (dashed curve). In addition, the cross coupling induces a substantial effect on the second channel such that y_2 (solid curve) substantially deviates from its reference value, which is equal to zero.

For not diagonally-dominant systems only a full MIMO design, i.e., a design that explicitly takes into account the cross couplings present in the plant, can produce a satisfactory system behavior. The introduction of such methods is one of the main objectives of this lecture.

Remark: For systems with strong cross couplings, such as the heat exchanger with $k = 10000\ \mathrm{W/m^2\ K}$, one might be tempted to try to *decouple* the interaction using an appropriate "decoupling filter" $F(s)$. Indeed, for a "square" plant $P(s) \in \mathbb{C}^{m\times m}$ and a diagonal desired plant dynamics

$$Q(s) = \operatorname{diag}\left(\frac{b_i(s)}{a_i(s)}\right) = \operatorname{diag}\left(\frac{b_{\mu,i}s^{\mu} + \ldots + b_{1,i}s + b_{0,i}}{a_{\nu,i}s^{\nu} + \ldots + a_{1,i}s + a_{0,i}}\right), \quad i = 1, \ldots, m \tag{1.26}$$

with sufficiently large relative degrees $r_i = \nu_i - \mu_i$ the decoupling filter $F(s)$ has the form

solid: $k = 10000$ W/K m^2; dashed: $k = 100$ W/K m^2

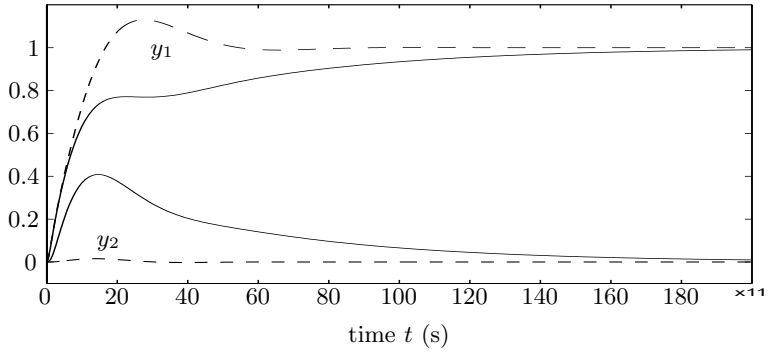

Figure 1.10: Closed-loop step response $r_1(t) = h(t)$, $r_2(t) = 0$ with two "one-loop-at-a-time" control systems as shown in Figure 1.7.

$$F(s) = P^{-1}(s) \cdot Q(s) \tag{1.27}$$

Placing this filter at the input of the plant yields (seemingly) the desired result

$$P(s) \cdot F(s) = P(s) \cdot P^{-1}(s) \cdot Q(s) = Q(s) \tag{1.28}$$

such that the design of a suitable controller (seemingly) is much easier (m independent SISO control problems). However, this approach is not recommended for the following reasons:

- If the plant $P(s)$ contains unstable eigenvalues or non-minimumphase zeros this approach yields not controllable unstable modes.
- Modeling errors will always be present such that a correct plant inversion is not possible.
- Decoupling requires some part of the control authority[10], which is not available anymore to achieve the true control objectives.

Particularly the last point is of great importance. A MIMO system offers additional opportunities to achieve the desired performance by exploiting the available cross couplings. In this sense, cross couplings should not be considered a nuisance, but an opportunity to achieve higher bandwidths, better disturbance compensations, less overshoot, etc.

[10] In reality, all control signals are limited [11], such that using the available amplitudes, i.e., the control authority, in an efficient way is a must in all designs.

1.2 Representation of MIMO Systems

Finite-dimensional, linear, and time-invariant MIMO systems are often described in the time domain using a state space formulation

$$\begin{aligned} \frac{\mathrm{d}}{\mathrm{d}t}x(t) &= A \cdot x(t) + B \cdot u(t), \quad x(t) \in \mathbb{R}^n, \quad u(t) \in \mathbb{R}^m, \quad x(0) = x_0 \\ y(t) &= C \cdot x(t) + D \cdot u(t), \quad y(t) \in \mathbb{R}^p \end{aligned} \tag{1.29}$$

Unlike in the SISO case, $u(t)$ and $y(t)$ are not scalar values anymore. Hence m is referring to the number of inputs and p to the number of outputs. n describes the number of states to represent the MIMO system in the state space representation.

Such a description is well-defined only if it is obtained by a modeling process based on "physical first laws." If only the input/output (IO) behavior is known (say, by measuring the impulse responses of the $p \times m$ channels), then there are infinitely many sets of matrices $\{A, B, C, D\}$ that produce the same IO behavior. Moreover, most of these sets will have more than the minimum number of states n required to reproduce the observed IO behavior (see Section 1.3).

In all subsequent steps it is assumed that all state, input and output variables used in the description in Equation (1.29) are normalized properly. Such a normalization is of fundamental importance for many system analysis and synthesis methods. In fact, all of these methods produce meaningful results only if all variables have similar magnitudes in regular operating conditions. Students not familiar with normalization and linearization techniques are referred to the text [11].

The Laplace transformation of Equation (1.29) yields

$$s \cdot X(s) - x_0 = A \cdot X(s) + B \cdot U(s) \tag{1.30}$$

hence

$$X(s) = (s\,I - A)^{-1} \cdot B \cdot U(s) + (s\,I - A)^{-1} \cdot x_0 \tag{1.31}$$

and

$$Y(s) = \left[C \cdot (s\,I - A)^{-1} \cdot B + D\right] \cdot U(s) + C \cdot (s\,I - A)^{-1} \cdot x_0 \tag{1.32}$$

If only the input/output (IO) behavior is of interest, the frequency domain representation

$$Y(s) = \left[C \cdot (s\,I - A)^{-1} \cdot B + D\right] \cdot U(s) = P(s) \cdot U(s) \tag{1.33}$$

is sufficient. Notice that $P(s)$ contains only the controllable and observable parts of Equation (1.29).

For SISO systems without delays, the transfer function in Equation (1.33) was shown to be the ratio of two polynomials in s

$$P(s) = \frac{b_m s^m + \cdots + b_1 s + b_0}{s^n + a_{n-1} s^{n-1} + \cdots + a_1 s + a_0} = \frac{b(s)}{a(s)} \tag{1.34}$$

In the MIMO case the transfer function in Equation (1.33) is a $p \times m$ matrix of such rational functions

$$P(s) = \begin{bmatrix} P_{1,1}(s) & P_{1,2}(s) & \dots & P_{1,m}(s) \\ P_{2,1}(s) & P_{2,2}(s) & \dots & P_{2,m}(s) \\ \vdots & \vdots & \ddots & \vdots \\ P_{p,1}(s) & P_{p,2}(s) & \dots & P_{p,m}(s) \end{bmatrix} \tag{1.35}$$

where each element of $P(s)$ is a SISO transfer function

$$P_{i,j}(s) = \frac{b_{m,i,j} s^m + \cdots + b_{1,i,j} s + b_{0,i,j}}{s^n + a_{n-1,i,j} s^{n-1} + \cdots + a_{1,i,j} s + a_{0,i,j}} = \frac{b_{i,j}(s)}{a_{i,j}(s)} \tag{1.36}$$

Note that m in Equation (1.35) denotes the number of inputs while in Equations (1.34) and (1.36) it denotes the order of the numerator polynomial. In Equation (1.36) the index j denotes the j-th input and the index i denotes the i-th output of the plant, respectively.

Quick Check 1.2.1: A MIMO system has two inputs, three outputs and four internal states. State the dimensions of the state-space matrices A, B, C and D as well as the transfer function $P(s)$. ⌟

1.3 System Realization

The transformation from the internal form in Equation (1.29) to the IO form in Equation (1.33) is trivial. Sometimes, however, the inverse problem must be solved, for instance when IO measurements of an otherwise unknown system are available and an internal description must be found.[11] Compared to the SISO case, this transformation (sometimes referred to as *realization problem*) is much more difficult in the case of MIMO systems, the main reason for that being the lack of information of what choice of system coordinates is appropriate. An example shown below will serve to illustrate these difficulties.

In the SISO case the solution of the realization problem is simple. There are infinitely many possible choices of suitable coordinates that realize the

[11] One can argue that this problem is not well-posed. However, there are examples where an internal description of the system must be available, for instance when a numerical controller design algorithm requires this data as input.

system's IO behavior with an internal description of minimal order. Canonical forms that yield simple structures of $\{A, b, c, d\}$ are used often. As an example, the realization of the transfer function in Equation (1.34) in the controller canonical form is shown below.

$$\left[\begin{array}{c|c} A & b \\ \hline c & d \end{array}\right] = \left[\begin{array}{cccccc|c} 0 & 1 & 0 & \cdots & \cdots & 0 & 0 \\ 0 & 0 & 1 & 0 & \cdots & 0 & 0 \\ \vdots & & \ddots & \ddots & \ddots & \vdots & \vdots \\ \vdots & & & 0 & 1 & 0 & 0 \\ 0 & \cdots & \cdots & \cdots & 0 & 1 & 0 \\ -a_0 & -a_1 & \cdots & \cdots & -a_{n-2} & -a_{n-1} & 1 \\ \hline b_0 & \cdots & b_m & 0 & \cdots & 0 & 0 \end{array}\right] \tag{1.37}$$

In the MIMO case the realization problem is more difficult to solve and requires advanced mathematical tools. The main problem is that "naive" straightforward solutions are not minimal, i.e., contain non-controllable and/or non-observable parts.

For instance the system

$$P(s) = \begin{bmatrix} \frac{2}{s+1} & \frac{3}{s+2} \\ \frac{1}{s+1} & \frac{1}{s+1} \end{bmatrix} \tag{1.38}$$

has the following "naive realization"

$$\begin{aligned} \frac{\mathrm{d}}{\mathrm{d}t}x(t) &= \begin{bmatrix} -1 & 0 & 0 & 0 \\ 0 & -2 & 0 & 0 \\ 0 & 0 & -1 & 0 \\ 0 & 0 & 0 & -1 \end{bmatrix} \cdot x(t) + \begin{bmatrix} 1 & 0 \\ 0 & 1 \\ 1 & 0 \\ 0 & 1 \end{bmatrix} \cdot u(t) \\ y(t) &= \begin{bmatrix} 2 & 3 & 0 & 0 \\ 0 & 0 & 1 & 1 \end{bmatrix} \cdot x(t) \end{aligned} \tag{1.39}$$

which is not minimal (in this example, the system $\{A, B, C, 0\}$ is neither completely controllable nor completely observable). There are methods which permit to derive directly minimal-order system realizations. However, the mathematical concepts needed for that approach are beyond this first course on MIMO systems. Interested students are referred to [13] or subsequent courses in the system dynamics and controls curriculum.

1.4 System Stability, Controllability and Observability

Most system *analysis* results valid for SISO systems in the time domain remain true for MIMO systems. For instance:

1. The stability properties of the system $\{A, B, C, D\}$ are determined by the eigenvalues of A. Exactly the same rules that have been formulated for SISO systems also apply for MIMO systems.
2. The system $\{A, B, C, D\}$ is completely controllable iff[12] the matrix

$$\mathcal{R}_n = [B, A\,B, \ldots, A^{n-1}B] \in \mathbb{R}^{n\times(n\cdot m)} \tag{1.40}$$

   has full rank n (the matrix $\mathcal{R}_n$ has full rank n iff it has n linearly independent columns).
3. The system $\{A, B, C, D\}$ is completely observable iff the matrix

$$\mathcal{O}_n = [C^{\mathrm{T}}, A^{\mathrm{T}}\,C^{\mathrm{T}}, \ldots, (A^{n-1})^{\mathrm{T}}C^{\mathrm{T}}]^{\mathrm{T}} \in \mathbb{R}^{(n\cdot p)\times n} \tag{1.41}$$

   has full rank n (the matrix $\mathcal{O}_n$ has full rank n iff it has n linearly independent rows).

All of these results pertain to the *open-loop* system properties. The stability analysis of closed-loop systems in the time domain is not difficult as well. If a plant $\{A, B, C, 0\}$ and a controller $\{F, G, H, 0\}$ with

$$\frac{\mathrm{d}}{\mathrm{d}t}z(t) = F \cdot z(t) + G \cdot e(t), \quad u(t) = H \cdot z(t)$$
$$F \in \mathbb{R}^{q\times q}, \quad G \in \mathbb{R}^{q\times p}, \quad H \in \mathbb{R}^{m\times q}$$

are connected in the standard feedback configuration, the closed-loop system is asymptotically stable iff all eigenvalues of the matrix

$$\begin{bmatrix} A & B\,H \\ -G\,C & F \end{bmatrix} \tag{1.42}$$

have strictly negative real parts.

Quick Check 1.4.1: Draw the closed-loop system interconnection of the plant $\{A, B, C, 0\}$ and the controller $\{F, G, H, 0\}$ and verify Equation (1.42). ⌟

Even the Nyquist theorem can be extended to MIMO systems. If a plant $P(s)$ and a controller $C(s)$ are connected in the standard feedback configuration, the closed-loop system will be asymptotically stable iff the Nyquist plot defined by

[12] The abbreviation "iff" stands for "if and only if."

$$\mathcal{N} = \det\left(I + P(j\,\omega)\cdot C(j\,\omega)\right), \quad \omega \in [-\infty, +\infty] \tag{1.43}$$

encircles the origin $n_0/2+n_+$ times (counting counter-clockwise encirclements as being positive), where n_0 is the number of marginally stable and n_+ is the number of unstable stable poles of the loop gain $L(s) = P(s)\cdot C(s)$.

Unfortunately, this result does not provide the same level of information as the SISO Nyquist theorem does. In fact, the operator det(...) "destroys" important information that describes the interconnection pattern between the individual channels such that the closed loop, while being stable, can perform very poorly. The MIMO Nyquist result is immediately applicable only in the case of diagonally dominant systems. For MIMO systems that are not diagonally dominant more advanced design tools must be introduced.

1.5 System Poles and Zeros

If the transfer function in Equation (1.33) only has one input and one output, the poles are simply the roots of the denominator polynomial and the zeros are the roots of the numerator polynomial. In the MIMO case, however, the poles and zeros of a transfer function *matrix* $P(s)$ are not found as easily.

Example 1.5.1 (A Third-Order System [10]). Consider the 2×2 system

$$P(s) = \begin{bmatrix} \frac{2}{s+1} & \frac{3}{s+2} \\ \\ \frac{1}{s+1} & \frac{1}{s+1} \end{bmatrix} \tag{1.44}$$

It is easy to see that the zeros and poles of the four SISO entries are $\zeta = \infty$ and $\pi_1 = -1$, $\pi_2 = -2$. But what are the poles of the MIMO system, especially, what are the multiplicities of these poles? Does the MIMO system not have any finite zeros as well? ⌟

The answer to these questions, even for non-square matrices $P(s)$, is found using the concept of *matrix minors*, which are the determinants of all square submatrices that can be formed from $P(s)$. A *maximum minor* is a minor that is formed using a submatrix with the largest possible dimension. For square matrices $P(s)$, the only maximum minor corresponds to the matrix determinant itself.

With these definitions, the following result holds true [13]:

The poles of $P(s)$ are the roots of the least common denominator of all minors of $P(s)$. These poles are the eigenvalues of a minimal realization $\{A, B, C, D\}$ of the input-output behavior of the system.

Example 1.5.2 (A Third-Order System, continued). The minors of $P(s)$ defined in Equation (1.44) are

$$\frac{2}{s+1},\ \frac{3}{s+2},\ \frac{1}{s+1}, \frac{1}{s+1},\ \frac{1-s}{(s+1)^2(s+2)} \tag{1.45}$$

The least common denominator is, therefore, the polynomial

$$p(s) = (s+1)^2 \cdot (s+2) \tag{1.46}$$

and the poles π_i of $P(s)$ are -1, -1, and -2. Since there are three poles in this example, a minimal-order internal description $\{A, B, C, D\}$ of the system must have $n = 3$ as system order, as only completely observable and controllable poles are relevant in $P(s)$. ⌟

Note that each pole of $P(s)$ must be a pole of one of the SISO entries in $P(s)$. However, the multiplicity is not simply found by summing up the number of occurrences of that pole in the $p \times m$ entries of $P(s)$.

Closely related to the poles are the zeros of the transfer function in Equation (1.33). In a SISO setting the zeros are those complex frequencies ζ_i for which $P(\zeta_i) = 0$. For MIMO systems a similar reasoning is true; however, since a MIMO system has *vectors* as inputs, not only the frequencies play a role, but also the directions.

If the internal description Equation (1.29) of a MIMO system is known, a possible definition of the *transmission* zeros of the corresponding transfer function Equation (1.33) can be defined as follows. Assuming an initial condition $x(0) = 0$, the system output $y(t)$ vanishes for finite intervals only if the linear equations

$$\begin{aligned} (sI - A) \cdot X(s) - B \cdot U(s) &= 0 \\ C \cdot X(s) + D \cdot U(s) &= 0 \end{aligned} \tag{1.47}$$

are satisfied. These homogeneous linear equations have a nontrivial solution iff the matrix

$$\begin{bmatrix} (sI - A) & -B \\ C & D \end{bmatrix} \tag{1.48}$$

is singular. The values $s = \zeta_i$ for which this is true are the transmission zeros of the system described by Equation (1.33).

As with SISO systems, the zeros of a MIMO system in input-output form can be found analyzing its transfer function $P(s)$ (see [10] for more details):

The zeros of $P(s)$ are the roots of the greatest common divisor of the numerators of the maximum minors of $P(s)$ after normalization to have the pole polynomial of $P(s)$ as denominators. These zeros are also zeros of a minimal realization $\{A, B, C, D\}$ of the input-output behavior of the system.

Example 1.5.3 (A Third-Order System, continued). The only maximum minor of $P(s)$ is

$$\frac{1-s}{(s+1)^2 \cdot (s+2)} \tag{1.49}$$

which is already normalized by the pole polynomial. Therefore, there is only one zero at $\zeta = 1$. Notice that none of the entries of $P(s)$ had a finite zero. The zero found at 1 (a nonminimumphase zero!) is strictly due to the MIMO structure of the system. ⌟

The internal description $\{A, B, C, D\}$ of the IO description $P(s)$ must be of minimal order, otherwise additional zeros and poles appear, which cancel out. Also, if $P(s)$ is square, the zeros of $P(s)$ are simply the poles of $P^{-1}(s)$.

As in the SISO case, a MIMO system that has one (or more) zero with positive real part will be referred to as being nonminimumphase. Such systems are more difficult to control than minimumphase systems, i.e., the achievable bandwidths are limited by the nonminimumphase zeros.

Notice that a MIMO system can have poles and zeros at the same frequency s without incurring a pole-zero cancellation [19]. For instance the 2×2 transfer function

$$P(s) = \begin{bmatrix} \dfrac{s+2}{s+1} & 0 \\ 0 & \dfrac{s+1}{s+2} \end{bmatrix} \tag{1.50}$$

has a pole and a zero at $s = -1$ and $s = -2$. In fact, the minors of $P(s)$ are

$$\frac{s+2}{s+1}, \quad \frac{s+1}{s+2}, \quad \frac{(s+2)\cdot(s+1)}{(s+1)\cdot(s+2)} = 1 \tag{1.51}$$

and the least common denominator is $(s+1)\cdot(s+2)$, which shows that the system has one pole at $s = -1$ and one at $s = -2$. Since $P(s)$ is square, there is only one maximum minor equal to 1. After normalization to have the pole polynomial $(s+2)\cdot(s+1)$ as denominator, this maximum minor is defined by the fraction

$$\frac{(s+2)\cdot(s+1)}{(s+2)\cdot(s+1)} \tag{1.52}$$

such that the greatest common divisor of the numerator is simply $(s+2)\cdot(s+1)$. Accordingly, the system has one zero at $s = -2$ and one at $s = -1$. This seemingly contradictory result is a consequence of the fact that in MIMO systems a direction is associated with each pole and zero. A cancellation takes place only if the frequency *and* the direction of a pole and a zero coincide.

The directions $\delta_{\pi,i}^{\text{in, out}}$ associated with the pole π_i are defined by

$$P(s)|_{s=\pi_i} \cdot \delta_{\pi,i}^{\text{in}} = \infty \cdot \delta_{\pi,i}^{\text{out}} \tag{1.53}$$

where $\delta_{\pi,i}^{\text{in}}$ is the input and $\delta_{\pi,i}^{\text{out}}$ the output pole direction.

Similarly, the directions $\delta_{\zeta,j}^{\text{in, out}}$ associated with the zero ζ_j are defined by

$$P(s)|_{s=\zeta_j} \cdot \delta_{\zeta,j}^{\text{in}} = 0 \cdot \delta_{\zeta,j}^{\text{out}} \tag{1.54}$$

where $\delta_{\zeta,j}^{\text{in}}$ is the input and $\delta_{\zeta,j}^{\text{out}}$ the output zero direction.

An approach to compute the directions is to use the singular value decomposition Equation (2.21) introduced later in Section 2.3. For square $m \times m$ systems, the directions may be obtained by[13]

$$P(s)|_{s\to\pi_i+\varepsilon} = U_i \cdot \Sigma_i \cdot V_i^{\mathrm{T}} \quad \Rightarrow \quad \delta_{\pi,i}^{\text{in}} \approx V_i(:,1), \quad \delta_{\pi,i}^{\text{out}} \approx U_i(:,1),$$

or

$$P(s)|_{s\to\zeta_j+\varepsilon} = U_j \cdot \Sigma_j \cdot V_j^{\mathrm{T}} \quad \Rightarrow \quad \delta_{\zeta,j}^{\text{in}} \approx V_j(:,m), \quad \delta_{\zeta,j}^{\text{out}} \approx U_j(:,m),$$

respectively, where ε is an arbitrary small number.

Quick Check 1.5.1: Show that the input directions associated with the zero and the pole at -1 of the transfer function in Equation (1.50) do not coincide. ⌟

Example 1.5.4 (A Third-Order System, continued). The pole directions associated with the three poles $\pi_1 = -1$, $\pi_2 = -1$, and $\pi_3 = -2$ of the transfer function matrix $P(s)$ in Equation (1.44), rounded to two digits, are

$$\delta_{\pi,1}^{\text{in}} = \begin{bmatrix} 0.97 \\ 0.23 \end{bmatrix}, \qquad \delta_{\pi,1}^{\text{out}} = \begin{bmatrix} 0.85 \\ 0.53 \end{bmatrix}$$

$$\delta_{\pi,2}^{\text{in}} = \begin{bmatrix} -0.23 \\ 0.97 \end{bmatrix}, \qquad \delta_{\pi,2}^{\text{out}} = \begin{bmatrix} -0.53 \\ 0.85 \end{bmatrix}$$

$$\delta_{\pi,3}^{\text{in}} = \begin{bmatrix} 0.00 \\ -1.00 \end{bmatrix}, \qquad \delta_{\pi,3}^{\text{out}} = \begin{bmatrix} -1.00 \\ 0.00 \end{bmatrix}$$

Similarly, the directions associated with the only finite zero $\zeta = 1$ are

$$\delta_{\zeta,1}^{\text{in}} = \begin{bmatrix} -0.71 \\ 0.71 \end{bmatrix}, \qquad \delta_{\zeta,1}^{\text{out}} = \begin{bmatrix} -0.45 \\ 0.89 \end{bmatrix}$$

⌟

[13] Using Matlab's notation, $M(:,k)$ denotes the vector formed by the k-th column of the matrix M. Also, these expressions assume the ordering of the singular values according to the convention used in Matlab, i.e., $\Sigma(1,1)$ is the largest and $\Sigma(m,m)$ the smallest singular value.

2

Relative-Gain Arrays and Singular Values

2.1 Introduction

In this section, the relative-gain array (RGA) is introduced, which is a tool that permits to systematically assess how "MIMO-similar" a given system is. Subsequently, singular values of matrices are introduced and the application of these tools to describe the frequency-domain behavior of MIMO systems is discussed.

2.2 Relative-Gain Arrays

The first question that arises when a controller for an $m \times m$ MIMO plant has to be synthesized is if m well-designed SISO controllers can yield a satisfactory closed-loop system behavior or if a "true" MIMO design is necessary to reach that goal. This question can be answered by inspecting the *relative-gain array* $\mathrm{RGA}(s)$ of the plant $P(s)$. If $\mathrm{RGA}(s) \approx I$ then the plant is diagonally dominant and controlling one loop at a time can yield acceptable results. In the other case a full MIMO control system design is necessary.

The basic idea of the RGA analysis is explained using a 2×2 plant as an example. Figure 2.1 shows the two different system structures analyzed below. To compute the element $(1,1)$ of the $\mathrm{RGA}(s)$, the loop from y_2 to u_2 is closed with a SISO controller $C_{22}(s)$ and the resulting transfer function from u_1 to y_1 is computed (for space reasons the independent variable s is omitted below)

$$y_1 = \frac{P_{11}(1 + P_{22}C_{22}) - P_{12}C_{22}P_{21}}{1 + P_{22}C_{22}} \cdot u_1 \tag{2.1}$$

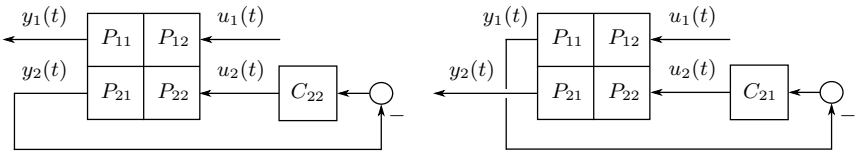

Figure 2.1: System structure used to derive the RGA matrix of a 2×2 plant; left for the element $[\mathrm{RGA}(s)]_{11}$ and right for $[\mathrm{RGA}(s)]_{12}$.

Two extreme cases can now be distinguished:

- First assume almost open-loop conditions ($C_{22} \approx 0$): in this case the transfer function $u_1 \to y_1$ is approximately equal to P_{11}.
- Second assume high controller gains ($P_{22}C_{22} \gg 1$): in this case the transfer function $u_1 \to y_1$ is approximately equal to $\left(P_{11}P_{22} - P_{12}P_{21}\right)/P_{22}$.

The element $(1,1)$ of the matrix $\mathrm{RGA}(s)$ is now defined as the ratio between these two transfer functions

$$[\mathrm{RGA}]_{11} = P_{11} / \left(\frac{P_{11}P_{22} - P_{12}P_{21}}{P_{22}} \right)$$

$$= \frac{P_{11}P_{22}}{P_{11}P_{22} - P_{12}P_{21}} \tag{2.2}$$

By repeating these calculations with a controller C_{11} that closes the loop from y_1 to u_1 the result $[\mathrm{RGA}(s)]_{22} = [\mathrm{RGA}(s)]_{11}$ is obtained.

The main point is now that if the plant is diagonally dominant, the term $[\mathrm{RGA}(s)]_{11}$ must be close to 1 because in this case the channel $u_1 \to y_1$ is not affected substantially by the presence of C_{22} (similar open-loop and closed-loop behaviors). As Equation (2.2) shows, this is the case if $P_{12} \cdot P_{21}$ is much smaller than $P_{11} \cdot P_{22}$. If $[\mathrm{RGA}(s)]_{11}$ substantially differs from 1, the MIMO interactions (as defined by P_{12} and P_{21}) are important, such that a SISO-similar approach is not recommended.

To compute the element $[\mathrm{RGA}(s)]_{21}$, the transfer function $u_1 \to y_2$ is analyzed closing the loop from y_1 to u_2, as shown on the right side of Figure 2.1. As in the previous case, the element $[\mathrm{RGA}(s)]_{21}$ is the ratio between the resulting open-loop ($C_{21} \approx 0$) transfer function and the resulting high-gain ($P_{12}C_{21} \gg 1$) transfer function. The final result obtained after a few steps is

$$[\mathrm{RGA}]_{21} = \frac{-P_{12}P_{21}}{P_{22}P_{11} - P_{21}P_{12}} \tag{2.3}$$

Quick Check 2.2.1: Verify Equation (2.3). ⌟

Again, it can be shown that $[\mathrm{RGA}(s)]_{12} = [\mathrm{RGA}(s)]_{21}$. These scalars are close to zero iff $P_{12} \cdot P_{21} \ll P_{22} \cdot P_{11}$. Therefore, if $[\mathrm{RGA}(s)]_{12} = [\mathrm{RGA}(s)]_{21}$ substantially differ from 0, the MIMO interactions (as defined by $P_{12} \cdot P_{21}$) are important and a SISO-similar approach is not recommended.

For a general square MIMO system $P(s)$ the RGA is defined by

$$\mathrm{RGA}(s) = P(s) \ .\times P(s)^{-T} \tag{2.4}$$

where the operator $.\times$ denotes element-wise multiplication (as `.*` in Matlab) and $P^{-T} = (P^{-1})^{\mathrm{T}} = (P^{\mathrm{T}})^{-1}$.

The following observations are often useful:

- The columns and the rows of $\mathrm{RGA}(s)$ always add up to 1.
- The RGA is invariant with respect to scaling, i.e., for any regular diagonal matrices D_i the equation $\mathrm{RGA}[P(s)] = \mathrm{RGA}[D_1 \cdot P(s) \cdot D_2]$ holds true.
- The RGA of a triangular matrix $P(s)$ is the identity matrix I.[1]
- In feedback control applications, the input/output pairing should be chosen such that the input i is paired with the output j whenever $[\mathrm{RGA}(s)]_{j,i}$ is close to 1.

Summarizing, if $\mathrm{RGA}(s)$ is substantially different from I for some frequencies s that are important for the design, the cross-coupling gains are important and MIMO approaches must be used to control the plant $P(s)$. If $\mathrm{RGA}(s) \approx I$ for all frequencies s of interest, then the individual channels can be controlled well "one loop at a time" using m SISO controllers.

Quick Check 2.2.2: Consider the RGA matrix

$$RGA(s) = \begin{bmatrix} 0 & 1 \\ 1 & 0 \end{bmatrix} \tag{2.5}$$

Is it sufficient to control this plant with two SISO controllers or should a real MIMO approach be used? ⌟

For the example of the heat exchanger discussed in Section 1.1, the RGA has the form

$$\mathrm{RGA}(s) = \begin{bmatrix} \dfrac{(\tau\, s+1)^2}{(\tau\, s+1)^2 - \sigma^2} & \dfrac{-\sigma^2}{(\tau\, s+1)^2 - \sigma^2} \\ \dfrac{-\sigma^2}{(\tau\, s+1)^2 - \sigma^2} & \dfrac{(\tau\, s+1)^2}{(\tau\, s+1)^2 - \sigma^2} \end{bmatrix} \tag{2.6}$$

[1] This confirms that triangular systems are "almost SISO" and often can be controlled well using SISO approaches.

or, at the special frequency $s = 0$ (static gain)

$$\mathrm{RGA}(0) = \begin{bmatrix} \dfrac{1}{1-\sigma^2} & \dfrac{-\sigma^2}{1-\sigma^2} \\ \dfrac{-\sigma^2}{1-\sigma^2} & \dfrac{1}{1-\sigma^2} \end{bmatrix} \tag{2.7}$$

This result permits an interesting physical interpretation. The definition of the parameter σ in Equation (1.8) is repeated here for convenience

$$\sigma = \frac{k \cdot F}{\dot{m} \cdot c + k \cdot F} \tag{2.8}$$

Since the physical parameters $\{k, F, \dot{m}, c\}$ must be greater than zero, the inequality $0 < \sigma < 1$ is satisfied in all cases. If the heat exchange capability $k \cdot F$ is much smaller than the enthalpy transported by the water flow $\dot{m} \cdot c$, the parameter $\sigma \approx 0$ and the $\mathrm{RGA}(s) \approx I$. In this case, the plant is diagonally dominant because the amount of heat exchanged between the two channels is small compared to the heat transported in each strand.

In the other extreme case, i.e., if $k \cdot F \gg \dot{m} \cdot c$, the parameter $\sigma \approx 1$ and the magnitudes of all elements of the $\mathrm{RGA}(s)$ become very large. In this case the plant is not diagonally dominant and breaking one loop at a time will not work. This RGA analysis corroborates the findings of Subsection 1.1.2 where it was shown that two SISO PI controllers were able to control the plant well when the heat-transfer coefficient k was small, while this approach failed for large values of k.

2.3 Singular Values of Real and Complex Matrices

This section recalls some definitions and results of linear (matrix) algebra. These ideas will be used in the following section to define the generalization of the frequency response $P(j\,\omega)$ of a transfer function $P(s)$ when $P(s)$ describes a MIMO system. Note that first the analysis is done for real-valued variables. The generalization to complex-valued variables is done later in this section.

The starting point is the definition of the *induced norm* $||M||$ of a linear transformation

$$y = M \cdot u, \quad u \in \mathbb{R}^m, \; y \in \mathbb{R}^p, \; M \in \mathbb{R}^{p \times m} \tag{2.9}$$

The induced norm of a linear transformation is defined as follows

$$||M|| = \max_{||u|| \neq 0} \frac{||y||}{||u||} = \max_{||u||=1} ||y|| \tag{2.10}$$

where $||x||$ denotes any norm of the vector x. For each vector norm $||x||$ the result of Equation (2.10) induces the corresponding "matrix norm" $||M||$, hence the name.

For the important example of the norm operator $||x||$ being the Euclidean norm $||x|| = \sqrt{x^{\mathrm{T}} \cdot x}$ (the *inner product* or *2-norm*), the induced norm of M is given by[2]

$$||M|| = \max_i \left(\sigma_i(M)\right), \quad \sigma_i(M) = \sqrt{\lambda_i(M^{\mathrm{T}} \cdot M)} \tag{2.11}$$

where λ_i are the eigenvalues of the matrix $M^{\mathrm{T}} \cdot M$.[3] Since by construction $M^{\mathrm{T}} \cdot M$ is symmetric and positive semi-definite, its eigenvalues all are real and non-negative.

Quick Check 2.3.1: Show that $M^{\mathrm{T}} \cdot M$ is positive semi-definite. ⌟

The non-negative real scalars[4] σ_i, with $i = 1, \ldots, \min(p, m)$, are referred to as the *singular values* of the matrix $M \in \mathbb{R}^{p \times m}$. Similar to the determinant or the eigenvalues of M, these singular values give important information regarding the properties of the linear mapping represented by the matrix M.

The proof of Equation (2.11) uses Lagrange's method for constrained optimization. According to Equation (2.10), the objective function to be maximized is given by the expression

$$L = ||y||^2 + \lambda \cdot \left(1 - ||u||^2\right) \tag{2.12}$$

$$= u^{\mathrm{T}} \cdot M^{\mathrm{T}} \cdot M \cdot u + \lambda \cdot \left(1 - u^{\mathrm{T}} \cdot u\right) \tag{2.13}$$

where the variable λ is used to include the constraints into the objective function. The necessary conditions for a local maximum are

$$\frac{\partial L}{\partial u} = 0, \text{ and } \frac{\partial L}{\partial \lambda} = 0 \tag{2.14}$$

In this special case

$$\frac{\partial L}{\partial u} = 2 \cdot u^{\mathrm{T}} \cdot M^{\mathrm{T}} \cdot M - 2 \cdot \lambda \cdot u^{\mathrm{T}} \tag{2.15}$$

Accordingly, the optimal solution u^* must satisfy the homogeneous equation

[2] Some authors prefer to use the symbol $||M||_2$ to denote the matrix norm induced by the 2-norm operator. In this course, the subscript 2 is omitted where it becomes clear from the context to simplify the notation.

[3] Note that Equation (2.11) is only valid if the matrix M is real-valued. For complex-valued M see Equation (2.25).

[4] If the rank ρ of M is smaller than $\min(p, m)$ then $k = \min(p, m) - \rho$ singular values are zero.

$$(\lambda \cdot I - M^{\mathrm{T}} \cdot M) \cdot u^* = 0 \tag{2.16}$$

and a non-trivial u^* exists iff

$$\det\left(\lambda \cdot I - M^{\mathrm{T}} \cdot M\right) = 0 \tag{2.17}$$

The scalars λ_i that satisfy this equation are, by definition, the eigenvalues of $M^{\mathrm{T}} \cdot M$. As mentioned above, $M^{\mathrm{T}} \cdot M$ is a symmetric and positive semi-definite matrix (by construction). Therefore, its eigenvalues λ_i and their square roots $\sigma_i = \sqrt{\lambda_i}$ are real and non-negative.

Quick Check 2.3.2: Show that for any x, $c^{\mathrm{T}} \in \mathbb{R}^n$ and $Q = Q^{\mathrm{T}} \in \mathbb{R}^{n \times n}$ the following expressions are valid

$$\frac{\partial}{\partial x}(c \cdot x) = c$$

and

$$\frac{\partial}{\partial x}\left(x^{\mathrm{T}} \cdot Q \cdot x\right) = 2 \cdot x^{\mathrm{T}} \cdot Q$$

⌟

With this result and using the definition in Equation (2.10) of the induced norm, it is easy[5] to see that

$$||M||^2 = \max_{||u|| \neq 0} \frac{||y||^2}{||u||^2} = \max_{||u||=1} \frac{u^{\mathrm{T}} \cdot M^{\mathrm{T}} \cdot M \cdot u}{u^{\mathrm{T}} \cdot u} = \max_i \left(\sigma_i^2\right) \tag{2.18}$$

A geometric interpretation for the example $u, y \in \mathbb{R}^2$ and

$$M = \begin{bmatrix} 1.3 & 0.1 \\ 1.5 & -1 \end{bmatrix} \tag{2.19}$$

is shown in Figure 2.2. Its left part shows the mapping of all points with $||u|| = 1$ to an ellipse (in the general case $n > 2$ a hyper ellipsoid). A general point u° (denoted by $\circ$ and a dashed line) is mapped to a point on that ellipse (denoted by $\circ$ and a solid line). The right plot shows the same mapping for the two special points u° and u^* that are mapped to those points y° with the maximum and y^* with the minimum distance from the origin. The corresponding solid lines are the semi-axes of the ellipsoid and the dashed lines are the eigenvectors of the matrix $M^{\mathrm{T}} \cdot M$. The length of y° is the maximum singular value and, therefore, the induced norm $||M||$. Similarly, the length of y^* is the minimum singular value and represents a lower bound for the norm $||y||$ of all vectors $y = M \cdot u$ with $||u|| = 1$.

[5] Multiply Equation (2.16) "from the left" by the vector $(u^*)^{\mathrm{T}}$.

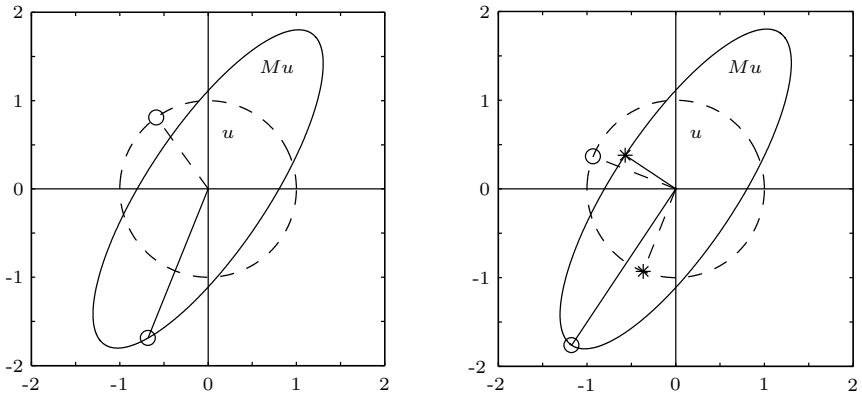

Figure 2.2: Illustration of the geometric interpretation of the singular values of a 2×2 matrix.

The results obtained above can be summarized by the inequality

$$\sigma_{\min}(M) \leq \frac{||y||}{||u||} \leq \sigma_{\max}(M), \quad ||u|| \neq 0 \tag{2.20}$$

where it is assumed that $\sigma_{\min}(M)$ is the minimum and $\sigma_{\max}(M)$ the maximum singular value of M.

Singular values play an important role in understanding the geometric properties of linear mappings represented by the matrix M. Any matrix $M \in \mathbb{R}^{p \times m}$ can be written using a *singular value decomposition* as follows

$$M = U \cdot \Sigma \cdot V^{\mathrm{T}} \tag{2.21}$$

where the matrices $U \in \mathbb{R}^{p \times p}$ and $V \in \mathbb{R}^{m \times m}$ are *unitary* matrices, i.e.,

$$U \cdot U^{\mathrm{T}} = I_{p \times p}, \quad V \cdot V^{\mathrm{T}} = I_{m \times m}$$

and where the only non-zero elements of $\Sigma \in \mathbb{R}^{p \times m}$ are the singular values of M, i.e.,

$$[\Sigma]_{i,j} = 0 \ \forall \ i \in [1, p] \neq j \in [1, m]$$

and

$$[\Sigma]_{i,j} = \sigma_k \ \forall \ i = j = k \in [1, \min(p, m)]$$

The geometric interpretation associated with this decomposition is that every mapping represented by M can be decomposed into first an isometric transformation[6] represented by V^{T}, then a scaling projection represented

[6] Such transformations are essentially rotations and, therefore, preserve the length of the vectors transformed. In general, reflections through the origin are possible as well.

by Σ, and finally another isometry represented by U. Since fast and robust numerical algorithms exist for the computation of the singular value decomposition of high-order matrices M, this concept has many useful applications in system theory and in many other engineering domains.

Quick Check 2.3.3: Explain why the eigenvalues of M are not good quantifiers of the mapping M. Use the example

$$M = \begin{bmatrix} 0 & 1 \\ \varepsilon & 0 \end{bmatrix}$$

with $0 < \varepsilon \ll 1$. Show that its singular values are a better choice. ⌟

So far only real-valued variables have been considered. The generalization to the case of $M \in \mathbb{C}^{p\times m}$ is not difficult. The starting point is the definition of the Euclidean norm of a complex scalar $z = a + j\,b$ (a, $b \in \mathbb{R}$)

$$||z||^2 = a^2 + b^2 = (a - j\,b) \cdot (a + j\,b) = \overline{z} \cdot z \tag{2.22}$$

where the notation $\overline{z}$ denotes complex conjugation. For a complex vector $v \in \mathbb{C}^n$ with $v_i = a_i + j\,b_i$ and $i = 1, \ldots, n$, its norm is defined as

$$||v||^2 = \sum_{i=1}^{n} a_i^2 + b_i^2 = \sum_{i=1}^{n} (a_i - j\,b_i) \cdot (a_i + j\,b_i) = \overline{v}^{\mathrm{T}} \cdot v \tag{2.23}$$

The linear mapping in Equation (2.9) is now represented by the complex matrix M

$$y = M \cdot u, \quad u \in \mathbb{C}^m, \; y \in \mathbb{C}^p, \; M \in \mathbb{C}^{p\times m} \tag{2.24}$$

The induced norm of M is defined in Equation (2.10). Repeating the analysis shown above for the complex case yields the analogous result

$$||M|| = \sigma_{\max}(M) = \max_i \sqrt{\lambda_i(\overline{M}^{\mathrm{T}} \cdot M)} \tag{2.25}$$

where the matrix $\overline{M}^{\mathrm{T}}$ is the transpose and complex conjugate of the matrix M. In particular, if $||u|| = 1$ the norm of y must satisfy the inequality

$$\sigma_{\min}(M) \leq ||y|| \leq \sigma_{\max}(M) \tag{2.26}$$

Since the matrix $\overline{M}^{\mathrm{T}} \cdot M$ is Hermitian[7] by definition, its eigenvalues are all non-negative real numbers. Therefore, Equation (2.26) makes perfectly sense also for complex variables. The eigenvectors of $\overline{M}^{\mathrm{T}} \cdot M$ are always orthogonal, hence linearly independent, even if multiple eigenvalues exist. However, in general they consist of complex-valued entries.

[7] A matrix Q is Hermitian if $Q = \overline{Q}^{\mathrm{T}}$, i.e., if it is equal to its complex conjugate and transpose. **Remark**: In Matlab the operator ' denotes transposition *and* complex conjugation.

3

Frequency Responses of MIMO Systems

3.1 Introduction

In the SISO case, the frequency response of the plant $P(j\,\omega)$ has been shown to be a powerful tool for the analysis *and* the synthesis of the closed-loop system. In this section, the frequency response of MIMO systems is analyzed.

3.2 Frequency Responses of MIMO Systems

The key observation in SISO systems was that an asymptotically stable plant $P(s)$ when driven by a harmonic input $u(t)$, produces an output $y(t)$ that has a first transient (complicated) and a second steady-state (simple) part.

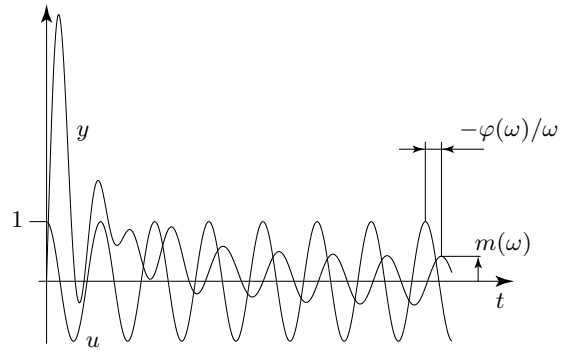

Figure 3.1: Transient and steady-state response of a linear SISO system to a harmonic input.

To be more specific, if the input to a SISO plant is defined by

$$u(t) = \cos(\omega\, t) \cdot h(t) \tag{3.1}$$

the plants's output in steady-state can be described by

$$y_\infty(t) = |P(j\,\omega)| \cdot \cos\left(\omega\, t + \angle P(j\,\omega)\right) \tag{3.2}$$

Both the magnitude $m(\omega) = |P(j\,\omega)|$ and the phase $\varphi(\omega) = \angle P(j\,\omega)$ are functions of the frequency ω. These functions can be visualized either together in Nyquist plots or separately in Bode plots, which have the advantage of explicitly showing the relationship between frequency and magnitude or phase.

The generalization of these frequency responses to MIMO systems is not straightforward. In particular, there is no obvious way to define a scalar phase information. As shown below, only conservative bounds of the magnitude of *phasors*[1] can be derived, which provide information similar to the magnitude plots in SISO systems.

Generalizing the situation to the MIMO case, the input $u(t)$ is now a vector of harmonic functions[2]

$$u(t) = \begin{bmatrix} \mu_1 \cdot \cos(\omega\, t + \varphi_1) \cdot h(t) \\ \mu_2 \cdot \cos(\omega\, t + \varphi_2) \cdot h(t) \\ \cdots \\ \mu_m \cdot \cos(\omega\, t + \varphi_m) \cdot h(t) \end{bmatrix} \tag{3.3}$$

Quick Check 3.2.1: How does the motion of a two-dimensional input phasor $u(t) = [u_1(t), u_2(t)]$ with $\mu_1 = \mu_2 = 1$ in the u_1-u_2-plane look like? Consider four different cases:

1) $\varphi_2 - \varphi_1 = 0$
2) $\varphi_2 - \varphi_1 = \pi/2$
3) $\varphi_2 - \varphi_1 = \pi$
4) $\varphi_2 - \varphi_1 = \pi/4$

What happens to these phasors when you change μ_1 or μ_2? What if you change the frequency ω? ⌟

[1] In this course the term phasor is used to refer to a "vector with a phase." A precise definition follows below. Note that this terminology is not standard.

[2] Note that the excitation frequency ω must be the same in each channel, but the phase φ_i and the amplitude μ_i can vary.

After Laplace transformation, the input vector (3.3) can be written as

$$U(s) = \mathrm{e}^{\Phi \cdot s/\omega} \cdot \mu \cdot \frac{s}{s^2 + \omega^2} \tag{3.4}$$

where

$$\Phi = \mathrm{diag}(\varphi_i) \in \mathbb{R}^{m \times m}, \quad \text{and} \quad \mu = [\mu_1, \ldots, \mu_m]^{\mathrm{T}} \in \mathbb{R}^m \tag{3.5}$$

Quick Check 3.2.2: Show that (3.4) is the Laplace transform of (3.3). ⌟

It is worth noting that in the time domain the three elements:

1) function of time $\cos(\omega\, t)$;
2) individual input channel amplitudes μ_i
3) individual input channel phase φ_i

are integrated into the expression in Equation (3.3) such that they cannot be analyzed individually. In the frequency domain they are separated in three elements:

1) function of frequency $\frac{s}{s^2+\omega^2}$;
2) individual input channel amplitudes μ
3) individual input channel phase $\mathrm{e}^{\Phi \cdot s/\omega}$

that are connected by simple multiplication and, thus, much easier to analyze individually.

Assuming the plant $P(s)$ to be asymptotically stable, the output $y_\infty(t)$ of the MIMO system in steady-state conditions is described by the equations[3]

$$y_\infty(t) = \begin{bmatrix} \nu_1 \cdot \cos(\omega\, t + \psi_1) \cdot h(t) \\ \nu_2 \cdot \cos(\omega\, t + \psi_2) \cdot h(t) \\ \cdots \\ \nu_m \cdot \cos(\omega\, t + \psi_m) \cdot h(t) \end{bmatrix} \tag{3.6}$$

and in the frequency domain this vector can be written as

$$Y_\infty(s) = \mathrm{e}^{\Psi \cdot s/\omega} \cdot \nu \cdot \frac{s}{s^2 + \omega^2} \tag{3.7}$$

[3] As usual, a square system is analyzed, i.e., the number of outputs p is equal to the number of inputs m.

where

$$\Psi = \mathrm{diag}(\psi_i) \in \mathbb{R}^{m\times m}, \quad \text{and} \quad \nu = [\nu_1, \ldots, \nu_m]^{\mathrm{T}} \in \mathbb{R}^m \tag{3.8}$$

As shown in [11], the steady-state system behavior is described by taking the limit $s \to j\,\omega$ and the resulting frequency response matrix $P(j\,\omega)$ has the form

$$P(j\omega) = \begin{bmatrix} P_{1,1}(j\omega) & P_{1,2}(j\omega) & \ldots & P_{1,m}(j\omega) \\ P_{2,1}(j\omega) & P_{2,2}(j\omega) & \ldots & P_{2,m}(j\omega) \\ \ldots & \ldots & \ddots & \ldots \\ P_{m,1}(j\omega) & P_{m,2}(j\omega) & \ldots & P_{m,m}(j\omega) \end{bmatrix} \tag{3.9}$$

As the system is linear, the steady-state output phasor $\mathrm{e}^{j\,\Psi} \cdot \nu$ must satisfy the equation

$$\mathrm{e}^{j\,\Psi} \cdot \nu = P(j\,\omega) \cdot \mathrm{e}^{j\,\Phi} \cdot \mu \tag{3.10}$$

The key idea, with which the frequency response concepts of SISO systems can be (partially) generalized to MIMO systems, is now to look for the extreme cases. To be more specific, for each fixed frequency ω the induced norm of the plant is defined by

$$||P(j\,\omega)|| = \max_{||\mathrm{e}^{j\,\Phi}\cdot\mu||\neq 0} \frac{||\mathrm{e}^{j\,\Psi}\cdot\nu||}{||\mathrm{e}^{j\,\Phi}\cdot\mu||} = \max_{||\mathrm{e}^{j\,\Phi}\cdot\mu||=1} ||\mathrm{e}^{j\,\Psi}\cdot\nu|| \tag{3.11}$$

where the Euclidean norms used in this expression are defined in Equation (2.23). With this definition, it is straightforward to see that

$$||\mathrm{e}^{j\,\Phi}\cdot\mu|| = ||\mu||, \quad \text{and} \quad ||\mathrm{e}^{j\,\Psi}\cdot\nu|| = ||\nu|| \tag{3.12}$$

such that Equation (3.11) can also be written as

$$||P(j\,\omega)|| = \max_{||\mu||\neq 0} \frac{||\nu||}{||\mu||} = \max_{||\mu||=1} ||\nu|| \tag{3.13}$$

Therefore, as introduced in Equation (2.25), the maximum "amplification" that the plant $P(s)$ produces in steady-state is given by $\sigma_{\max}\,(P(j\omega))$, where the singular values of $P(j\,\omega)$ are defined by

$$\sigma_i(P(j\,\omega)) = \sqrt{\lambda_i(\overline{P}^{\mathrm{T}}(j\,\omega)\cdot P(j\,\omega))} \tag{3.14}$$

Figure 3.2 shows how the matrix $P(j\omega_0)$ at a specific frequency ω_0 can be interpreted as a mapping transforming one phasor into another. In the case that the phasor $\mathrm{e}^{j\,\Phi}\cdot\mu$ is the eigenvector of $\overline{P}^{\mathrm{T}}(j\,\omega_0)\cdot P(j\,\omega_0)$ that is associated to $\sigma_{\max}$, the output phasor $\mathrm{e}^{j\,\Psi}\cdot\nu$ has the largest possible norm $||\nu||$, which is the case for the example shown in Figure 3.2. Note that the singular values $\sigma_i(P(j\,\omega))$ are functions of the frequency ω, i.e., for each *fixed* frequency ω_0 a singular-value problem must be solved. Matlab provides dedicated commands, such as the `sigma` routine; use the `help` command for more information.

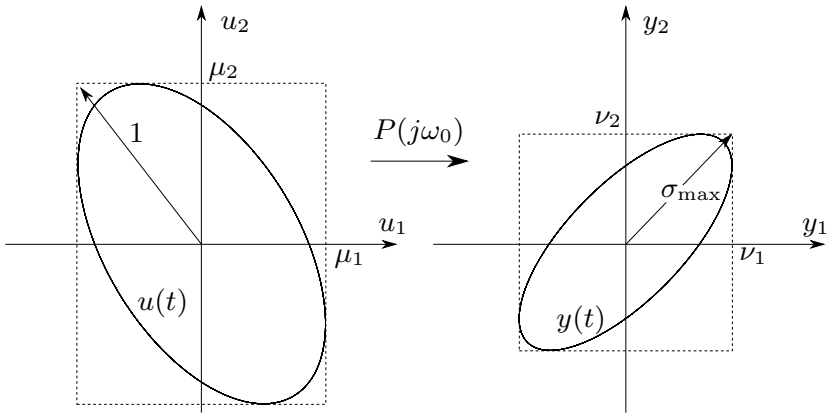

Figure 3.2: Frequency response matrix $P(j\omega_0) \in \mathbb{C}^{2\times 2}$ at a specific frequency ω_0 interpreted as a mapping of one phasor to another phasor.

The result in Equation (2.20) shows that, provided the input satisfies the condition $||\mu|| = 1$, the output phasor $\mathrm{e}^{j\,\Psi} \cdot \nu$ will always satisfy the constraints

$$\min_i \sigma_i(P(j\,\omega)) \leq ||\nu|| \leq \max_i \sigma_i(P(j\,\omega)) \tag{3.15}$$

At each fixed frequency ω_0, the maximum and minimum singular values $\sigma_{\max}(\omega_0)$ and $\sigma_{\min}(\omega_0)$ indicate the limits within which the norm of the phasor $\mathrm{e}^{j\,\Psi} \cdot \nu$ of the output $y(t)$ must lie in steady-state conditions. These bounds are conservative: equality is possible only when $\mathrm{e}^{j\,\Phi} \cdot \mu$ is an eigenvector of the matrix $\overline{P}(j\omega_0)^{\mathrm{T}} \cdot P(j\omega_0)$. Moreover, Equation (3.15) provides worst-case estimations only, i.e., at each time t the signal $y(t)$, in general, will have a magnitude smaller than $\sigma_{\max} \cdot ||\mu||$ even if $\mathrm{e}^{j\,\Phi} \cdot \mu$ is an eigenvector of $\overline{P}(j\omega_0)^{\mathrm{T}} \cdot P(j\omega_0)$. The reason for that is that the scalar signals $y_i(t)$, in general, are not in phase such that these signals will not reach their maximum value at the same time.

This can be illustrated best using an example, e.g., the heat exchanger model derived in Section 1.1. The equations of that system are shown below for the case in which different mass flows and volumes are present in the hot and in the cold strand.[4] The new numerical values are

$$\overset{*}{m}_1 = 0.5\,\mathrm{kg/s},\ \overset{*}{m}_2 = 0.2\,\mathrm{kg/s},\ V_1 = 0.01\,\mathrm{m}^3,\ V_2 = 0.02\,\mathrm{m}^3$$

and

$$\rho = 1000\,\mathrm{kg/m}^3,\ \mathrm{c} = 4200\,\mathrm{J/(kg\,K)},\ F = 2\,\mathrm{m}^2,\ k = 2000\,\mathrm{W/(m}^2\,\mathrm{K)}$$

Accordingly, the time constants $\tau_1 \neq \tau_2$ and the gains $\beta_1 \neq \beta_2$ and $\sigma_1 \neq \sigma_2$ will be different for each channel. The system's state-space description has the following system matrices ($C = I$ and $D = 0$ remain unchanged)

[4] Otherwise the singular values are not distinguishable at higher frequencies.

$$A = \begin{bmatrix} -1/\tau_1 & \sigma_1/\tau_1 \\ \sigma_2/\tau_2 & -1/\tau_2 \end{bmatrix}, \quad B = \begin{bmatrix} \beta_1/\tau_1 & 0 \\ 0 & \beta_2/\tau_2 \end{bmatrix} \tag{3.16}$$

With these matrices it is straightforward to compute the system's transfer function matrix $P(s)$ and, from that, its frequency response matrix $P(j\,\omega)$. Computing the singular values of this matrix $P(j\,\omega)$ for all frequencies in the interval $\omega \in [0.001, 1]$ rad/s yields the plot shown in Figure 3.3.

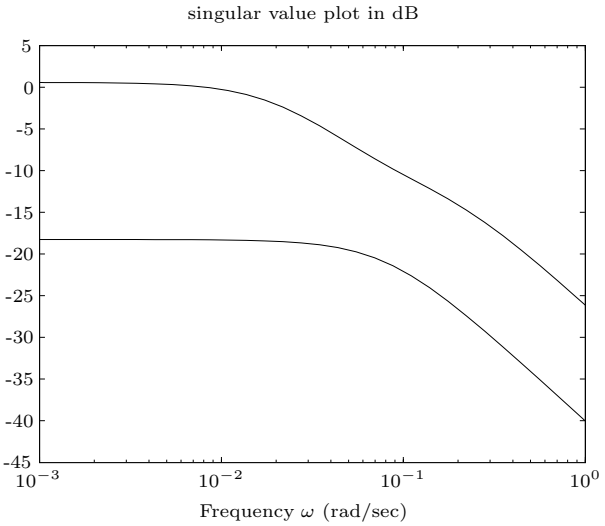

Figure 3.3: Plot of the two singular values of the heat exchanger model.

To better understand the concept of phasors, the behavior of the system for a single frequency ω_0 is analyzed in more detail. Taking $\omega_0 = 0.1$ rad/s yields

$$P(j\,\omega_0) = C \cdot (j\,\omega_0 \cdot I - A)^{-1} \cdot B + D \tag{3.17}$$

$$= \begin{bmatrix} 0.1861 - j\,0.1986 & -0.0131 - j\,0.0430 \\ -0.0327 - j\,0.1074 & 0.0252 - j\,0.0793 \end{bmatrix} \tag{3.18}$$

The singular values of $P(j\,\omega_0)$ are

$$\sqrt{\lambda_i\left(\overline{P}(j\,\omega_0)^{\mathrm{T}} \cdot P(j\,\omega_0)\right)} = \{\sigma_{\max}, \sigma_{\min}\} \approx \{0.2990, 0.0789\} \tag{3.19}$$

and the corresponding eigenvectors of $\overline{P}(j\,\omega_0)^{\mathrm{T}} \cdot P(j\,\omega_0)$ are

$$\zeta_{\max} = \begin{bmatrix} 0.9182 - j\,0.3525 \\ 0.1806 \end{bmatrix} \tag{3.20}$$

$$= \mathrm{e}^{j\,\Phi_{\max}} \cdot \mu_{\max} = \begin{bmatrix} \mathrm{e}^{-j\,0.367} & 0 \\ 0 & \mathrm{e}^{0} \end{bmatrix} \cdot \begin{bmatrix} 0.9836 \\ 0.1806 \end{bmatrix} \tag{3.21}$$

and

$$\zeta_{\min} = \begin{bmatrix} 0.1686 - j\,0.0647 \\ -0.9836 \end{bmatrix} \tag{3.22}$$

$$= \mathrm{e}^{j\,\Phi_{\min}} \cdot \mu_{\min} = \begin{bmatrix} \mathrm{e}^{j\,2.774} & 0 \\ 0 & \mathrm{e}^{0} \end{bmatrix} \cdot \begin{bmatrix} 0.1806 \\ 0.9836 \end{bmatrix} \tag{3.23}$$

If the input is chosen to be

$$u(t) = \begin{bmatrix} 0.9836 \cdot \cos(0.1 \cdot t - j\,0.367) \\ 0.1806 \cdot \cos(0.1 \cdot t) \end{bmatrix} \tag{3.24}$$

the individual amplitudes of the output will have the values $\nu_{\max,1} \approx 0.2740$ and $\nu_{\max,2} \approx 0.1196$ and, as expected,

$$\sigma_{\max} = \sqrt{\nu_{\max,1}^2 + \nu_{\max,2}^2} = \sqrt{0.2740^2 + 0.1196^2} = 0.2990. \tag{3.25}$$

The corresponding input and output signals are shown in Figure 3.4. Figure 3.5 shows a three-dimensional representation of the same input and output signals. Once the system has reached steady-state conditions, both output signals $y_1(t)$ and $y_2(t)$ are harmonic functions of the frequency $\omega_0 = 0.1$ rad/s. However, the phase lags are not the same and, therefore, the signal $y(t)$ *never* has the magnitude $||y(t)|| = \sigma_{\max}(P(j\,0.1)) = 0.2990$ (the two signals do not have their maximum values at the *same* time t).

Figure 3.6 shows a view of the input signal in Equation (3.24) and the resulting steady-state output signal $y_\infty(t)$ with the time t as an implicit parameter.[5] This figure illustrates the meaning of the scalars $\mu_{\max,1}$ and $\mu_{\max,2}$, and $\nu_{\max,1}$ and $\nu_{\max,2}$, respectively. The key point is the observation that there is no time $t = t^*$ for which $y_1(t^*) = \nu_{\max,1}$ *and* $y_2(t^*) = \nu_{\max,2}$. This is an immediate consequence of the fact that the two channels have different phase lags. These phase lags are due to the direct couplings $P_{ii}(s)$, but also due to the cross couplings $P_{ij}(s)$, such that there is no obvious way to include the phase information in the following considerations.

The other extreme is reached when the input is chosen to be

[5] Looking at Figure 3.5, Figure 3.6 is simply the projection along the time axis onto the u_1, u_2 plane.

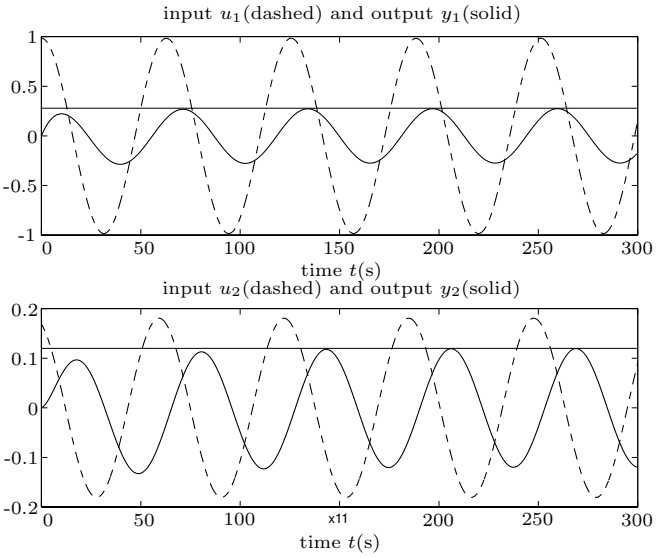

Figure 3.4: Response of the heat exchanger model to the input $u(t)$ in Equation (3.24) (steady-state output amplitudes 0.2740 and 0.1196).

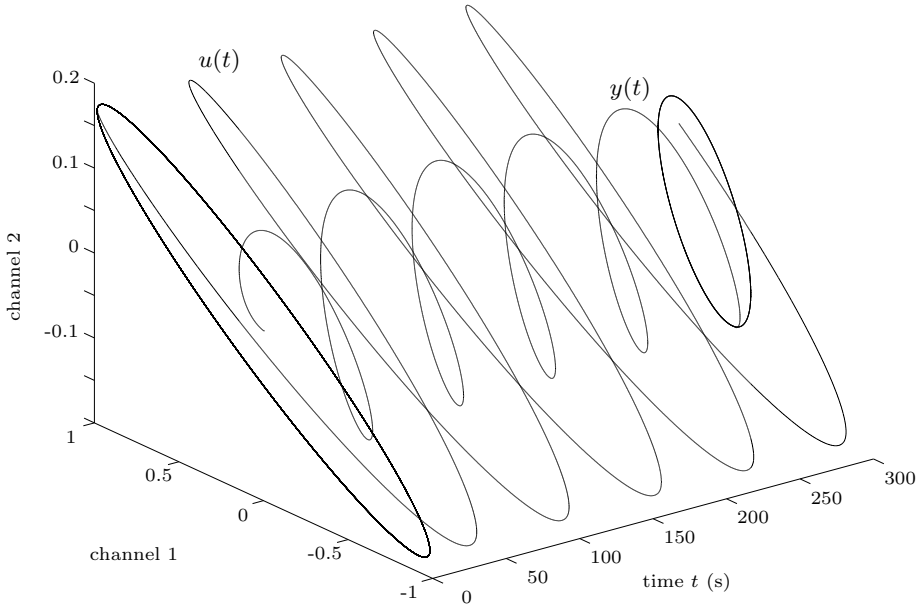

Figure 3.5: Three-dimensional view of the input $u(t)$ (larger spiral) and output $y(t)$ (smaller spiral) signals shown in Figure 3.4, transient and steady-state signals.

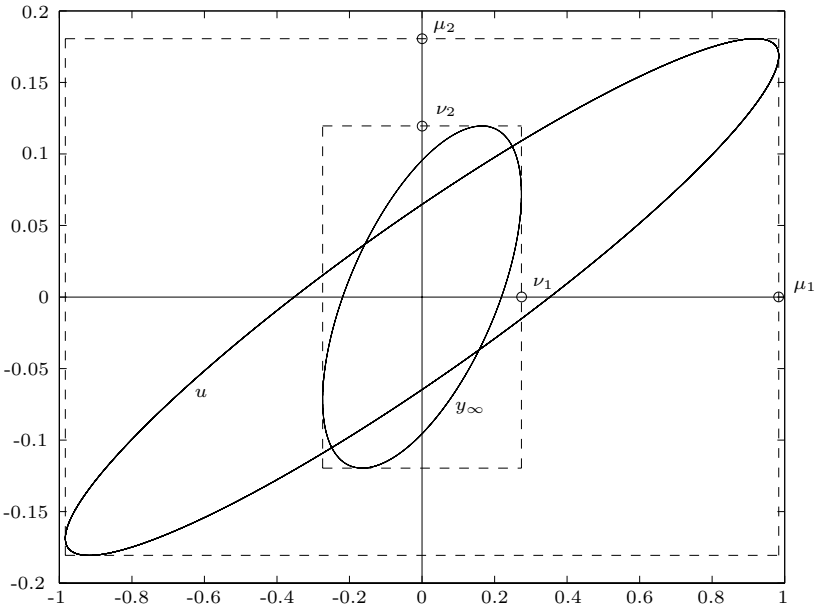

Figure 3.6: Projection of the input signal $u(t)$ and the steady-state part of the output signal $y(t)$ shown in Figure 3.5.

$$u(t) = \begin{bmatrix} 0.1806 \cdot \cos(0.1 \cdot t + 2.774) \\ 0.9836 \cdot \cos(0.1 \cdot t) \end{bmatrix} \tag{3.26}$$

The corresponding input and output signals are shown in Figure 3.7. In this case the smallest possible value of the peak values of the amplitudes is obtained $\sqrt{0.03154^2 + 0.07229^2} = \sigma_{\min}$.

These results of the heat exchanger example have a "nice" physical interpretation:

- Having the two inputs in phase (most of the time the input temperature variations have the same sign), yields a stronger output temperature variation than in the case where the hot input temperature rises when the cold input temperature falls.
- The magnitude of the cross-coupling gain from the hot to the cold side ($P_{2,1} = -0.033 - j\,0.107$) is larger than the magnitude of the cross-coupling gain from the cold to the hot side ($P_{1,2} = -0.013 - j\,0.043$). Accordingly, since the total input temperature variations are limited by the constraint $||u|| = 1$, the amplitude of u_1 is chosen larger than that of u_2 if a large effect has to be achieved, as can be seen in $\zeta_{\max}$.

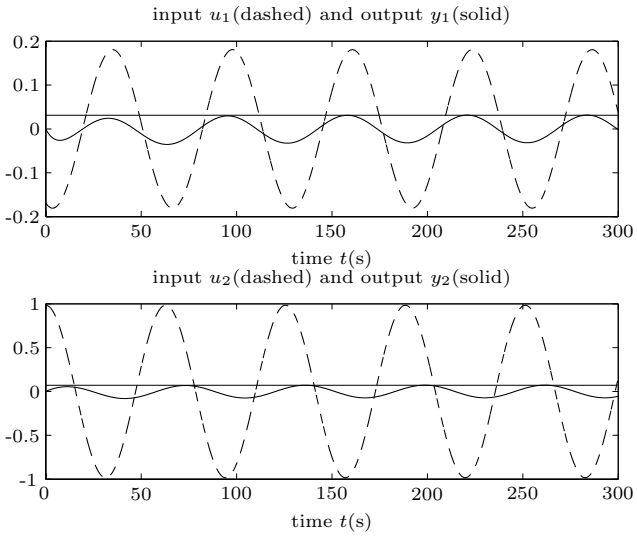

Figure 3.7: Response of the heat exchanger model to the input $u(t)$ in Equation (3.26) (steady-state output amplitudes 0.03154 and 0.07229).

- The same arguments show that in the case where the effect has to be as small as possible, almost all input action needed to satisfy $||u|| = 1$ is placed in u_2, which has the smaller effect on the hot side.
- Note that in steady state the norm $||y(t)||$ is smaller than $\sigma_{\mathrm{m}in}$. Again, this is a consequence of the fact that there is a phase lag between the two components of the vector $y(t)$. In this sense, $\sigma_{\mathrm{m}in}$ is an upper bound of the lower limit for $||y(t)||$.

3.3 Concluding Remarks

In this chapter it was shown that in the MIMO case there is no immediate counterpart to the Nyquist or Bode diagrams that proved to be so useful in the SISO case.[6] The only available frequency response tools are the singular value plots. These plots have some similarities to the magnitude plots in Bode diagrams. However, they only contain extreme-case information.

To be more specific, inequality in Equation (3.15) provides useful information regarding the extreme-case signal amplification (attenuation). Plotting all singular values for all frequencies (see for instance Figure 3.3) yields an *estimation* of the maximum and the minimum magnitude of the output signal

[6] This is a warning of the difficulties to be expected in MIMO design problems.

$y(t)$ in steady-state conditions for the case that the input $u(t)$ is a harmonic signal.

Singular values are used by many modern controller synthesis methods to formulate meaningful optimization problems. For any system $G(s)$ that has all of its poles in $\mathbb{C}_-$ (their real parts are strictly negative) it is possible to find the maximum singular values of $G(s)$ for $s \in \mathbb{C}_+$ by analyzing the frequency response $G(j\,\omega)$.[7]

The norm defined by

$$||G(s)||_\infty = \max_\omega \left(\max_i \sigma_i(G(j\,\omega)) \right) \tag{3.27}$$

is a very useful *system norm*. In particular, the norm of the combination of two systems is not larger than the product of the two individual system norms

$$||G_1(s) \cdot G_2(s)||_\infty \leq ||G_1(s)||_\infty \cdot ||G_2(s)||_\infty \tag{3.28}$$

The most important drawback of the inequality in Equation (3.15) is that it does not contain any phase information. In fact, since each channel has a different phase lag, there is no neat way to extract any characteristic information that is useful, e.g., to assess the system stability.

Aside from the transfer function of the plant, many other transfer functions can be mapped by singular-value plots, for instance the complementary sensitivity $T(s)$, the sensitivity $S(s)$, and the return difference $Q(s)$

$$T(s) = (I + P(s) \cdot C(s))^{-1} \cdot P(s) \cdot C(s) \tag{3.29}$$

$$S(s) = (I + P(s) \cdot C(s))^{-1} \tag{3.30}$$

$$Q(s) = I + P(s) \cdot C(s) \tag{3.31}$$

Note that the Equations (3.29) to (3.31) have been derived by breaking the loop at the controller input. In contrast to the SISO case, for MIMO systems the choice of the loop-breaking point is not irrelevant.

Example 3.3.1 (Complementary Sensitivities of an $m \times m$ System). Consider the square system shown in Figure 3.8. Breaking the loop at the controller input yields the following transfer function $r \to y$ (for space reasons the independent variable s is omitted in some equations below)

$$\begin{aligned} e = r - P \cdot C \cdot e \quad &\Rightarrow \quad (I + P \cdot C) \cdot e = r \\ &\Rightarrow \quad e = (I + P \cdot C)^{-1} \cdot r \\ y = P \cdot C \cdot e \quad &\Rightarrow \quad y = P \cdot C \cdot (I + P \cdot C)^{-1} \cdot r \end{aligned}$$

[7] This is a consequence of the maximum-modulus theorem, which states that a function that is analytic in a region Γ attains its maximum at the boundaries $\partial\Gamma$ of that region [11].

In this case, the complementary sensitivity is

$$T_1(s) = P(s) \cdot C(s) \cdot (I + P(s) \cdot C(s))^{-1}$$

Recalling that $(A \cdot B)^{-1} = B^{-1} \cdot A^{-1}$ it can be shown that $T_1(s)$ is equal to $T(s)$:

$$\begin{aligned} T_1(s) &= P(s) \cdot C(s) \cdot (I + P(s) \cdot C(s))^{-1} \\ &= \Big((I + P(s) \cdot C(s)) \cdot (P(s) \cdot C(s))^{-1}\Big)^{-1} \\ &= \Big((P(s) \cdot C(s))^{-1} + I\Big)^{-1} \\ &= \Big((P(s) \cdot C(s))^{-1} \cdot (I + P(s) \cdot C(s))\Big)^{-1} \\ &= (I + P(s) \cdot C(s))^{-1} \cdot P(s) \cdot C(s) \\ &= T(s) \end{aligned}$$

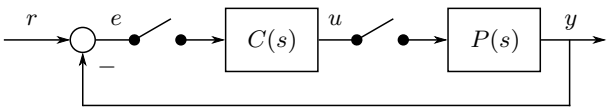

Figure 3.8: MIMO closed-loop system

Repeating the same analysis, but now breaking the loop at the plant's input yields the following transfer function $r \to y$

$$\begin{aligned} u = C \cdot (r - P \cdot u) \quad &\Rightarrow \quad (I + C \cdot P) \cdot u = C \cdot r \\ &\Rightarrow \quad u = (I + C \cdot P)^{-1} \cdot C \cdot r \\ y = P \cdot u \quad &\Rightarrow \quad y = P \cdot (I + C \cdot P)^{-1} \cdot C \cdot r \end{aligned}$$

In this case, the complementary sensitivity is

$$T_2(s) = P(s) \cdot (I + C(s) \cdot P(s))^{-1} \cdot C(s)$$

It is straightforward to see that $T_1(s) = T_2(s)$ and either form may be used. However, the order of the transfer functions $P(s)$ and $C(s)$ must be kept as shown above. ⌟

Quick Check 3.3.1: Prove that $T_1(s) = T_2(s)$. ⌟

Singular value plots play an important role in the design of MIMO control systems. Those results valid for SISO systems that can be formulated using Bode *magnitude* plots only can be transferred easily to MIMO systems using singular value plots. For instance, the robustness of a SISO control loop $L(s)$ is quantified using its minimum return difference

$$\mu_{\min} = \min_{\omega}(|1 + L(j\,\omega)|)$$

In MIMO systems similar ideas can be used, generalizing this expression to

$$\mu_{\min} = \min_{\omega}\left(\min_{i}\sigma_i\left(I + L(j\,\omega)\right)\right)$$

Another example is the worst-case disturbance amplification $||S||_\infty$ expressed in SISO systems with the help of the sensitivity function $S(s)$ of the closed-loop system

$$||S||_\infty = \max_{\omega}(|S(j\,\omega)|)$$

which can be generalized for MIMO systems to

$$||S||_\infty = \max_{\omega}\left(\max_{i}\sigma_i\left(S(j\,\omega)\right)\right)$$

Other examples will be shown in the next chapter. Singular values are, therefore, a very useful object when analyzing MIMO systems. However, one should never forget that these scalars only convey a worst-case information.

Part II

Time Domain MIMO Controller Design

4

Overview and Introduction

Compared to the SISO case, the design of MIMO control systems is substantially more difficult. The main reason is that input and output signals, as well as poles and zeros of the transfer functions now have directions[1] in which they act, such that strong interactions between the individual IO channels can be present. In these cases, iterative loop-shaping approaches that are based on intuitive design rules, in general, do not work well. Only systematic and model-based design approaches can produce good results. It has to be emphasized that these interactions are not an inherent drawback; on the contrary, with appropriate design methods, they can be exploited to improve the overall system behavior.

Several design methods have been developed, starting around 1960 when the "modern" state-space formulations became available. The starting point of all powerful MIMO design methods is the formulation of an optimization problem. Two main families of design methods are used today:

- the $\mathcal{H}_2$ methods, which minimize the $\mathcal{H}_2$-norm, i.e., the mean value, of a suitable error signal over all frequencies in the frequency domain and which simultaneously can be understood as an optimization problem in the time domain; and
- the $\mathcal{H}_\infty$ methods, which formulate an optimization problem in the frequency domain and which minimize the $\mathcal{H}_\infty$-norm, i.e., the worst possible value of a suitable error signal over all frequencies.

Despite the fact that their problem formulations are rather different, the solutions to both approaches are remarkably similar. Several main points are worth mentioning:

[1] See Section 1.5 for a discussion of this concept.

- in both approaches, first, the state $x(t)$ is *assumed* to be accessible (directly measurable) and the problem is solved under this condition yielding a linear feedback law $u(t) = -K \cdot x(t)$;
- in a second step an estimation $\hat{x}(t)$ of the unknown state vector $x(t)$ is obtained using the available signals and *state observers* that have the same order as the system itself (the concept behind such observers is explained in Chapter 6);
- the estimation $\hat{x}(t)$ is then used to compute the feasible control signal $u(t) = -K \cdot \hat{x}(t)$ utilizing the feedback gain obtained for the simplified case (this is referred to as an output feedback structure and the substitution of $x(t)$ by $\hat{x}(t)$ is referred to as the certainty equivalence principle); and
- the actual computation of the parameters of the controller and the observer requires the solution of two Riccati equations (quadratic matrix equations).

In this text, the discussion of MIMO control systems focuses on the $\mathcal{H}_2$ approach using its time-domain interpretation. It allows to introduce the main ideas of MIMO control requiring relatively few mathematical technicalities. The weak point of the $\mathcal{H}_2$ methods is the missing direct link to robustness arguments. Robustness against modeling errors is, therefore, not included explicitly in the design process but must be verified and, if necessary, improved a posteriori using iterative design processes.

The $\mathcal{H}_\infty$ approach permits the explict inclusion of robust stability and robust performance requirements into the design process. This is accomplished with suitable weighting transfer functions that formalize the design goals. These transfer functions are used to define an extended system whose order is equal to the order of the resulting controller. Accordingly, the order of $\mathcal{H}_\infty$ controllers is, in general, larger than the order of the plant. A short introduction to $\mathcal{H}_\infty$ control explaining its basic concept will be given in Chapter 11 and a brief overview on how to use it is shown in a case study in Appendix A.3. More details on $\mathcal{H}_\infty$ control systems can be found, for instance, in the monograph [21].

Of course, this list of synthesis methods could be extended to include many other approaches. Some have become obsolete (e.g., Nyquist-array methods) and some are not recommended (e.g., pole-placement methods[2]).

[2] In the MIMO case, the choice of good pole locations is not trivial, i.e., poles chosen based on arguments valid for SISO systems often turn out to be unacceptable in the MIMO case. Again, this is a consequence of the fact that in MIMO systems a direction is associated to each pole.

5

Infinite-Horizon LQR Controller

5.1 Introduction

This chapter focuses on the time-domain interpretation of the $\mathcal{H}_2$-norm minimization approach for the case that the state vector is accessible. The resulting controllers are referred to as LQR controllers (see below for an explanation of this acronym) and they serve as a starting point to introduce and discuss more general MIMO controller design techniques. As mentioned in the last chapter, the LQR controller design scheme can also be understood as a minimization of the $\mathcal{H}_2$-norm of a suitable error signal in the frequency domain. This frequency domain interpretation is discussed briefly in Chapter 9. It demonstrates the drawbacks of the LQR controller and motivates the strengths of the H_∞ controller design technique discussed in Chapter 11.

5.2 Infinite-Horizon LQR Problem Formulation

The problem to be solved in this section can be formulated as follows.

Given a linear and time-invariant system

$$\frac{\mathrm{d}}{\mathrm{d}t}x(t) = A \cdot x(t) + B \cdot u(t), \quad x(0) \neq 0, \quad x(t) \in \mathbb{R}^n, \; u(t) \in \mathbb{R}^m \tag{5.1}$$

find the control signal $u^{\mathrm{opt}}(t)$ that solves the optimal control problem

$$u^{\mathrm{opt}}(t) = \min_{u(t)} J(u(t)) \tag{5.2}$$

where the objective function is defined by

$$J(u(t)) = \int_0^\infty \left(x^{\mathrm{T}}(u(t)) \cdot Q \cdot x(u(t)) + u^{\mathrm{T}}(t) \cdot R \cdot u(t)\right) \mathrm{d}t \tag{5.3}$$

The optimization shown in Equation (5.2) seeks to find a control signal $u^{\mathrm{opt}}(t)$ out of all possible control signals $u(t)$ that minimizes the quadratic cost function $J(u(t))$ in Equation (5.3). For the problem to be well-posed, the weighting matrices Q and R must satisfy the conditions

$$Q = Q^{\mathrm{T}} \in \mathbb{R}^{n\times n},\ Q \geq 0, \quad \text{and} \quad R = R^{\mathrm{T}} \in \mathbb{R}^{m\times m},\ R > 0 \tag{5.4}$$

The conditions in Equation (5.4) require that deviations from zero of both $x(t)$ and $u(t)$ can only enter the cost function positively and that the control signal $u(t)$ is not allowed to diverge to infinity.

Indeed, the cost function is minimized only if

$$\lim_{t\to\infty} u(t) = 0 \tag{5.5}$$

$$\lim_{t\to\infty} x(t) = 0 \tag{5.6}$$

as otherwise $J(u^{\mathrm{opt}}(t))$ becomes infinite. As a consequence, these conditions guarantee that the control signal u^{opt} yields an asymptotically stable closed-loop system.

The formulation of the optimization problem in Equation (5.2) is referred to as the *infinite-horizon regulator problem*: the system state $x(t)$, initialized at $x(0) \neq 0$, is asymptotically regulated to its origin $x = 0$. Since the convergence is asymptotic, an infinite horizon is required to find a solution to the problem.

The expression *LQR* (Linear Quadratic Regulator) refers to the linear system description, the quadratic cost function and the regulator problem setting. The restriction to a regulator problem might give the impression that the solution presented below is of limited value. However, this is not true because several other control problem formulations (reference tracking, disturbance rejection, etc.) can be reformulated to fit the regulator problem setting, as it will be shown in Section 5.5.

Interpretation of the LQR Problem in the SISO Case

The LQR problem formulation has an intuitive interpretation in the SISO case, in particular if the plant is assumed to have an output $y(t) = c \cdot x(t)$ and the output vector c is used[1] to form the state weighting matrix: $Q = c^{\mathrm{T}} \cdot c$. In this case the state-dependent part of the cost function can be written as

$$x(t)^{\mathrm{T}} \cdot Q \cdot x(t) = x(t)^{\mathrm{T}} \cdot c^{\mathrm{T}} \cdot c \cdot x(t) = (c \cdot x(t))^{\mathrm{T}} \cdot c \cdot x(t) = y^2(t) \tag{5.7}$$

and the complete cost function results as

[1] The pair $\{A, c\}$ is assumed to be completely observable in this formulation.

$$J(u(t)) = \int_0^\infty \left(y^2(u(t)) + r \cdot u^2(t)\right) \mathrm{d}t = \underbrace{\int_0^\infty y^2(u(t))\,\mathrm{d}t}_{E_y} + r \cdot \underbrace{\int_0^\infty u^2(t)\,\mathrm{d}t}_{E_u} \tag{5.8}$$

with only one scalar design parameter $r > 0$ remaining.

The integral from $t = 0 \to \infty$ of a signal squared corresponds to its energy content. A small r indicates that the energy E_u of the control signal is not important relative to the energy E_y of the resulting error signal.[2] Accordingly, the optimal control signal $u^{\mathrm{opt}}(t)$ will be relatively large in the beginning in order to drive $y(t)$ to zero quickly. This situation is often referred to as the *cheap control* case, as the control energy is assumed to be readily available.

The other limit case $r \to \infty$ is referred to as the *expensive control* situation. In this case, E_u will be relatively small and E_y relatively large.

Quick Check 5.2.1: What happens for $r = 0$ or for $r = \infty$? Can you explain why neither case is useful in practice? ⌟

5.3 Infinite-Horizon LQR Problem Solution and Proof

Solution

The optimal solution to the standard LQR problem defined in Section 5.2 is surprisingly simple, *viz.* a time-invariant and linear function of the system state

$$u^{\mathrm{opt}}(t) = -K \cdot x(t) \tag{5.9}$$

The constant controller gain K is defined by

$$K = R^{-1} \cdot B^{\mathrm{T}} \cdot \Phi \tag{5.10}$$

where the matrix Φ is the only positive definite solution of the algebraic matrix Riccati equation[3]

$$\Phi \cdot B \cdot R^{-1} \cdot B^{\mathrm{T}} \cdot \Phi - \Phi \cdot A - A^{\mathrm{T}} \cdot \Phi - Q = 0 \tag{5.11}$$

The symmetry of Equation (5.11) requires that $\Phi = \Phi^{\mathrm{T}}$, and the constraint $\Phi > 0$ applies, i.e., Φ must be positive definite. A positive definite solution $\Phi > 0$ is guaranteed to exist if[4]

[2] Remember that the control system solves a regulator problem, in which 0 is the reference value for $y(t) = c \cdot x(t)$.

[3] A $q \times r$ matrix equation is a list of $q \cdot r$ individual scalar equations: every entry in the matrix equation has to hold.

[4] Less restrictive conditions guarantee a solution to exist, namely $\{A, B\}$ are detectable and $\{A, \widetilde{C}\}$ are stabilizable. In that case, however, it is not guaranteed that $\Phi > 0$.

c1: the pair $\{A, B\}$ is completely controllable; and

c2: the pair $\{A, \widetilde{C}\}$ is completely observable,

where the matrix $\widetilde{C}$ is the full-rank decomposition of the weight Q, i.e.,

$$Q = \widetilde{C}^{\mathrm{T}} \cdot \widetilde{C}, \quad \widetilde{C} \in \mathbb{R}^{p \times n}, \quad \text{where} \quad p = \operatorname{rank}(Q) \leq n \tag{5.12}$$

Condition c2 guarantees that the scalar $x^{\mathrm{T}}(t) \cdot Q \cdot x(t)$ contains sufficient information about the state variables such that the criterion in Equation (5.2) formulates a meaningful trade-off problem. The matrix $\widetilde{C}$ is not related to the output matrix C of the plant $y(t) = C \cdot x(t)$. However, one can *choose* $Q = C^{\mathrm{T}} \cdot C$ and thereby penalize the true output signal $y(t)$ in the cost function as shown above in the example of a SISO system.

Figure 5.1 illustrates a closed-loop system with a linear state-feedback controller in place.

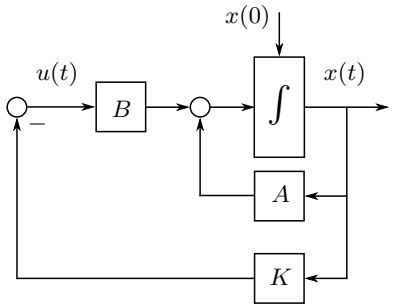

Figure 5.1: State-space representation of a linear state-feedback controlled system.

For the solution of the Riccati Equation in Equation (5.11) reliable numerical algorithms are known which are implemented in standard CACSD[5] tools. Matlab provides the `lqr` command and below the notation

```
K=lqr(A,B,Q,R)
```

will be used to refer to the solution Equation (5.9) of Equation (5.11) of the LQR problem.

Sufficiency Proof

The proof that the feedback introduced in Equation (5.9) with Φ satisfying Equation (5.11) indeed minimizes the objective function formulated in Equation (5.3) is given next. This sufficiency proof uses the idea of completing the

[5] This acronym stands for Computer Aided Control System Design.

squares. The proof of necessity, i.e., that *only* Equation (5.9) with Φ satisfying Equation (5.11) minimizes the objective function in Equation (5.3), is much more difficult. Interested readers are referred to [1].

The starting point is rewriting Equation (5.11) as follows

$$Q = \Phi \cdot B \cdot R^{-1} \cdot B^{\mathrm{T}} \cdot \Phi - \Phi \cdot A - A^{\mathrm{T}} \cdot \Phi \tag{5.13}$$

With that the objective function in Equation (5.2) can be written as (for space reason all time dependencies are omitted)

$$\begin{aligned} J &= \int_0^\infty \left(x^{\mathrm{T}} \cdot \Phi \cdot B \cdot R^{-1} \cdot B^{\mathrm{T}} \cdot \Phi \cdot x + u^{\mathrm{T}} \cdot R \cdot u\right) \mathrm{d}t \\ &\quad - \int_0^\infty \left(x^{\mathrm{T}} \cdot \left(A^{\mathrm{T}} \cdot \Phi + \Phi \cdot A\right) \cdot x\right) \mathrm{d}t \end{aligned} \tag{5.14}$$

Completing the squares yields

$$\begin{aligned} J &= \int_0^\infty \left((x^{\mathrm{T}} \cdot \Phi \cdot B \cdot R^{-1} + u^{\mathrm{T}}) \cdot R \cdot (R^{-1} \cdot B^{\mathrm{T}} \cdot \Phi \cdot x + u)\right) \mathrm{d}t \\ &\quad - \int_0^\infty \left(x^{\mathrm{T}} \cdot \Phi \cdot B \cdot R^{-1} \cdot R \cdot u + u^{\mathrm{T}} \cdot R \cdot R^{-1} \cdot B^{\mathrm{T}} \cdot \Phi \cdot x\right) \mathrm{d}t \\ &\quad - \int_0^\infty \left(x^{\mathrm{T}} \cdot \left(A^{\mathrm{T}} \cdot \Phi + \Phi \cdot A\right) \cdot x\right) \mathrm{d}t \end{aligned} \tag{5.15}$$

Simplifying this expression yields

$$\begin{aligned} J &= \int_0^\infty \left((R^{-1} \cdot B^{\mathrm{T}} \cdot \Phi \cdot x + u)^{\mathrm{T}} \cdot R \cdot (R^{-1} \cdot B^{\mathrm{T}} \cdot \Phi \cdot x + u)\right) \mathrm{d}t \\ &\quad - \int_0^\infty \left((u^{\mathrm{T}} \cdot B^{\mathrm{T}} + x^{\mathrm{T}} \cdot A^{\mathrm{T}}) \cdot \Phi \cdot x + x^{\mathrm{T}} \cdot \Phi \cdot (B \cdot u + A \cdot x)\right) \mathrm{d}t \end{aligned} \tag{5.16}$$

which, using Equation (5.1) can be written as

$$\begin{aligned} J &= \int_0^\infty \left((R^{-1} \cdot B^{\mathrm{T}} \cdot \Phi \cdot x + u)^{\mathrm{T}} \cdot R \cdot (R^{-1} \cdot B^{\mathrm{T}} \cdot \Phi \cdot x + u)\right) \mathrm{d}t \\ &\quad - \int_0^\infty \left(\tfrac{\mathrm{d}}{\mathrm{d}t} x^{\mathrm{T}} \cdot \Phi \cdot x + x^{\mathrm{T}} \cdot \Phi \cdot \tfrac{\mathrm{d}}{\mathrm{d}t} x\right) \mathrm{d}t \end{aligned} \tag{5.17}$$

or

$$\begin{aligned} J &= \int_0^\infty \left((R^{-1} \cdot B^{\mathrm{T}} \cdot \Phi \cdot x + u)^{\mathrm{T}} \cdot R \cdot (R^{-1} \cdot B^{\mathrm{T}} \cdot \Phi \cdot x + u)\right) \mathrm{d}t \\ &\quad - \int_0^\infty \tfrac{\mathrm{d}}{\mathrm{d}t} \left(x^{\mathrm{T}} \cdot \Phi \cdot x\right) \mathrm{d}t \end{aligned} \tag{5.18}$$

The objective function J can be finite only if the state $x(t)$ converges to 0 as time t goes to ∞. Accordingly, the second term in the last equation is equal to

$$\int_0^\infty \frac{\mathrm{d}}{\mathrm{d}t} \left(x^{\mathrm{T}}(t) \cdot \Phi \cdot x(t)\right) \mathrm{d}t = x^{\mathrm{T}}(t) \cdot \Phi \cdot x(t)\big|_0^\infty = -x^{\mathrm{T}}(0) \cdot \Phi \cdot x(0) \tag{5.19}$$

and, therefore, the objective function can be written as

$$J = \int_0^\infty \xi^{\mathrm{T}}(t) \cdot R \cdot \xi(t) \;\; \mathrm{d}t + x^{\mathrm{T}}(0) \cdot \Phi \cdot x(0) \tag{5.20}$$

where

$$\xi(t) = R^{-1} \cdot B^{\mathrm{T}} \cdot \Phi \cdot x(t) + u(t) \tag{5.21}$$

Since $R > 0$, by definition, the value of $\xi(t)$ that minimizes the objective function is $\xi(t) = 0 \; \forall t \in [0, \infty)$, which proves that the feedback law in Equation (5.9) is indeed the optimal solution. Morever, the value of the objective function in the optimal case is

$$J^{\mathrm{opt}} = x^{\mathrm{T}}(0) \cdot \Phi \cdot x(0) \tag{5.22}$$

an infromation that was missing so far.

5.4 Properties of Infinite-Horizon LQR Controllers

Here, the three most important properties of any closed control loop are discussed for the LQR case, i.e., its stability, its robustness and its disturbance rejection properties.

5.4.1 Stability Properties

An LQR closed-loop controlled system is guaranteed to be asymptotically stable, even if the linear system to be controlled is unstable. From Figure 5.1 it can be seen that the closed-loop system follows the dynamics of an autonomous linear system with state matrix $A - B \cdot K$

$$\frac{\mathrm{d}}{\mathrm{d}t} x(t) = (A - B \cdot K) \cdot x(t), \quad x(0) = x_0 \tag{5.23}$$

If the conditions c1 and c2 stated in Section 5.3 are satisfied, the closed-loop system matrix $A - B \cdot K$ is guaranteed to be a Hurwitz matrix, i.e., all eigenvalues of $A - B \cdot K$ must have negative real parts and therefore the closed-loop controlled system converges to zero for any initial state $x(0) \neq 0$.

5.4.2 Robustness Properties

The robustness of a stable closed-loop control system is a quantitative measure of how "far away" it is from instability. The robustness properties of a closed-loop transfer function $T(s)$ can be assessed using any open-loop transfer function $L(s)$ as long as they relate to each other as follows

$$T(s) = \frac{L(s)}{1 + L(s)} \tag{5.24}$$

In the standard SISO feedback control-loops analyzed so far, the open-loop transfer function used was $L(s) \stackrel{\text{def}}{=} P(s) \cdot C(s)$, that is from control error e to system output y, see Figure 5.2.

In an LQR control loop, however, there is no obvious way to open the closed-loop at the output since the complete state is fed back. Alternatively, the robustness properties can be assessed breaking the loop as shown in Figure 5.3, resulting in

$$L_{\text{LQR}}(s) = K \cdot (sI - A)^{-1} \cdot B \tag{5.25}$$

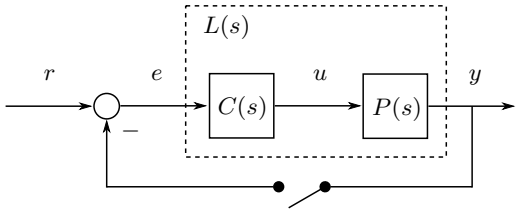

Figure 5.2: Open-loop of a standard feedback control-loop.

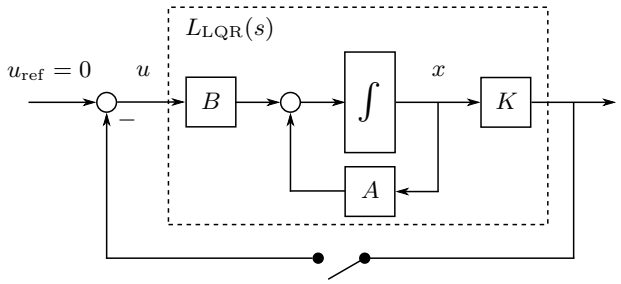

Figure 5.3: Open-loop of a linear state-feedback controlled system.

Comparing Figure 5.3 to Figure 5.2 reveals that $L_{\mathrm{LQR}}(s)$ and $L(s)$ fit identically into the resulting closed-loop structure and therefore the same measures of robustness can be used, namely the Nyquist stability theorem in the SISO case and the minimum return difference in the general MIMO case.

Interesting assertions about the robustness of the closed control loop can be proven under the conditions that $L_{\mathrm{LQR}}(s)$ is obtained using $R = r \cdot I$ (see e.g. [1] or [2]). In this case, the minimum return difference $\mu_{\min,\mathrm{LQR}}$ can be shown to satisfy always the inequality

$$\mu_{\min,\mathrm{LQR}} = \min_{\omega} \left(\min_{i} \sigma_i \left(I + L_{\mathrm{LQR}}(j\,\omega) \right) \right) \geq 1, \tag{5.26}$$

which corresponds to excellent robustness margins. Notice that this result is not surprising as the LQR solution utilizes the full state vector to form the feedback control signal.

In the SISO case, condition Equation (5.26) can be simplified to

$$\mu_{\min,\mathrm{LQR}} = \min_{\omega} \left(|1 + L_{\mathrm{LQR}}(j\,\omega)| \right) \geq 1 \tag{5.27}$$

and this result has a nice frequency-domain interpretation: the Nyquist plot of the SISO loop gain $L_{\mathrm{LQR}}(j\omega)$ does not enter a circle with radius 1 around the critical point -1.

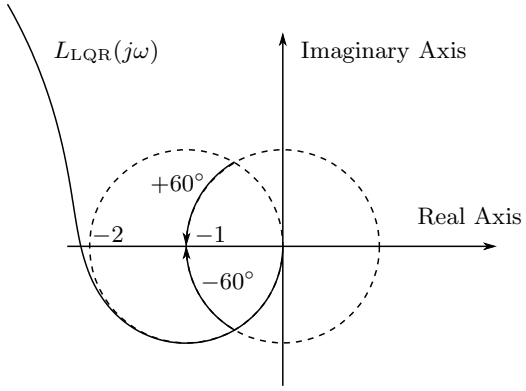

Figure 5.4: Nyquist diagram of the open loop gain L_{LQR} of an LQR controlled SISO system (see Figure A.6 discussed in detail in Appendix A.2)

The result of Equation (5.27) can be translated into guarantees on the phase and gain margin of the SISO LQR loop. For the following discussion, recall that the phase margin and the gain margin of a SISO loop gain $L(j\omega)$ are used to quantify its robustness with respect to pure gain *or* pure phase modeling errors, i.e., the true loop gain $L_{\mathrm{t}}(j\omega)$ is assumed to have the form

$$L_{\mathrm{t}}(j\omega) = \mathrm{e}^{-j\cdot\alpha} \cdot k \cdot L(j\omega) \tag{5.28}$$

and the associated closed loop is assumed to remain stable for any phase errors *or* gain errors that satisfy the conditions[6]

$$\begin{array}{rcl} k & \in & [k_{\min}, k_{\max}] \\ \alpha & \in & [\alpha_{\min}, \alpha_{\max}] \end{array} \tag{5.29}$$

From Equation (5.27) it follows that in the LQR case these limits satisfy the conditions

$$\begin{array}{rcl} k_{\min} & \leq & 0.5 \\ k_{\max} & = & \infty \\ \alpha_{\min} & \leq & -60^\circ \\ \alpha_{\max} & \geq & 60^\circ \end{array} \tag{5.30}$$

As Figure 5.4 shows, in general the limits are not attained and even more robust control loops result.

Improving Robustness

The robustness properties of the standard LQR controllers can be improved further in the following way. Instead of the solution Φ of the standard Riccati Equation (5.11), the solution Φ_β of the following modified Riccati equation is used to form the state-feedback gain in Equation (5.9).

$$\frac{1}{\beta} \cdot \Phi_\beta \cdot B \cdot R^{-1} \cdot B^{\mathrm{T}} \cdot \Phi_\beta - \Phi_\beta \cdot A - A^{\mathrm{T}} \cdot \Phi_\beta - Q = 0 \tag{5.31}$$

For tuning parameters $\beta > 1$ the resulting loop gain as defined in Equation (5.25) has the property

$$\min_{\omega} \left(\min_{i} \sigma_i \left(\beta\, I + L(j\,\omega) \right) \right) \geq \beta \tag{5.32}$$

In the SISO case, the condition in Equation (5.32) correnspponds to a circle with radius β around the point $-\beta$ in the Nyquist plot, as illustrated in Figure 5.5.

In the limit case $\beta \to \infty$ the Riccati Equation in Equation (5.31) is reduced to the Lyapunov equation

$$-\Phi_\infty \cdot A - A^{\mathrm{T}} \cdot \Phi_\infty - Q = 0 \tag{5.33}$$

In this case, the loop gain $L_\infty(s) = K_\infty \cdot (s\, I - A)^{-1} \cdot B$ with

[6] It is important to keep in mind that if phase and gain deviations are present *simultaneously* these margins are no longer meaningful (for more details see [11]).

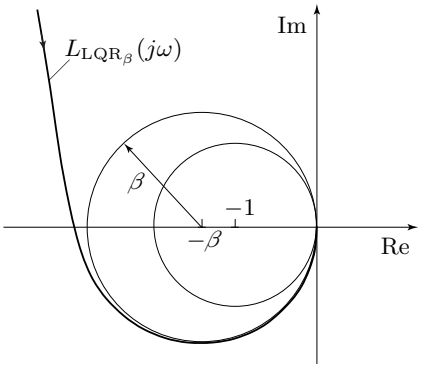

Figure 5.5: Exemplary Nyquist diagram of the open-loop gain transfer function $L_{LQR_\beta}(s) = k_\beta\,(s\,I - A)^{-1}b$, with k_β computed using Equation (5.31).

$$K_\infty = R^{-1} \cdot B^{\mathrm{T}} \cdot \Phi_\infty$$

is strictly positive real. In the SISO case, this is equivalent to a loop gain whose Nyquist curve $L_\infty(j\,\omega)$ remains in the real-positive complex plane. Unfortunately, a stabilizing solution Φ_∞ exists iff A is a Hurwitz matrix, i.e., if the uncontrolled linear system is stable to begin with.

5.4.3 Disturbance Rejection Properties

In general the closed-loop LQR control loop as shown in Figure 5.1 is not able to reject constant disturbances completely. This is due to the lack of integrating behavior.[7]

For the case of a constant disturbance $w(t) = w_\infty \cdot h(t)$ at the system input, as shown in Figure 5.6, the resulting system is described by

$$\frac{\mathrm{d}}{\mathrm{d}t}x(t) = (A - B \cdot K) \cdot x(t) + B \cdot w_\infty \cdot h(t), \quad x(0) = x_0 \tag{5.34}$$

As mentioned above, the closed-loop system matrix $A - B \cdot K$ is Hurwitz by design and, therefore, the system remains asymptotically stable even in the presence of a constant input disturbance. However, the state of the closed-loop system will asymptotically converge to a constant value $\lim_{t\to\infty} x(t) = x_\infty$ that is not equal to zero anymore

[7] If the plant itself has integrating behavior, i.e., if it has at least one eigenvalue in the origin, some disturbance rejection properties can be expected. However, in general, even in that situation an LQR controller cannot reject *all* possible disturbances.

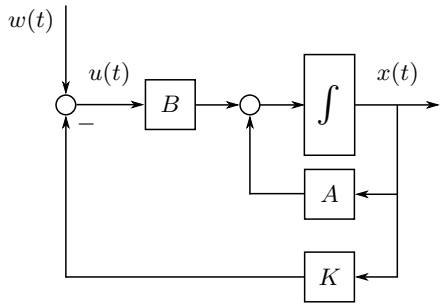

Figure 5.6: State-space representation of a linear state-feedback controlled system with input disturbance $w(t)$.

$$\frac{\mathrm{d}}{\mathrm{d}t}x_\infty = 0 = (A - B \cdot K) \cdot x_\infty + B \cdot w_\infty \cdot h(t) \tag{5.35}$$

$$\rightarrow x_\infty = -(A - B \cdot K)^{-1} B \cdot w_\infty \tag{5.36}$$

In Subsection 5.5.2 it will be show how the LQR control scheme can be extended to include integrative behavior that leads to a zero steady-state control error even in the presence of non-vanishing disturbances.

Quick Check 5.4.1: Is the matrix $A - B \cdot K$ always invertible? ⌟

5.4.4 Conclusion

The fact that using the LQR controller design method is fairly simple but still guarantees a stable control loop with a significant robustness margin is the main result of this section. The fact that disturbances are not rejected completely in the standard LQR formulation is a minor issue. In Subsection 5.5.2, it will be shown that the problem formulation can be recast such that when the standard LQR scheme is applied, disturbance rejection can be guaranteed as well.

The following points summarize the key results:[8]

- The LQR controller is a *linear* and *time-invariant* feedback of the state variable $x(t)$.
- The resulting closed-loop system matrix $A - B \cdot K$ is guaranteed to be a Hurwitz matrix, i.e., all eigenvalues of $A - B \cdot K$ have negative real parts.
- The conditions c1 and c2 are sufficient, but not necessary for a solution to the LQR problem to exist. Less restrictive conditions are known that guarantee a meaningful solution as well, see [9].

[8] Readers interested in the complete proofs of these assertions are referred to [1].

- The resulting controller is not an optimal controller in the sense that it is the *best possible* one. The term optimal only refers to the fact that the controller is obtained as the solution to an optimization problem.
- The matrices Q and R are the "tuning knobs" with which the controller properties are influenced in a systematic way. The choice of meaningful weights is not trivial.
- The loop gain in Equation (5.25) always has excellent robustness properties. For the particular choice

$$R = r \cdot I_{m\times m}, \quad r > 0 \tag{5.37}$$

  these properties have a straightforward interpretation in the frequency domain as shown in Equation (5.26) for the MIMO, and Equation (5.27) for the SISO case, respectively.
- It is simple to prove that Equation (5.11) indeed yields a solution to the LQR problem (see proof above), but it is more difficult to prove that this solution is the only one.
- For the solution of the Riccati Equation in Equation (5.11) reliable numerical algorithms are known which are implemented in standard CACSD tools. Matlab provides the `lqr` command and in this text the notation

```
K=lqr(A,B,Q,R)
```

  will be used to refer to Equation (5.9), the solution of the LQR problem.

5.5 Some Extensions of the Infinite-Horizon LQR Controller

The following paragraphs will show how the standard LQR problem formulation can be extended to add disturbance rejection and enable reference tracking. Note that all of the extended control loops shown in the following paragraphs still have the same stability and robustness properties as the standard LQR control loop defined in Section 5.4.

5.5.1 State Reference Tracking

As shown in Subsection 5.4.1, the standard LQR scheme controls the system to the equilibrium point $u_\infty = x_\infty = 0$. In Subsection 5.4.3, it was shown that if a constant disturbance w_∞ is added to the input of an LQR closed-loop system, in general, its state converges to a different equilibrium state $x_\infty \neq 0$.

In the following paragraphs, extensions of the standard LQR controller are introduced that enable controlling the system to a desired equilibrium state x_∞ (if that is feasible) and to completely reject constant input disturbances w_∞.

A linear system can have many constant equilibrium states x_∞. Each one of them is related to a chosen constant input u_∞ and together, state x_∞ and input u_∞ must fulfill the steady-state equation

$$\lim_{t\to\infty} \frac{\mathrm{d}}{\mathrm{d}t} x(t) = A \cdot x_\infty + B \cdot u_\infty = 0 \tag{5.38}$$

The pair $\{u_\infty = 0,\ x_\infty = 0\}$ is always one possible equilibrium point, but there may be more. Indeed, all pairs $\{u_\infty,\ x_\infty\}$ that satisfy Equation (5.38) are admissible as well. If the matrix A is invertible (the plant has no poles in the origin) then this set is described by

$$X_\infty = \{\xi \in \mathbb{R}^n \mid \xi = A^{-1} \cdot B \cdot \nu,\ \ \nu \in \mathbb{R}^m\} \tag{5.39}$$

If the matrix A is singular, then a non-trivial solution to Equation (5.38) exists if $x_\infty \in \ker\{A\}$ (in this case $u_\infty = 0$) or if the range of A and the range of B have an intersection.

Quick Check 5.5.1: Assume the matrices $\{A, b\}$ describe a second-order SISO system in controllability canonical form and assume that the matrix A has only eigenvalues in the origin. Is there a non-trivial solution $\{x_\infty, u_\infty\} \neq \{0, 0\}$ to Equation (5.38)? ⌟

In the following it is assumed that a nontrivial equilibrium x_∞, u_∞ exists. In this case, new coordinates Δu and Δx can be defined with respect to that equilibrium point as follows

$$\begin{aligned} \Delta x(t) &= x(t) - x_\infty \\ \Delta u(t) &= u(t) - u_\infty \end{aligned} \tag{5.40}$$

In these new coordinates, the system dynamics are described by

$$\frac{\mathrm{d}}{\mathrm{d}t} \Delta x(t) = A \cdot \Delta x(t) + B \cdot \Delta u(t) \tag{5.41}$$

The cost function of the LQR problem formulation in the new coordinates is

$$J(\Delta u(t)) = \int_0^\infty \Big(\Delta x(t)^\top \cdot Q \cdot \Delta x(t) + \Delta u(t)^\top \cdot R \cdot \Delta u(t) \Big) \mathrm{d}t \tag{5.42}$$

The system dynamics in Equation (5.41) and the cost function in Equation (5.42) are identical to the standard LQR formulation in Section 5.2, only the variable names are different. As a result, the optimal solution is identical to the solution of the standard LQR formulation, namely the static linear state-feedback matrix K

$$\Delta u(t) = -K \cdot \Delta x(t) \tag{5.43}$$

The feedback gain K is the solution to the Riccati equations of the original problem. The resulting closed-loop system is shown in Figure 5.7a. It illustrates that the system asymptotically converges to zero in the newly defined coordinates $\Delta x(t)$ while in the original coordinates $x(t)$, it converges to the equilibrium state x_∞.

Alternatively, the closed-loop system can be drawn as shown in Figure 5.7b. The control signal $u(t)$ in Equation (5.44) consists of the original linear state-feedback $-K \cdot x(t)$ plus an additional constant term $K \cdot x_\infty + u_\infty$. This term can be calculated inserting the definitions in Equation (5.40) into Equation (5.43).

$$\begin{aligned} u(t) &= -K \cdot (x(t) - x_\infty) + u_\infty \\ &= -K \cdot x(t) + K \cdot x_\infty + u_\infty \end{aligned} \tag{5.44}$$

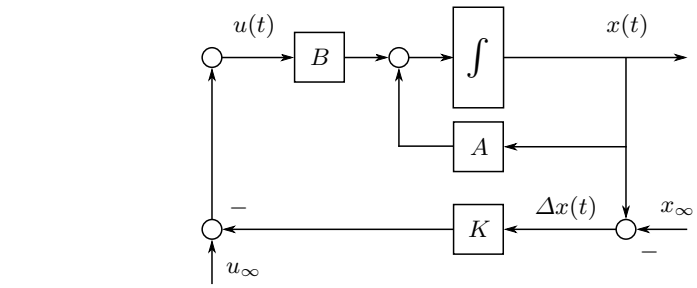

(a)

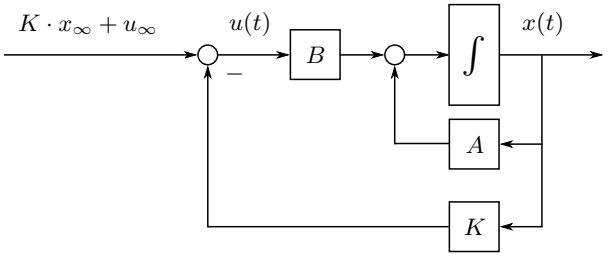

(b)

Figure 5.7: LQR closed-loop extended by an additional constant input to control the system state to the desired equilibrium state x_∞.

Quick Check 5.5.2: Show that the system illustrated in Figure 5.7 fulfills Equation (5.38) in steady-state. ⌟

5.5.2 Output Reference Tracking

In practice, a control engineer usually is interested in controlling the system output variable $y(t)$ and not the system state $x(t)$. Therefore, in this section, the plant description in Equation (5.1) is extended to include the real (physical) measurements $y(t)$ and a control system extension is shown that allows to control the system output to a chosen reference signal.

To achieve this objective, the LQR control loop is extended to enable the tracking of piecewise *constant* reference signals as defined in Equation (5.46). In many applications only such reference signals are encountered. However, the theory of LQR controllers can be extended to deal with fully time-varying reference signals. Unfortunately, in that case, the resulting controller is not time-invariant anymore and also not causal. A brief introduction of these ideas is given below in Section 5.6.

Here, the simpler situation of constant reference signals is analyzed first. The starting point is the usual plant dynamics

$$\begin{aligned} \frac{\mathrm{d}}{\mathrm{d}t}x(t) &= A \cdot x(t) + B \cdot u(t), \quad && x(t) \in \mathbb{R}^n,\, u(t) \in \mathbb{R}^m \\ y(t) &= C \cdot x(t), && y(t) \in \mathbb{R}^m \end{aligned} \tag{5.45}$$

and reference signals $r(t) \in \mathbb{R}^m$ having this special form (the signal $h(t) \in \mathbb{R}$ is the standard Heaviside function)

$$r(t) = \begin{bmatrix} r_1 \\ r_2 \\ \vdots \\ r_m \end{bmatrix} \cdot h(t) = r_\infty \cdot h(t) \tag{5.46}$$

The plant is assumed to be strictly proper ($D = 0$) and the number of outputs is assumed to be the same as the number of inputs ("square system").

The first assumption is not very restrictive but it simplifies the mathematical details considerably and it is, therefore, adopted here. All results presented below can be extended to proper systems ($D \neq 0$). Interested readers are referred to [1]. The second assumption is justified by engineering arguments. If a plant has $p > m$ outputs, where m is the number of inputs, some of the outputs cannot be controlled independently. These $p - m$ outputs are linearly dependent on the remaining m outputs and, thus, can be discarded.[9] If a plant has $p < m$ outputs, $m - p$ inputs are not necessary to control the plant outputs

[9] These $p-m$ output signals provide valuable additional information and, therefore, can be used to improve the behavior of the m main control channels. A typical example are cascaded [11] or observer-based controllers (see Chapter 6).

and, for cost reasons, in general these expensive actuators will be omitted in the first place.

The idea of controlling the system to an equilibrium state x_∞ as discussed in Subsection 5.5.1 can be used to control the system to a constant reference r_∞ for the system output. For this approach to work, the reference signal r_∞ must correspond to an equilibrium point x_∞ that results in the desired constant system output y_∞, i.e.,

$$r_\infty = y_\infty = C \cdot x_\infty \tag{5.47}$$

The extension of the standard LQR control system that enables an output-reference tracking for the special case defined in Equation (5.46) is illustrated in Figure 5.8. The additional input signal $u_r(t)$ is a linear function of the reference signal $r(t)$ (a justification of this result follows shortly)

$$u_r(t) = \underbrace{-\left(C \cdot (A - B \cdot K)^{-1} \cdot B\right)^{-1}}_{\Gamma} \cdot r(t) \tag{5.48}$$

The feedforward matrix Γ is guaranteed to exist if the transfer function $P(s)$ of the open-loop system

$$P(s) = C \cdot (s \cdot I - A)^{-1} \cdot B \tag{5.49}$$

has no zeroes in the origin (see [15] for a proof of this assertion).

Quick Check 5.5.3: Assume that the system Equation (5.45) is a SISO system. Give an intuitive explanation of this condition. ⌟

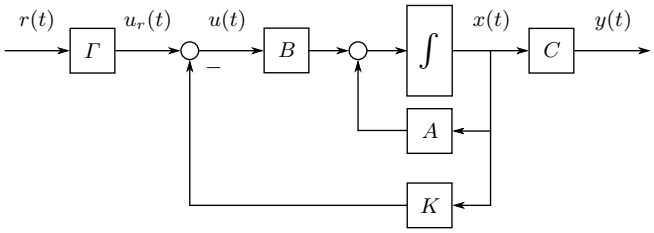

Figure 5.8: Extended LQR control system with output reference signal $r(t)$ defined in Equation (5.46).

With Figure 5.8, the matrix Γ can be derived using the transfer function from $r(t)$ to $y(t)$ and using the final-value theorem of the Laplace transformation [11]

$$\lim_{t\to\infty} y(t) = \lim_{s\to 0} s \cdot C \cdot (s\,I - (A - B \cdot K))^{-1} \cdot B \cdot \Gamma \cdot R(s) \tag{5.50}$$

$$= \lim_{s\to 0} s \ \cdot C \cdot (s\,I - (A - B \cdot K))^{-1} \cdot B \cdot \Gamma \cdot r_\infty \cdot \frac{1}{s} \tag{5.51}$$

$$= C \cdot (-A + B \cdot K)^{-1} \cdot B \cdot \Gamma \cdot r_\infty \tag{5.52}$$

As a consequence, for $\lim_{t\to\infty} y(t) = y_\infty$ to be equal to r_∞ the matrix Γ must satisfy the equation[10]

$$\Gamma = -\left(C \cdot (A - B \cdot K)^{-1} \cdot B\right)^{-1} \tag{5.53}$$

as announced in Equation (5.48).

Note that the motivation behind this feedforward structure is identical to the full state reference tracking scheme discussed in Subsection 5.5.1. Both schemes control the system to an equilibrium state x_∞ using an additional constant input signal. They are therefore a different implementation of the same idea. As a result, the system shown in Figure 5.8 asymptotically converges to the reference signal $r(t)$ as defined in Equation (5.46). In the standard LQR control case this corresponds to the system state asymptotically converging to zero.

5.5.3 Rejection of Constant Disturbances - LQRI Controllers

In the standard LQR formulation discussed in Section 5.2, no integral action is present in the controller. Therefore, disturbances in the control loop are not rejected completely. Any systematic approach to remedy this situation using the LQR design method uses the idea to extend the system.

The extended system consists of the real system itself plus additional elements at its input or at its output that provide integral action. The standard LQR scheme is then applied to the extended system resulting in a linear feedback of both the original system states $x(t)$ and the additional integrator states $v(t)$. In the final implementation of the resulting controller, which is referred to as LQRI controller, the integrator states are included into the controller, enabling integral control action. In this text, this procedure is illustrated by extending the system with integral action at its output.

Figure 5.9 illustrates the extended system description. The m error signals $e(t) = r(t) - y(t)$ are fed into m integrators whose output can be constant iff $e(t) = 0$, i.e., iff all of the output errors are zero.

[10] Using the fact that $(-M)^{-1} = -(M^{-1})$.

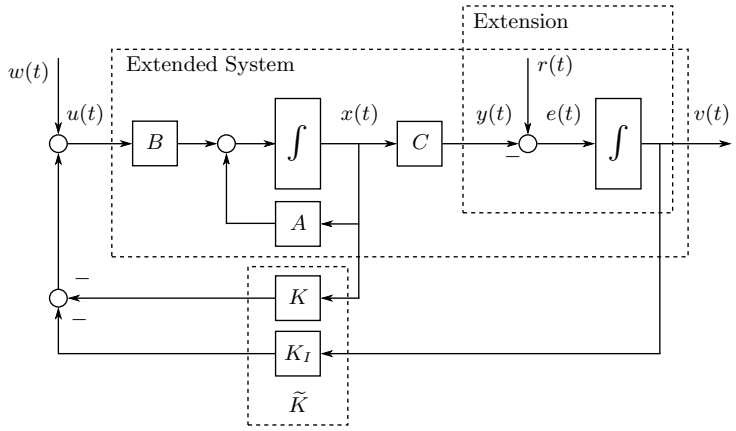

Figure 5.9: LQRI controller structure with individual parts highlighted: the extension, the extended system and the linear feedback gain $\widetilde{K}$ for the extended system.

The extended system can be represented using the extended state vector

$$\widetilde{x}(t) = \begin{bmatrix} x(t) \\ v(t) \end{bmatrix} \in \mathbb{R}^{n+m} \tag{5.54}$$

The dynamics of the extended system are described by

$$\frac{\mathrm{d}}{\mathrm{d}t}\tilde{x}(t) = \begin{bmatrix} A \cdot x(t) + B \cdot (u(t) + w(t)) \\ r(t) - y(t) \end{bmatrix} \tag{5.55}$$

$$= \begin{bmatrix} A & 0 \\ -C & 0 \end{bmatrix} \cdot \begin{bmatrix} x(t) \\ v(t) \end{bmatrix} + \begin{bmatrix} B \\ 0 \end{bmatrix} \cdot (u(t) + w(t)) + \begin{bmatrix} 0 \\ I \end{bmatrix} \cdot r(t) \tag{5.56}$$

$$= \widetilde{A} \cdot \widetilde{x}(t) + \widetilde{B}_u \cdot u(t) + \widetilde{B}_r \cdot r(t) + \widetilde{B}_u \cdot w(t) \tag{5.57}$$

with the following definitions that will be used below

$$\widetilde{A} = \begin{bmatrix} A & 0 \\ -C & 0 \end{bmatrix}, \quad \widetilde{B}_u = \begin{bmatrix} B \\ 0 \end{bmatrix}, \quad \widetilde{B}_r = \begin{bmatrix} 0 \\ I \end{bmatrix} \tag{5.58}$$

The standard LQR controller design method can now be applied to the extended system. With the system matrices $\widetilde{A}$ and $\widetilde{B}_u$ and the weighting matrix $\widetilde{Q}$ the optimal state-feedback gain matrix $\widetilde{K}$ can be computed using the approach[11] introduced in Section 5.3. A possible choice for the extended the weighting matrix $\widetilde{Q}$ has the following form

[11] The matrix $R = r \cdot I$ with $r \in \mathbb{R}_+$ remains unchanged.

$$\widetilde{Q} = \begin{bmatrix} Q & 0 \\ 0 & Q_I \end{bmatrix}, \quad \text{with} \quad Q_I = \begin{bmatrix} \gamma_1 & 0 & \dots & 0 \\ 0 & \gamma_2 & \dots & 0 \\ \vdots & \vdots & \ddots & \vdots \\ 0 & 0 & \dots & \gamma_m \end{bmatrix}$$

The matrix Q_I, allows to adjust the amount of integral action applied to each control error e_i using the real-valued scalars $\gamma_i > 0$, which are, therefore, additional tuning parameters.

Using Matlab notation the solution to the LQRI problem is given by

```
K_tilde = lqr(A_tilde,B_u_tilde,Q_tilde,r*eye(m,m))
```
(5.59)

The feedback gain matrix $\widetilde{K}$ can be partitioned into two distinct submatrices. The first submatrix $K \in \mathbb{R}^{m \times n}$ is the feedback gain for the system states $x(t)$, while the second submatrix $K_I \in \mathbb{R}^{m \times m}$ is the feedback gain for the integrator states $v(t)$.

$$\widetilde{K} = \begin{bmatrix} K, & K_I \end{bmatrix}, \quad K \in \mathbb{R}^{m \times n}, \quad K_I \in \mathbb{R}^{m \times m} \tag{5.60}$$

When implementing this controller, one has to keep in mind that the real system does not contain the integrator states $v(t)$ introduced in Figure 5.9 . Therefore, those states have to be included in the controller. The blocks in Figure 5.9 can be rearranged as illustrated in Figure 5.10. Arranged this way, the integral control action that guarantees a zero steady-state error is well visible.

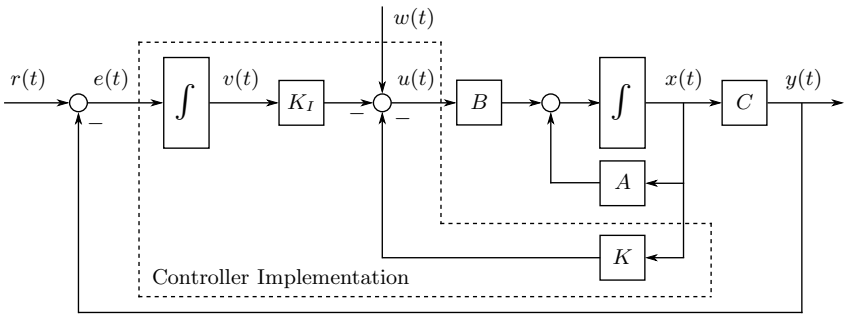

Figure 5.10: LQRI controller structure rearranged. The shaded area represents the controller to be implemented.

If there are no disturbances acting on the control loop and if the reference signal is $r = 0$, the extended control system forces all states $x(t)$ and $v(t)$ to zero. If there are some constant disturbances anywhere in the control loop or if the reference signal is nonzero, the integral action still guarantees that $\lim_{t\to\infty} e(t) = 0$.

Quick Check 5.5.4: Show that the dynamics $\frac{\mathrm{d}}{\mathrm{d}t}\widetilde{x}(t)$ of the extended state defined in Equation (5.55) are identical for both representations in Figures 5.9 and 5.10. ⌟

Combined Reference Tracking and Disturbance Rejection

The integral control action of the LQRI controller not only rejects constant disturbances, but it also guarantees a zero steady-state error when constant non-zero reference values are imposed, i.e., $\lim_{t\to\infty} y(t) = r_\infty$. Therefore, one might be tempted to utilize it for reference tracking as well. However, the reference tracking performance can be improved substantially by using feedforward control action. This is justified by the fact that a feedback controller requires some error to be present in the first place before it can take any corrective actions, while a feedforward controller can act immediately when the step change in the reference value occurs. Since the structure of such a two-degree of freedom controller and the calculation of the feedforward and feedback gains are straightforward, its use is recommended strongly.

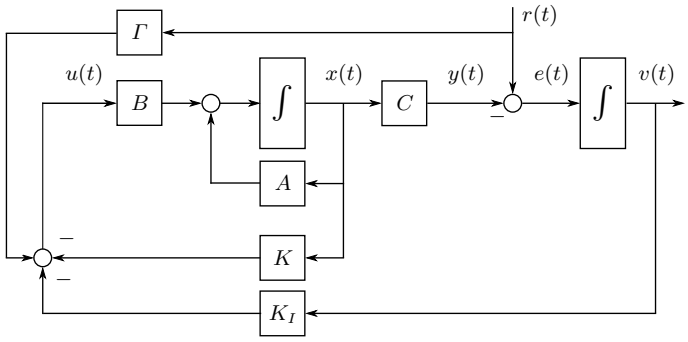

Figure 5.11: LQRI controller structure including the reference feedforward gain Γ.

Figure 5.11 shows how to combine both extensions (integral action and feedforward control) introduced above. The gain Γ is defined in Equation (5.48) and the gains K and K_I in Equation (5.60). Note that the state vector $v(t)$ consisting of the m integrator states is not part of the real plant and must therefore be implemented in the control system.

The control system illustrated in Figure 5.11 is essentially a PID^{n-1} controller with feedforward action. The system output $y(t)$ is a linear combination of the states and potentially their $(n-1)$-th integrals. Therefore, the states $x(t)$ that are fed back are related to the system output itself (P-part of the controller) and to its derivatives, up to the $(n-1)$-th order (D^{n-1}-part of the controller). The I-part of the controller is due to the feedback of the integrated control error.

As with all controllers with integral part, anti reset windup and bumpless transfer between manual and automatic operation are important issues when realizing such controllers. Interested readers are referred to [11] for a first discussion of these issues and indications to further reading.

5.6 Finite Horizon LQR

So far, only constant reference signals have been discussed. If time-varying reference signals are present and if these signals are known at the outset, then more general optimal control methods exist that produce better results. In Subsection 5.6.1 a brief summary of these ideas is given for linear systems. Students interested in a more detailed discussion are referred to subsequent lectures or, e.g., to the text [1]. As a preparation for the discussion of time-varying reference signals, in this section the *finite-horizon* LQR case is analyzed first.

In the finite-horizon formulation, the optimization is accomplished over a finite time interval $t \in [t_a, t_b]$. Since the solution to this finite horizon LQR problem is time-dependent, the system description can be assumed to be time-dependent as well. In this case, Equations (5.1) and (5.2) can be generalized as follows

$$\frac{\mathrm{d}}{\mathrm{d}t}x(t) = A(t)\cdot x(t) + B(t)\cdot u(t), \quad x(t)\in\mathbb{R}^n,\ u(t)\in\mathbb{R}^m, \quad x(t_a) = x_a \tag{5.61}$$

$$J(u) = x^{\mathrm{T}}(t_b)\cdot P\cdot x(t_b) + \int_{t_a}^{t_b} \left(x^{\mathrm{T}}(u(t))\cdot Q(t)\cdot x(u(t)) + u^{\mathrm{T}}(t)\cdot R(t)\cdot u(t)\right)\mathrm{d}t \tag{5.62}$$

where $P\in\mathbb{R}^{n\times n}$ and[12] $P = P^{\mathrm{T}} \geq 0$ penalizes deviations of the final state from the origin (in contrast to the infinite-horizon case, one cannot assume anymore the final state to be zero).

The feedback law in Equation (5.9) now has the form

$$u(t) = -K(t)\cdot x(t), \quad \text{where} \quad K(t) = R^{-1}(t)\cdot B^{\mathrm{T}}(t)\cdot \Phi(t) \tag{5.63}$$

[12] The other matrices $\{A(t), B(t), Q(t), R(t)\}$ for all $t\in[t_a, t_b]$ have the same dimensions as those defined in Equations (5.1) and (5.4).

The matrix $\Phi(t)$ is the solution of the differential matrix Riccati equation

$$\frac{\mathrm{d}}{\mathrm{d}t}\Phi(t) = \Phi(t)\cdot B(t)\cdot R^{-1}(t)\cdot B^{\mathrm{T}}(t)\cdot\Phi(t) - \Phi(t)\cdot A(t) - A^{\mathrm{T}}(t)\cdot\Phi(t) - Q(t) \quad (5.64)$$

with the *final* condition

$$\Phi(t_b) = P \quad (5.65)$$

As in the time-invariant case, $\Phi(t) = \Phi^{\mathrm{T}}(t)$ by construction. The solution of Equation (5.64) is obtained by integrating backwards that differential equation, starting with the final condition in Equation (5.65). Any numerical solver can be used to accomplish this task. The matrix $K(t)$ is then stored in an appropriate memory device. During the interval $t \in [t_a, t_b]$, the corresponding values are retrieved from that memory[13] as illustrated in Figure 5.12.

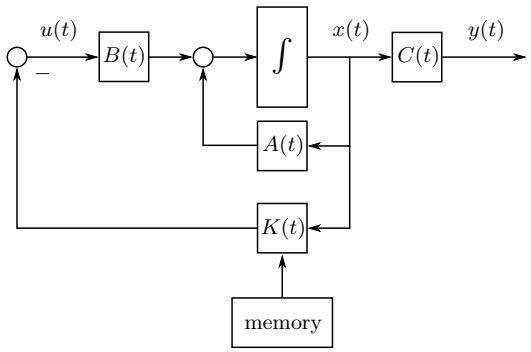

Figure 5.12: Block diagram of a time-varying LQR control system.

Notice that it is possible to realize the control system without the "memory" block by computing the solution to Equation (5.64) "online," i.e., starting at $t = t_a$ and continuously computing the solution $K(t)$ by forward integration of Equation (5.64). However, this is not recommended because the initial condition $K(t_a)$ must be computed a priori by backward integration of Equation (5.64) and because the matrix equation in Equation (5.64) is unstable in the forward direction. Small errors in the initial condition, therefore, will grow and render the numerical results useless.

Caveat: The system in Equation (5.61) is linear, but many of the results available for time-invariant linear systems do not hold in the time-variant case! For instance, the stability of the system in Equation (5.61) cannot be verified by any of the known approaches (Nyquist or Hurwitz criterion, eigenvalue location, etc.). The closed-loop system resulting from the combination of

[13] Some sort of interpolation is usually necessary.

Equations (5.61) and (5.63), for instance, is not guaranteed to be asymptotically stable. The control signal in Equation (5.63) just optimizes the objective function Equation (5.62) over the finite time interval $t \in [t_a, t_b]$.

5.6.1 LQR Feedforward Control Systems

In this problem setting, in the interval $[t_a, t_b]$ the output $y(t)$, defined by

$$y(t) = C(t) \cdot x(t) \tag{5.66}$$

of the system in Equation (5.61) should follow a *known* reference signal $r(t)$ as closely as possible without requiring too much control energy. This somewhat fuzzy problem formulation is rendered precise by introducing the objective function

$$\begin{aligned} J(u) =& (r(t_b) - y(t_b))^{\mathrm{T}} \cdot P \cdot (r(t_b) - y(t_b)) \\ &+ \int_{t_a}^{t_b} \left((r(t) - y(t))^{\mathrm{T}} \cdot Q(t) \cdot (r(t) - y(t)) + u^{\mathrm{T}}(t) \cdot R(t) \cdot u(t) \right) \mathrm{d}t \end{aligned} \tag{5.67}$$

that has to be minimized. In this formulation, all weights are symmetric and have the same dimension P, $Q(t)$, $R(t) \in \mathbb{R}^{m \times m}$. For the sake of simplicity, they are all assumed to be positive-definite.

The control signal $u(t)$ that minimizes this objective function is a combination of a feedback and a feedforward signal (two degrees of freedom, or 2-DOF controller)

$$u(t) = -K(t) \cdot x(t) + u_r(t) \tag{5.68}$$

Similarly to the feedback-only case, the optimal feedback gain $K(t)$ is defined by

$$K(t) = R^{-1}(t) \cdot B^{\mathrm{T}}(t) \cdot \Phi(t) \tag{5.69}$$

where the matrix $\Phi(t)$ is the solution of the differential Riccati equation

$$\frac{\mathrm{d}}{\mathrm{d}t}\Phi(t) = \Phi(t)\, B(t)\, R^{-1}(t)\, B^{\mathrm{T}}(t)\, \Phi(t) - \Phi(t)\, A(t) - A^{\mathrm{T}}(t)\, \Phi(t) - C^{\mathrm{T}}(t)\, Q(t)\, C(t) \tag{5.70}$$

Compared to Equation (5.64), only the last summand is different. As in the time-varying LQR case, the solution $\Phi(t)$ is obtained by backward integration of Equation (5.70) starting with the final condition

$$\Phi(t_b) = C^{\mathrm{T}}(t_b) \cdot P \cdot C(t_b) \tag{5.71}$$

The feedforward signal $u_r(t)$ in Equation (5.68) is formed with the help of an adjoint system

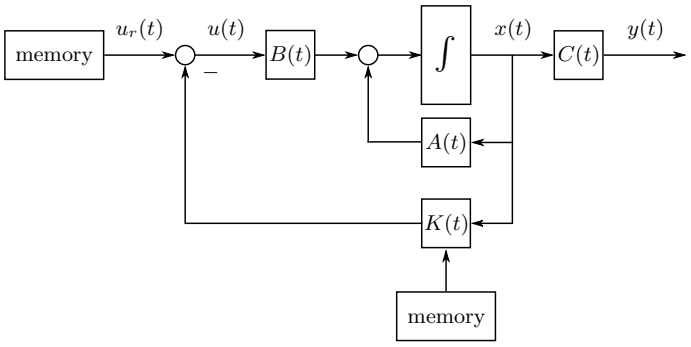

Figure 5.13: Feedforward and feedback LQR control system.

$$\frac{\mathrm{d}}{\mathrm{d}t}z(t) = -\left(A(t) - B(t)\cdot R^{-1}(t)\cdot B^{\mathrm{T}}(t)\cdot \Phi(t)\right)^{\mathrm{T}}\cdot z(t) - C^{\mathrm{T}}(t)\cdot Q(t)\cdot r(t) \tag{5.72}$$

whose final condition is defined by

$$z(t_b) = C^{\mathrm{T}}(t_b)\cdot P\cdot r(t_b) \tag{5.73}$$

It is important to emphasize that the reference signal $r(t)$ is the *same* signal that is used in Equation (5.67), i.e., the reference signal $r(t)$ must be known a priori. As for the solution of the Riccati Equation in Equation (5.70), Equation (5.72) must be solved by integrating backwards starting at the final condition. The feedforward signal $u_r(t)$ can then be formed as follows

$$u_r(t) = R^{-1}(t)\cdot B^{\mathrm{T}}(t)\cdot z(t) \tag{5.74}$$

Both the matrix $K(t)$ in Equation (5.69) and the vector signal $u_r(t)$ in Equation (5.74) must be computed "off line" before[14] the transient occurs and must then be stored in appropriate memory devices. Figure 5.13 illustrates this concept by showing a block diagram of such a 2-DOF control system.

[14] This makes this control system non-causal. The resulting control input, in general, will start to act on the system before any changes in the reference signal are visible, because that preemptive action minimizes the objective function Equation (5.67).

6

State Observer

6.1 Introduction

State-feedback controllers as discussed in the previous chapter cannot be realized in practice because only the plant output $y(t)$ and the plant input $u(t)$ are available for further processing in control algorithms. Nevertheless, the state-feedback approach is very powerful when combined with a filter (the *observer*) that is able to produce an *estimate* $\hat{x}(t)$ of the plant's true state variables $x(t)$, using only the plant's input and output signals. Figure 6.1 illustrates the concept of all observer-based output-feedback control loops. The closed-loop behavior of such systems is analyzed in Chapter 7. In this chapter, the structure and the design of the observer itself are discussed.

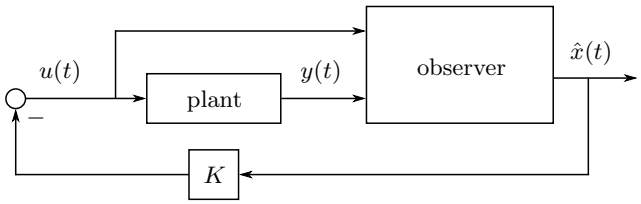

Figure 6.1: Block diagram of an observer-based output-feedback controller.

In the main part of this chapter, in Sections 6.2 to 6.4, it is assumed that none of the measured signals are contaminated by noise. The observer derived under these conditions is referred to as *Luenberger observer*. It is designed using the LQR methodology by reformulating the corresponding problem setting. In this case, the design weights used in the corresponding Riccati equations are arbitrary parameters that have to be chosen by the designer.

The second part of the chapter, Section 6.5, briefly treats the case in which the measured signals are contaminated by some noise. The resulting observer is referred to as *Kalman filter* and its general structure is identical to that of the Luenberger observer. Furthermore, similar to the Luenberger observer design process, the LQR methodology is used to design the Kalman filter. In the Kalman filter case, however, the design weights used in the corresponding Riccati equations are defined by specific statistical properties of the noise signals.

6.2 Problem Formulation

For a given a linear system

$$\begin{aligned} \frac{\mathrm{d}}{\mathrm{d}t}x(t) &= A \cdot x(t) + B \cdot u(t) \\ y(t) &= C \cdot x(t) \end{aligned} \tag{6.1}$$

and without access to the state vector $x(t)$, a linear full state observer[1] is used to get an estimate $\hat{x}(t)$ of the state vector $x(t)$.

The observer has access to all available signals which are the system input $u(t)$, the system output $y(t)$ and the current estimate $\hat{x}(t)$ of the system state $x(t)$. The dynamics of the observer are

$$\frac{\mathrm{d}}{\mathrm{d}t}\hat{x}(t) = F \cdot \hat{x}(t) + H \cdot u(t) + L \cdot y(t) \tag{6.2}$$

The matrices F, L, and H are yet undefined constant matrices.

The system in Equation (6.2) is defined to be a suitable observer for the system in Equation (6.1) if it fulfills two conditions:

c1 If the initial state estimate is perfect, i.e., $\hat{x}(0) = x(0)$, then the observer should estimate the future state perfectly, i.e., for all $u(t)$ and all $t > 0$ the estimation $\hat{x}(t)$ is equal to the system state $x(t)$.

c2 If the initial estimate is not perfect, i.e., if $\hat{x}(0) \neq x(0)$, then the observed state $\hat{x}(t)$ should asymptotically converge to the real system state $x(t)$, i.e., $\lim_{t\to\infty} \hat{x}(t) = x(t)$.

[1] Reduced-order observers that only reconstruct those parts of the state vector $x(t)$ that are not measured or nonlinear observers are also known, but not discussed here. For more details on the former see e.g. [15], and [14] on the latter.

6.3 Solution: Output Injection

Observer Structure

The block diagram of the linear full state observer is depicted in Figure 6.2. The key element is the output injection through the matrix L which allows the conditions c1 and c2 from above to be fulfilled. This particular observer structure is referred to as a *Luenberger observer* as introduced in [16].

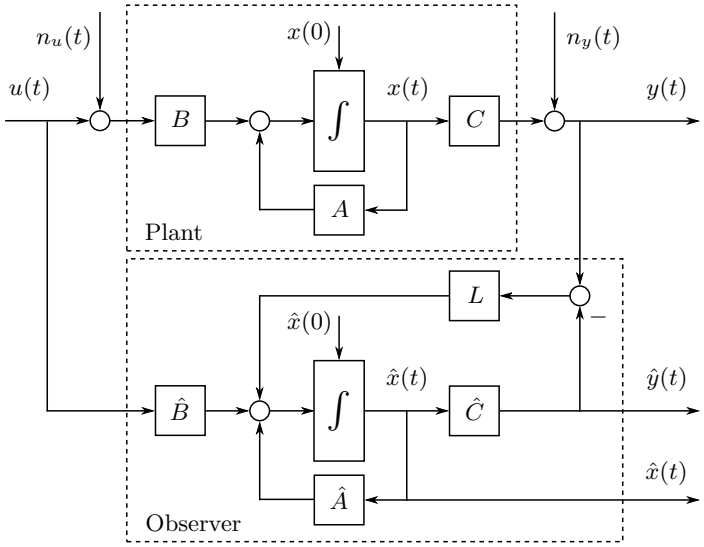

Figure 6.2: Block diagram of a Luenberger observer.

Quick Check 6.3.1: As Figure 6.2 shows, the signal $L{\cdot}(y(t){-}\hat{y}(t))$ is "injected" just in front of the integrator block. Explain why it is not possible to inject a signal at the same place in the plant. Explain why this is possible in the observer. ⌟

Observer Dynamics

The following derivation of the Luenberger observer structure in Figure 6.2 is based on the assumption that the observer matrices perfectly match the plant matrices, i.e., $\hat{A} = A$, $\hat{B} = B$, $\hat{C} = C$. Of course, this is usually not the case due to modeling and parameter identification errors. In the observer-based state-feedback controller design presented in Chapter 7, modeling errors will be accounted for by appropriate robustness margins. In addition the noise

signals $n_u(t)$ and $n_y(t)$ are assumed to be zero in this first analysis. The influence of such noise signals is briefly discussed at the end of this section and in Section 6.5.

The derivation also requires the definition of the state estimation error $x_\mathrm{e}(t)$ and its time derivative $\frac{\mathrm{d}}{\mathrm{d}t}x_\mathrm{e}(t)$.

$$x_\mathrm{e}(t) = x(t) - \hat{x}(t) \tag{6.3}$$

$$\frac{\mathrm{d}}{\mathrm{d}t}x_\mathrm{e}(t) = \frac{\mathrm{d}}{\mathrm{d}t}x(t) - \frac{\mathrm{d}}{\mathrm{d}t}\hat{x}(t) \tag{6.4}$$

Condition c1 requires that, if the initial state $x(0)$ is perfectly known, the time derivative of the resulting state estimation error in Equation (6.4) must be zero. Using Equations (6.1) and (6.2), this can be formulated as

$$\begin{aligned}\frac{\mathrm{d}}{\mathrm{d}t}x_\mathrm{e}(t) \stackrel{!}{=} 0 &= A \cdot x(t) + B \cdot u(t) - F \cdot \hat{x}(t) - H \cdot u(t) - L \cdot y(t) \\ &= A \cdot x(t) + B \cdot u(t) - F \cdot \hat{x}(t) - H \cdot u(t) - L \cdot C \cdot x(t) \\ &= (A - L \cdot C) \cdot x(t) - F \cdot \hat{x}(t) + (B - H) \cdot u(t) \\ &= ((A - L \cdot C) - F) \cdot x(t) + (B - H) \cdot u(t)\end{aligned} \tag{6.5}$$

In the last step, the state estimate $\hat{x}(t)$ was replaced with the real state $x(t)$ as required by condition c1. This equation must be true for arbitrary $x(t)$ and $u(t)$, which requires that

$$H = B \tag{6.6}$$

$$F = A - L \cdot C \tag{6.7}$$

The observer gain matrix L is an as yet undefined matrix with appropriate dimensions and constant entries. It will be used below to satisfy condition c2.

Condition c2 requires that the state estimation error $x_\mathrm{e}(t)$ asymptotically converges to zero for all initial conditions $x_\mathrm{e}(0) = x(0) - \hat{x}(0) \neq 0$. Using Equations (6.6) and (6.7), the dynamics of the estimation error result as

$$\begin{aligned}\frac{\mathrm{d}}{\mathrm{d}t}x_\mathrm{e}(t) &= A \cdot x(t) + B \cdot u(t) - F \cdot \hat{x}(t) - H \cdot u(t) - L \cdot y(t) \\ &= A \cdot x(t) + B \cdot u(t) - (A - L \cdot C) \cdot \hat{x}(t) - B \cdot u(t) - L \cdot C \cdot x(t) \\ &= A \cdot (x(t) - \hat{x}(t)) - L \cdot C \cdot (x(t) - \hat{x}(t)) \\ &= (A - L \cdot C) \cdot x_\mathrm{e}(t)\end{aligned} \tag{6.8}$$

As shown in Equation (6.8), if the replacements in Equations (6.6) and (6.7) are made, the estimation error follows the dynamics of an autonomous linear system. The required asymptotic estimation error convergence can therefore be guaranteed if the system matrix $A - L \cdot C$ is Hurwitz. The speed of this convergence is determined by the observer gain L.

6.4 Observer Gain Design

The ideas of the LQR design approach can be applied to find a suitable observer gain L as well. The application of the LQR scheme is very convenient and, moreover, as will be shown in Chapter 8, there is a structural benefit in the design process when later using the resulting observer in an observer-based state-feedback controller.

The starting point is the observation that the requirements for the observer dynamics $A - L \cdot C$ are identical to the ones for the state-feedback-controlled system dynamics $A - B \cdot K$. Both matrices are required to be Hurwitz and their structure is very similar, with only the roles of B and C interchanged. Transposing the system matrix of the estimation error dynamics produces

$$(A - L \cdot C)^{\mathrm{T}} = A^{\mathrm{T}} - C^{\mathrm{T}} \cdot L^{\mathrm{T}} \tag{6.9}$$

which corresponds exactly to the standard LQR problem formulation. Accordingly, this *dual problem setting* is equivalent to the LQR problem setting, provided the following replacements are made

$$\begin{aligned} A &\rightarrow A^{\mathrm{T}} \\ B &\rightarrow C^{\mathrm{T}} \\ Q = \bar{C}^{\mathrm{T}} \cdot \bar{C} &\rightarrow \bar{B} \cdot \bar{B}^{\mathrm{T}} \\ R = r \cdot I &\rightarrow q \cdot I \end{aligned} \tag{6.10}$$

where the matrix $\bar{B}$ is a chosen fictitious input matrix.[2] Using these correspondences, the same algorithms used to solve the standard LQR problem may be re-used to find a stabilizing observer gain L

$$L^{\mathrm{T}} = \frac{1}{q} \cdot C \cdot \Psi \tag{6.11}$$

If the pair $\{A, C\}$ is completely observable and the pair $\{A, \bar{B}\}$ is completely controllable, the matrix $\Psi = \Psi^{\mathrm{T}}$ is the only positive-definite solution of the following dual matrix Riccati equation

$$\frac{1}{q} \cdot \Psi \cdot C^{\mathrm{T}} \cdot C \cdot \Psi - \Psi \cdot A^{\mathrm{T}} - A \cdot \Psi - \bar{B} \cdot \bar{B}^{\mathrm{T}} = 0 \tag{6.12}$$

As in the standard problem, less restrictive conditions are necessary for the existence of a stabilizing solution Ψ.

[2] The matrix $\bar{B}$ can be chosen equal to the plant input matrix B, but this is not the only choice possible. Every $\bar{B}$ that makes the pair $\{A, \bar{B}\}$ completely controllable is, in principle, a valid choice.

To find the solution to this dual problem with Matlab, the command

```
L=lqr(A',C',B_bar*B_bar',q*eye(m,m))'
```

can be used.

Remark: One might be tempted to choose the eigenvalues of $A - L \cdot C$ significantly "faster"[3] than those of A (or later $A - B \cdot K$) in order to achieve a rapid convergence of the observed state $\hat{x}(t)$ to the true state $x(t)$. However, two unavoidable complications impose limitations:

- The observer is synthesized using an estimation $\{\hat{A}, \hat{B}, \hat{C}\}$ of the true system matrices $\{A, B, C\}$. Of course these matrices, in general, will be different. These and other modeling errors impose limits on the loop gain $L_{\mathrm{LQG}}(s)$ of the resulting control system as defined in Equation (7.7).
- As indicated Figure 6.2, the input signals to the observer will always be corrupted by some noise, i.e., $n_u(t) \neq 0$ and $n_y(t) \neq 0$. This fact imposes limits on the estimation error dynamics in Equation (6.8) as well.

The consequences of the first limitation will be analyzed in Chapter 7, while the limitations introduced by the noise are discussed below and in the next section.

Limitation due to Noise

Assuming $n_u(t) = 0$, but $n_y(t) \neq 0$, the dynamics of the state estimation error in Equation (6.8) have the form

$$\frac{\mathrm{d}}{\mathrm{d}t} x_{\mathrm{e}}(t) = (A - L \cdot C) \cdot x_{\mathrm{e}}(t) - L \cdot n_y(t) \tag{6.13}$$

The gain L has to satisfy two contradicting objectives:

- It should be chosen as large as possible, to increase the bandwidth of the error dynamics, i.e., to increase the speed with which initial state estimation errors $x_{\mathrm{e}}(0)$ converge to zero.
- It should also be chosen sufficiently small in order not to excite the observation-error dynamics by amplifying the measurement noise $n_y(t)$ that is fed back into the observer.

These contradictory requirements are best illustrated in an example. Figure 6.3 shows the transient behavior of the observation error of a third-order system, once without noise (upper plots) and once with noise (lower plots),

[3] In this context, "faster" means the real parts of the eigenvalues are smaller, i.e., more negative.

and once for a "slow" observer (left plots) and once for a "fast" observer (right plots). Clearly, without noise the "fast" observer performs better than the slow one (the estimation errors $x_{\mathrm{e,i}}(t)$ converge to zero faster), but much poorer when the unavoidable noise signals are included.

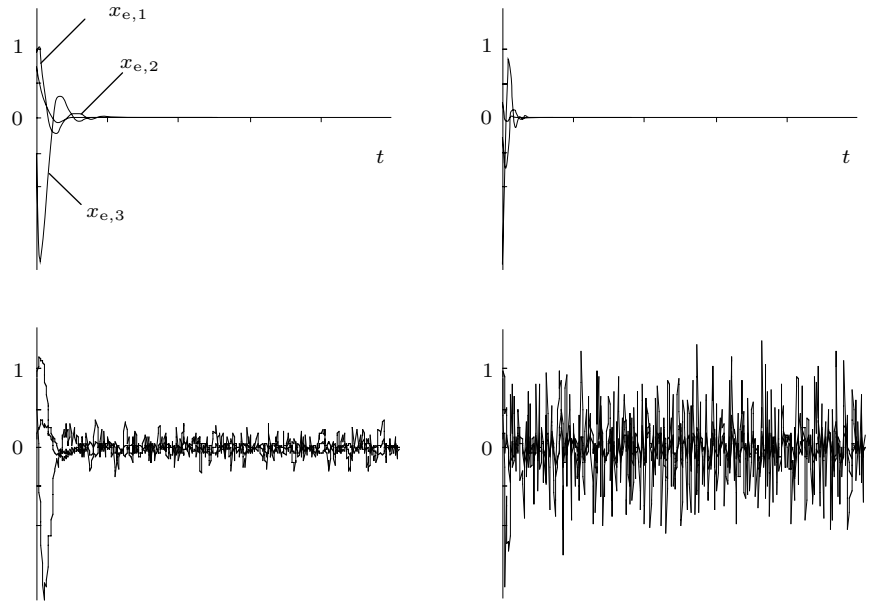

Figure 6.3: Transient behavior of the error dynamics of a third-order example. Left two plots: "slow" error dynamics, right two plots: "fast" error dynamics. Top two plots: no noise, bottom two plots: with noise.

If no information on the stochastic properties of the noise signals is available, the gain L must be found iteratively as the best compromise between fast error dynamics and acceptable noise amplifications. A rule of thumb is to choose the eigenvalues of $A - L \cdot C$ approximately three times "faster" than those of A (or $A - B \cdot K$, if the observer is to be used in an output-feedback loop).

6.5 Kalman Filters

In the absence of noise and with access to the exact system matrices $\{A, B, C\}$, the observer estimates the true system state perfectly, i.e., $\lim_{t\to\infty} \hat{x}(t) = x(t)$. If the noise signals $n_u(t)$ and $n_y(t)$ in Figure 6.2 are non-zero, the state estimation will always be influenced by that noise and the estimation error can not be brought to and kept at zero. However, if the noise signals are Gaussian zero-mean white noise signals and if their statistical properties are known, the variance of the observation error can be minimized. Moreover, in the limit $\lim_{t\to\infty}$, the mean value of $\hat{x}(t)$ corresponds to the expected value of $x(t)$. The resulting state estimator, a Kalman filter, has the same structure as the observer presented in Figure 6.2 and the corresponding observer gain L can be calculated using the LQR algorithms as well.

The theory of Kalman filtering forms the cornerstone of many powerful signal processing algorithms. One of its main advantages is that it offers a straightforward solution to the problem of *sensor fusion*, in which the information provided by several sensors measuring different physical variables are to be combined in a meaningful way.

A complete treatment of Kalman filtering is beyond the scope of this course. In particular a comprehensive analysis is possible only once a stochastic description of all signals and systems is available (interested readers are referred to [9] and [17]). Nevertheless, below a "sneak preview" of the main ideas is given for continuous-time systems.[4]

The plant whose state vector $x(t)$ is to be observed is described, as illustrated in Figure 6.2, by the equations

$$\frac{\mathrm{d}}{\mathrm{d}t}x(t) = A \cdot x(t) + B \cdot (u(t) + n_u(t)) \tag{6.14}$$

$$y_o(t) = C \cdot x(t) + n_y(t) \tag{6.15}$$

In the simplest case, the two noise signals $n_u(t)$ and $n_y(t)$ are uncorrelated zero-mean *white noise* signals. Without entering into the mathematical details of stochastic signals, a zero-mean white noise signal $n(t)$ is defined as a signal whose mean value and *covariance matrix*[5] are given by

$$\mathrm{E}\{n(t)\} = 0, \quad \mathrm{E}\left\{n(t) \cdot n^{\mathrm{T}}(\tau)\right\} = R \cdot \delta(t - \tau) \tag{6.16}$$

where the symbol $\mathrm{E}\{\ldots\}$ denotes the expectation operator, $\delta(\ldots)$ the Dirac function, and $R = R^{\mathrm{T}} \geq 0$ is a constant semi-positive definite real matrix. In

[4] In pratice, Kalman filters are realized using a discrete-time formulation. The main ideas are the same as in the continuos-time case, for more details see [4].

[5] These matrices are also known as auto-covariance matrices. For $t = \tau$ they describe the variance of the associated signals.

order to design a Kalman filter, the magnitudes of the covariance matrices of the two noise signals must be known, i.e., for the covariances

$$\begin{aligned} \mathrm{E}\left\{n_u(t) \cdot n_u^{\mathrm{T}}(\tau)\right\} &= R_u \cdot \delta(t-\tau), \quad R_u \geq 0 \\ \mathrm{E}\left\{n_y(t) \cdot n_y^{\mathrm{T}}(\tau)\right\} &= R_y \cdot \delta(t-\tau), \quad R_y > 0 \end{aligned} \tag{6.17}$$

the matrices $R_u \in \mathbb{R}^{m \times m}$ and $R_y \in \mathbb{R}^{p \times p}$ must be determined a priori, e.g., by a statistical analysis of the corresponding signals.

Once this information is available, a Kalman filter can be designed as follows. Its structure is the same as that of a standard state observer as shown in Figure 6.2. The only difference is that the observation error is fed back using that gain L_{K} that satisfies the following set of equations

$$L_{\mathrm{K}} = \Psi_{\mathrm{K}} \cdot C^{\mathrm{T}} \cdot R_y^{-1} \tag{6.18}$$

where the matrix $\Psi_{\mathrm{K}} = \Psi_{\mathrm{K}}^{\mathrm{T}} \in \mathbb{R}^{n \times n}$ is the only positive definite solution of the Riccati equation

$$\Psi_{\mathrm{K}} \cdot C^{\mathrm{T}} \cdot R_y^{-1} \cdot C \cdot \Psi_{\mathrm{K}} - A \cdot \Psi_{\mathrm{K}} - \Psi_{\mathrm{K}} \cdot A^{\mathrm{T}} - B \cdot R_u \cdot B^{\mathrm{T}} = 0 \tag{6.19}$$

The key point in this case is that the covariance matrices of the noise signals must be used in Equation (6.18) and Equation (6.19). A solution to this equation is guaranteed to exist if the pair $\{A, C\}$ is completely observable.

L_K can be found with Matlab using the command

```
L_K=lqr(A',C',B*R_u*B',R_y)'
```

The resulting filter estimates the state such that the observation error $x_{\mathrm{e}}(t) = x(t) - \hat{x}(t)$ has a mean value that asymptotically approaches zero and has the smallest possible variance.

7

LQG Controller

7.1 Introduction

Combining the full-state observer from Chapter 6 with a state-feedback control law, i.e., replacing Equation (5.9) by

$$u(t) = -K \cdot \hat{x}(t) \tag{7.1}$$

yields an output-feedback control system that can be implemented in practice. Such systems are often referred to as LQG loops.[1] The properties of the resulting open and closed-loop LQG systems are analyzed in this chapter that is organized as follows:

- Sections 7.2 and 7.3: The output of the state observers is used to close the feedback loop based on the state-feedback controller solution. The main properties of the resulting loop are analyzed.
- Section 7.4: The basic output-feedback structure is extended to enable reference tracking and disturbance rejection.
- Section 7.5: A step-by-step tutorial of how to design and implement an LQG controller with reference tracking and disturbance rejection capabilities is presented.

[1] The first two letters have the same meaning as in the LQR acronym and the letter G stands for Gaussian, a reference to the stochastic formulation of the observer design discussed in Section 6.5.

7.2 Standard LQG Controller Structure

The structure of an LQG-controlled system is depicted in Figure 7.1. The only difference in comparison to the standard LQR closed-loop system shown in Figure 5.1 is the addition of the observer which is used to estimate the state $x(t)$ of the plant.

For the discussion of the closed-loop dynamics, the switch is assumed to be closed. If the loop is opened at the shown location, a direct comparison to the LQR open-loop transfer function $L_{\mathrm{LQR}}(s)$ in Equation (5.25) is possible.

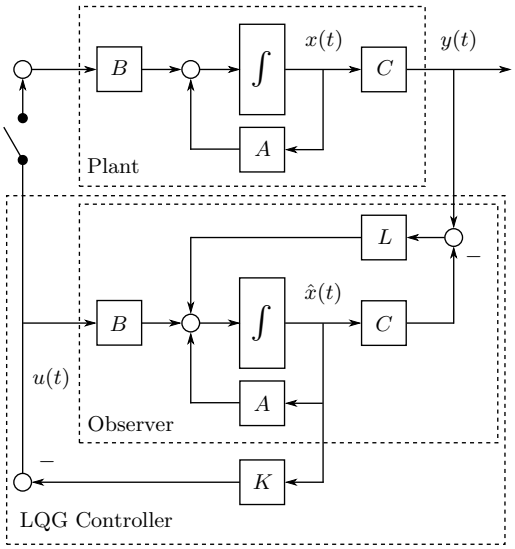

Figure 7.1: Block diagram of a standard LQG controlled system.

The dynamics of the closed-loop LQG controller structure in Figure 7.1 are described by

$$\begin{aligned} \frac{\mathrm{d}}{\mathrm{d}t}x(t) &= A \cdot x(t) - B \cdot K \cdot \hat{x}(t) \\ \frac{\mathrm{d}}{\mathrm{d}t}\hat{x}(t) &= (A - B \cdot K - L \cdot C) \cdot \hat{x}(t) + L \cdot C \cdot x(t) \end{aligned} \tag{7.2}$$

Defining a combined state vector $\widetilde{x}$

$$\widetilde{x}(t) = \begin{bmatrix} x(t) \\ \hat{x}(t) \end{bmatrix} \tag{7.3}$$

the closed-loop dynamics follow the dynamics of an autonomous linear system

$$\frac{\mathrm{d}}{\mathrm{d}t}\widetilde{x}(t) = \underbrace{\begin{bmatrix} A & -B \cdot K \\ L \cdot C & A - B \cdot K - L \cdot C \end{bmatrix}}_{\widetilde{A}_{\mathrm{cl}}} \cdot \widetilde{x}(t) \tag{7.4}$$

7.3 Properties of the Standard LQG Controller Structure

Analogously to the analysis of the properties of the standard LQR control loop in Section 5.4, the stability, robustness, and disturbance rejection properties of the standard LQG loop are analyzed here.

7.3.1 Stability Properties / Separation Principle

The most important fact is that all eigenvalues of the matrix A_{cl} in Equation (7.4) have strictly negative real parts and therefore the LQG closed-loop system is guaranteed to be asymptotically stable.

This assertion is easy to prove if the dynamics in Equation (7.4) are described in different coordinates. Instead of describing the system using the combined state vector $\widetilde{x}(t)$ as defined in Equation (7.4), a different combined state vector $\widetilde{z}(t)$ can be formed using the state vector $x(t)$ and the state estimation error $x_{\mathrm{e}}(t)$ as defined in Equation (6.3). The relevant properties of the system described in both coordinates $\widetilde{x}(t)$ or $\widetilde{z}(t)$ are identical as they are related to each other through a linear linear coordinate transformation

$$\widetilde{z} = \begin{bmatrix} x(t) \\ x_{\mathrm{e}}(t) \end{bmatrix} = \begin{bmatrix} x(t) \\ x(t) - \hat{x}(t) \end{bmatrix} = \begin{bmatrix} I_{n\times n} & 0_{n\times n} \\ I_{n\times n} & -I_{n\times n} \end{bmatrix} \cdot \widetilde{x} = T^{-1} \cdot \widetilde{x}$$

The system in Equation (7.4) expressed in the coordinates $\widetilde{z}$ exhibits the following dynamics

$$\frac{\mathrm{d}}{\mathrm{d}t}\widetilde{z}(t) = T^{-1} \cdot \widetilde{A}_{\mathrm{cl}} \cdot T \cdot \widetilde{z}(t) = \underbrace{\begin{bmatrix} A - B \cdot K & B \cdot K \\ 0_{n\times n} & A - L \cdot C \end{bmatrix}}_{\widetilde{A}_{\mathrm{cl}} \text{ in coordinates } \widetilde{z}} \cdot \widetilde{z}(t) \tag{7.5}$$

Due to the block structure of the system matrix in the coordinates $\widetilde{z}$, the eigenvalues λ_i can now be found directly and correspond to the combination of the eigenvalues of the two diagonal block matrices $A - B \cdot K$ and $A - L \cdot C$

$$\lambda_i(\widetilde{A}_{\mathrm{cl}}) = \lambda_i(T^{-1} \cdot \widetilde{A}_{\mathrm{cl}} \cdot T) = \lambda_i(A - B \cdot K) \ \cup \ \lambda_i(A - L \cdot C) \tag{7.6}$$

The matrix $A - B \cdot K$ corresponds to the system dynamics of the LQR loop and it is guaranteed to be Hurwitz by design. Similarly, the matrix $A - L \cdot C$ corresponds to the observer dynamics which is guaranteed to be Hurwitz as well if the gain L is computed using the dual LQR approach as described in Section 6.4. This conclusion, referred to as the *separation principle*, is very powerful. It implies that the state feedback controller and the full state observer can be designed and tuned independently of each other. As long as both of them are stable on their own, the resulting observer-based state feedback loop is guaranteed to be stable, too.

7.3.2 Robustness Properties

While a significant robustness is guaranteed for any LQR control system, there are no robustness guarantees whatsoever for a LQG control system. This point is briefly verified in this section.

The LQG open-loop transfer function can be compared to the LQR open-loop transfer function $L_{\mathrm{LQR}}(s)$ of Equation (5.25) if the LQG loop is opened at the location of the switch indicated in Figure 7.1. The resulting LQG open-loop transfer function is

$$L_{\mathrm{LQG}}(s) = K \cdot (s\,I - (A - B \cdot K - L \cdot C))^{-1} \cdot L \cdot C \cdot (s\,I - A)^{-1} \cdot B \quad (7.7)$$

The robustness of a LQG control system is expressed as usual using its minimum return difference

$$\mu_{\min,\mathrm{LQG}} = \min_{\omega} \left(\min_{i} \sigma_i \left(I + L_{\mathrm{LQG}}(j\,\omega) \right) \right) \quad (7.8)$$

Unfortunately, simple examples (see e.g. the case study "Levitating Sphere" in Appendix A.2, and in particular Figure A.8) show that $\mu_{\min,\mathrm{LQG}}$ can be arbitrarily close to zero, despite the fact that $\mu_{\min,\mathrm{LQR}} \geq 1$.

Therefore, although the LQG design is guaranteed to yield an asymptotically stable closed-loop system, that loop is not necessarily robust against modeling errors. Without that property, however, no control system is useful in practice. Accordingly, the robustness margins of any LQG design must be checked a posteriori. If these margins are insufficient, they must be improved using approaches such as the ones introduced in Chapter 8.

7.3.3 Disturbance Rejection Properties

As for the standard LQR controller, the standard LQG controller is in general not able to reject constant disturbances. This is to be expected since the only difference to the LQR controller is the fact that the state estimate $\hat{x}(t)$ is used in the feedback loop instead of the actual state $x(t)$. The analysis and conclusions of the disturbance rejection properties are, therefore, directly comparable to the discussion in the LQR case in Subsection 5.4.3.

7.3.4 Conclusion and Further Comments

A control loop designed using the standard LQG procedure yields a closed-loop system that:

1. is guaranteed to be asymptotically stable;
2. has no robustness guarantees;
3. is in general not able to reject disturbances; and
4. can in general not be used for reference tracking.

The first point is very useful, especially considering that the design process is straightforward. Regarding point two, the robustness of the resulting LQG control loop must always be checked a posteriori. If necessary, appropriate design iterations are required that achieve the desired robustness properties. A systematic and straightforward approach is presented in Section 8.2. Points three and four, reference tracking and disturbance rejection capabilities, can be included in the LQG design using the same ideas used for LQR controllers, as will be shown in Section 7.4.

7.4 Reference Tracking and Disturbance Rejection

Controller extensions that add reference tracking and disturbance rejection to the standard LQR controller were introduced and discussed in detail in Subsection 5.5.2. These extensions can be applied in the LQG case exactly as presented in the LQR case.[2] The resulting LQGI controller structure is illustrated in Figure 7.2. Note that, just like in the LQR controller, disturbance rejection and reference tracking can be added independently of each other.

The integral control action of the LQGI controller guarantees a zero steady-state error, i.e., $\lim_{t\to\infty} y(t) = r_\infty$, even in case of constant disturbances anywhere in the control loop and it enables a precise reference tracking as well. However, as discussed above, the reference tracking performance can be improved substantially by using a feedforward channel with gain Γ defined in Equation (5.48), as illustrated in Figure 7.2.

Note that the matrix Γ is not a function of the observer parameters. In the ideal case, the observer matrices $\{\hat{A}, \hat{B}, \hat{C}\}$ are identical to real system matrices $\{A, B, C\}$, which guarantees that $\lim_{t\to\infty} \hat{x}(t) = x(t)$ and, therefore,

[2] Instead of first extending the LQR structure with an observer and then extending the resulting controller to enable reference tracking/disturbance rejection, one can think of it as first adding reference tracking/disturbance rejection to the LQR controller and then introducing an observer.

the observer does not affect the control loop in steady-state. In a realistic case, however, observer and system matrices are not identical and a steady-state control error will remain. To eliminate that error source, therefore, integrating action must be included in practice.

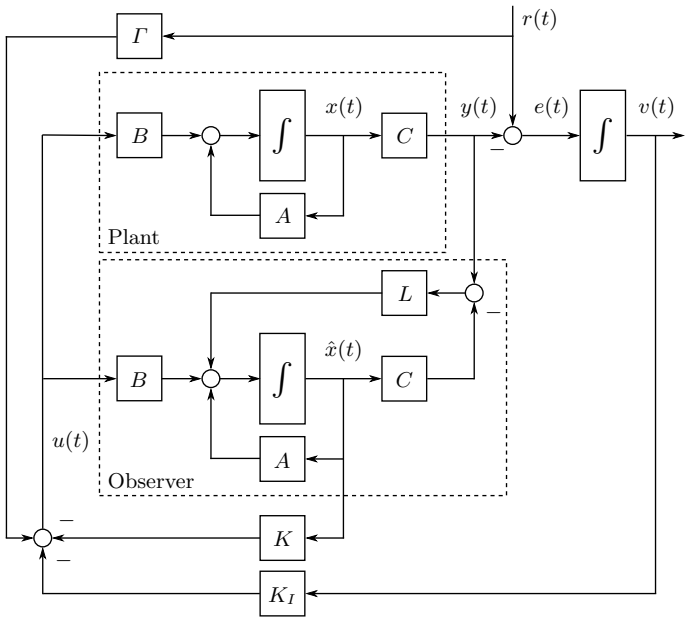

Figure 7.2: Complete system structure of an LQGI controller with feedforward on the reference signal.

7.5 Summary LQGI Controller Design

The complete LQGI controller structure shown in Figure 7.2 is presented again in a rearranged form in Figure 7.3. Using this structure, the feedback and feedforward parts of the controller can easily be identified.

This structure can be helpful or even necessary when implementing the controller in a given feedforward-feedback framework or when analyzing its stability and robustness properties, in which only the feedback part of the controller is relevant. More details can be found in the case studies in Appendix A.

As mentioned above, in a practical realization usually additional modules are needed (anti-reset windup systems, bumpless transfer schemes, etc.) and

the complete control system has to be transformed into a discrete-time equivalent in the (predominant) case that it is realized with the help of digital computers. More on these topics can be found e.e. in [11].

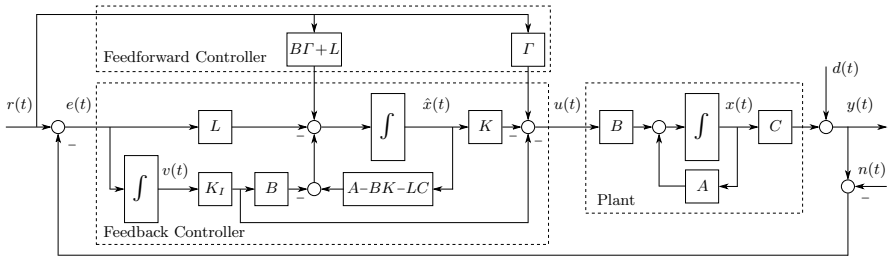

Figure 7.3: LQGI controller with feedforward on the reference signal. Identical to the controller illustrated in Figure 7.2, but with a clear separation of the feedforward and the feedback parts.

In a nutshell, a typical design procedure consists of the following steps:

1. Form the extended system $\{\widetilde{A},\, \widetilde{B},\, \widetilde{C}\}$ following the approach outlined in Subsection 5.5.3.
2. Design a suitable state-feedback control gain $\widetilde{K}$ for the extended system using Equation (5.59):

   ```
   K_tilde=lqr(A_tilde,B_u_tilde,Q_tilde,r*eye(m,m))
   ```

   and decompose it as illustrated in Equation (5.60)

   $$\widetilde{K} = \Big[K, \quad K_I\Big], \quad K \in \mathbb{R}^{m\times n}, \quad K_I \in \mathbb{R}^{m\times m}$$

   Start with simple weights ($R = r \cdot I$, etc.) and iterate on r and γ_i. If that is not sufficient, use more general weights until the desired system behavior is achieved.
3. Design an observer gain L for the original system $\{A,\, B,\, C\}$ using the duality approach introduced in Section 6.4

   ```
   L = lqr(A',C',B*B',q*eye(m,m))'
   ```

4. Calculate the feed-forward matrix Γ using Equation (5.48)

   $$\Gamma = -\left(C \cdot (A - B \cdot K)^{-1} \cdot B\right)^{-1}$$

   and add the feed-forward controller.

In Chapter 8 an additional iteration is introduced in step 2, with which the robustness of the control loop can be improved.

8

Loop Transfer Recovery (LTR)

As Figure A.8 in Appendix A.2 shows, the output-feedback LQG solution has a potential robustness problem. In this section, two iterative procedures are introduced, which can partially recover the excellent robustness properties of LQR loops for output feedback loops that have insufficient robustness margins. The general idea of all *loop-transfer recovery* (LTR) methods can be summarized as follows:

- First design a suitable state-feedback LQR controller that is known to yield "nice" loop gains.
- Set up a design procedure for an output-feedback controller with one iteration parameter (the "LTR gain").
- Increase the LTR gain until the loop gain $L_{\mathrm{LQG}}(s)$ of the output-feedback controller sufficiently approaches the loop gain $L_{\mathrm{LQR}}(s)$ of the state-feedback controller without violating the limits imposed by nonminimumphase zeros, noise and model uncertainty.

The two possible LTR iteration schemes presented below are referred to as *robustness recovery schemes*. Two approaches are discussed in this text:

- A "naive" approach that works only for minimumphase SISO systems, but which shows the main ideas with little mathematical effort.
- A systematic approach that also works for nonminimumphase MIMO systems, but which requires the solution of a series of LQR problems.

Both approaches recover as much as possible the robustness properties of a first LQR design.[1] The control system extensions discussed above (integral action and feedforward) can be used in the LTR framework as well.

[1] If the plant is nonminimumphase, the loop recovery will be limited by the nonminimumphase zeros.

8.1 A "Naive" Robustness Recovery Scheme

The SISO plant to be controlled is described as usual by the equations

$$\frac{\mathrm{d}}{\mathrm{d}t}x(t) = A \cdot x(t) + b \cdot u(t) \ , \qquad y(t) = c \cdot x(t) \tag{8.1}$$

and its transfer function

$$P(s) = c \cdot (s\,I - A)^{-1} \cdot b \ = \ \frac{c \cdot \mathrm{Adj}(sI - A) \cdot b}{\det(sI - A)} \tag{8.2}$$

The plant may be unstable, but it must be minimumphase. If state feedback were feasible, the loop transfer function of the LQR control system would be

$$L_{\mathrm{LQR}}(s) = k \cdot (sI - A)^{-1} \cdot b = \frac{k \cdot \mathrm{Adj}(sI - A) \cdot b}{\det(sI - A)} \tag{8.3}$$

The objective is now to find an *output* feedback controller $C(s)$ such that the resulting loop gain perfectly matches this $L_{\mathrm{LQR}}(s)$

$$C(s) \cdot P(s) = L_{\mathrm{LQR}}(s) \tag{8.4}$$

The straightforward "solution" to this problem is

$$C(s) = \frac{L_{\mathrm{LQR}}(s)}{P(s)} = \frac{k \cdot \mathrm{Adj}(sI - A) \cdot b}{c \cdot \mathrm{Adj}(sI - A) \cdot b} \tag{8.5}$$

This controller cancels the zeros of the plant with its poles[2] and replaces these zeros by the LQR zeros that are known to produce "nice" loop gains.

In general, $C(s)$ as defined in Equation (8.5) is not realizable because the degree $n-1$ of its numerator polynomial $k \cdot \mathrm{Adj}(sI - A) \cdot b$ exceeds the degree m of its denominator polynomial $c \cdot \mathrm{Adj}(sI - A) \cdot b$.[3] One solution to this problem is to combine $C(s)$ with a sufficient number of first-order lags with equal time constant τ

$$C(s) = \frac{k \cdot \mathrm{Adj}(sI - A) \cdot b}{c \cdot \mathrm{Adj}(sI - A) \cdot b \cdot (\tau s + 1)^{\kappa}} \tag{8.6}$$

The time constant τ is the main iteration parameter, as shown below, and the order κ has to be at least $n - 1 - m$.

[2] This is why the plant must be minimumphase: a pole/zero cancellation is acceptable only if the pole/zero has a negative real part.

[3] This is easy to see when $\{A, b, c\}$ are in controller canonical form. In Equation (A.2) this is confirmed for the levitating sphere example.

The resulting loop transfer function is

$$L(s) = \frac{k \cdot \mathrm{Adj}(sI - A) \cdot b}{\det(sI - A) \cdot (\tau s + 1)^{\kappa}} \tag{8.7}$$

The corner frequency $1/\tau$ determines the bandwidth of the loop transfer recovery. On the one hand, this LTR frequency may not be higher than the limits imposed by the model uncertainty and the noise present in the system. On the other hand, the LTR frequency must be sufficiently high to compensate for plant instabilities (see Figure A.9).

It is important to realize that the "naive" approach in Equation (8.6) does *not* always yield stabilizing controllers. For too small LTR bandwidths $1/\tau$, the resulting loop can be unstable because Equation (8.6) is not the result of an observer and state feedback combination. Therefore, the Separation Principle does not hold and stability is not guaranteed. Accordingly, stability and robustness must be verified after each iteration step using the well-known tools (Hurwitz criterion, Nyquist diagrams, etc.).

8.2 A Systematic Robustness Recovery Scheme

The starting point of the systematic robustness recovery scheme is a linear system $\{A, B, C\}$, for which an LQR controller gain K is computed. The resulting open-loop transfer function $L_{\mathrm{LQR}}(s)$ is derived in Equation (5.25) and repeated here for convenience

$$L_{\mathrm{LQR}}(s) = K \cdot (s\,I - A)^{-1} \cdot B \tag{8.8}$$

In a second step, an observer gain L is computed using the LQR machinery described in Section 6.4

```
L = lqr(A',C',B*B',q*eye(m,m))'
```
(8.9)

For this recovery scheme to work, it is important to choose the actual system matrix B in the weight $B \cdot B^{\mathrm{T}}$ in Equation (8.9). The resulting open-loop transfer function $L_{\mathrm{LQG}}(s)$ in Equation (7.7) is repeated here for convenience

$$L_{\mathrm{LQG}}(s) = K \cdot (s\,I - (A - B \cdot K - L \cdot C))^{-1} \cdot L \cdot C \cdot (s\,I - A)^{-1} \cdot B \tag{8.10}$$

The systematic recovery scheme is based on the fact that for minimumphase systems, in the limit case when the weight q in Equation (8.9) tends to zero, the open-loop transfer function $L_{\mathrm{LQG}}(s)$ approaches the open-loop transfer function $L_{\mathrm{LQR}}(s)$

$$\lim_{q \to 0} L_{\mathrm{LQG}}(s) = L_{\mathrm{LQR}}(s) \tag{8.11}$$

Therefore, if the weight q is reduced when designing the observer gain L, the LQG loop gain $L_{\mathrm{LQG}}(s)$ that has no robustness guarantees for larger values of q, approaches the LQR loop gain $L_{\mathrm{LQR}}(s)$ with significant robustness guarantees. The desired trade-off between robustness margin and noise rejection can thus be found iteratively.

If the linear system is extended with integrators at each output to enable disturbance rejection capabilities as outlined in Section 7.4, the resulting LQG loop approaches the LQR loop defined using the extended system matrices

$$\lim_{q \to 0} L_{\mathrm{LQG}}(s) = \widetilde{K} \cdot \left(s\, I - \widetilde{A} \right)^{-1} \cdot \widetilde{C} \tag{8.12}$$

Intuitive Justification

The following justification of Equation (8.11) is only valid for SISO systems with one state, i.e., $n = 1$. It is not a formal proof, but it is intended to intuitively justify the concepts of all LTR approaches. For a full proof valid also for general minimumphase MIMO systems, see [5].

Remember that the observer-based state estimation error follows the dynamics in Equation (6.8) which are repeated here for convenience

$$\frac{\mathrm{d}}{\mathrm{d}t} x_{\mathrm{e}}(t) = (A - L \cdot C) \cdot x_{\mathrm{e}}(t) \tag{8.13}$$

The cornerstone of the justification is the fact that in the limit case $q \to 0$, the observer gain results as

$$\lim_{q \to 0} |L| = \infty \tag{8.14}$$

which implies that the state estimation error dynamics converge infinitely fast. Therefore the observer state $\hat{x}(t)$ corresponds to the real state $x(t)$ and the open-loop transfer function $L_{\mathrm{LQG}}(s)$ approaches the open-loop transfer function $L_{\mathrm{LQR}}(s)$

$$\lim_{q \to 0} L_{\mathrm{LQG}}(s) = \lim_{|L| \to \infty} K \cdot \underbrace{(s\, I + L \cdot C)^{-1} \cdot L \cdot C}_{I} \cdot (s\, I - A)^{-1} \cdot B \tag{8.15}$$

$$= K \cdot (s\, I - A)^{-1} \cdot C \tag{8.16}$$

$$= L_{\mathrm{LQR}}(s) \tag{8.17}$$

The transfer function marked with identity I in Equation (8.15) corresponds to a system with a static gain of one and infinitely fast, stable dynamics. It therefore corresponds to the identity matrix I.

Quick Check 8.2.1: Why is it necessary that the system is of order $n = 1$ for this justification to be correct? ⌟

Applying the Systematic Robustness Recovery Scheme

The systematic robustness recovery scheme for an LQGI controller with integrative behavior consists of the following design steps:

1. Derive a linearized and normalized system model $\{A, B, C\}$ of the plant.
2. Extend the system with m integrators at each output as shown in Subsection 5.5.3 to get the extended system matrices $\{\widetilde{A}, \widetilde{B}\}$
3. Design a suitable state-feedback control gain $\widetilde{K}$ for the extended system using Equation (5.59)

```
K_tilde=lqr(A_tilde,B_u_tilde,Q_tilde,r*eye(m,m))
```

4. Analyze the resulting extended open-loop transfer function $L_{\mathrm{LQR}}(s)$ with respect to its properties (speed, overshoot, etc.)

$$L_{\mathrm{LQR}}(s) = \widetilde{K} \cdot \left(s\, I - \widetilde{A}\right)^{-1} \cdot \widetilde{B}$$

5. Design an observer gain L for the original system $\{A, B, C\}$ using the duality approach

```
L = lqr(A',C',B*B',q*eye(m,m))'
```

   The choice of the system matrix B in the weight $B \cdot B^{\mathrm{T}}$ penalizing the dual states is necessary.

6. Analyze the resulting open-loop frequency-domain properties using singular value plots of the return difference, and closed-loop time-domain properties using disturbance step plots.
7. Repeat steps 3 and 4 with *decreasing* values of q (the numerical value of q has no immediate interpretation). With decreasing values for q, the resulting open-loop transfer function $L_{\mathrm{LQG}}(s)$ approaches the ideal LQR open-loop transfer function $L_{\mathrm{LQR}}(s)$.

Some Final Remarks

- Perfectly reconstructing the LQR loop is *not* recommended. It yields high controller gains at high frequencies that may cause noise amplification.
- For nonminimumphase systems, perfectly reconstructing the LQR loop is not possible, i.e., Equation (8.11) is not valid. Since the LQG approach is based on an output-feedback observer, nonminimumphase zeros in the system would require unstable poles in the observer in order to fully reconstruct the state $x(t)$. However, if the plant is indeed nonminimumphase, the systematic LTR scheme will consider implicitly the limitations introduced by the nonminimumphase zeros, as discussed in [3].
- If the nonminimumphase zeros are at high frequencies, then "recovery" will take place in low frequencies, and for all practical purposes the presence of far-away nonminimumphase zeros does not degrade the low frequency reference tracking and disturbance rejection properties of the resulting closed loop. For more details see [20].

Part III

Frequency Domain MIMO Controller Design

9

Overview and Introduction

The disadvantage of the LQG/LTR procedure is that it offers no direct way to prescribe the frequency domain properties of the control loop. This direct link can be established using the design methods that are based on an $\mathcal{H}_\infty$ optimization. A first introduction to this approach is the content of Chapter 11.

The method proposed by Glover and McFarlane in Chapter 10 is a first step in the direction of developing a complete MIMO frequency domain theory. Since it can be applied without entering into too many mathematical details and since it uses the loop-shaping ideas introduced for SISO systems, it is presented briefly below and used in the case study in Appendix A.5.

The standard infinite-horizon LQR and LQG controllers in Chapters 5 and 7 were derived in the time domain due to the intuitive interpretation of the corresponding problem definitions. However, these controllers can also be interpreted in the frequency domain. The key to the transition from the time to the frequency domain interpretation is Parseval's Theorem

$$\int_0^\infty |x(t)|^2 \, \mathrm{d}t = \frac{1}{2\pi} \int_{-\infty}^\infty |X(\omega)|^2 \, \mathrm{d}\omega \tag{9.1}$$

Parseval's Theorem states the fact that the energy content of a signal $x(t)$ in the time domain is the same as the energy content of its Fourier transform $X(\omega)$ in the frequency domain. Appendix B.2 contains a proof of Parseval's Theorem.

This result can now be used to give a frequency-domain interpretation of the LQR approach. The simplest way to see that is by choosing the weighting matrices in the objective function used in the LQR design process as $Q = q \cdot I$ and $R = r \cdot I$, and applying Equation (9.1). With that the objective function can be expressed in the frequency domain as a sum of the weighted $\mathcal{H}_2$-norms of the frequency domain counterparts $X(\omega)$ and $U(\omega)$ of the system state and

the controller output, respectively

$$\begin{aligned} J &= \int_0^\infty \left(q \cdot x(t)^{\mathrm{T}} \cdot x(t) + r \cdot u^{\mathrm{T}}(t) \cdot u(t) \right) \mathrm{d}t \\ &= \int_0^\infty \left(q \cdot |x(t)|^2 + r \cdot |u(t)|^2 \right) \mathrm{d}t \\ &= \int_{-\infty}^\infty \left(q \cdot |X(\omega)|^2 + r \cdot |U(\omega)|^2 \right) \mathrm{d}\omega \end{aligned} \tag{9.2}$$

Frequency shaping in the LQR controller design process can be achieved using frequency-dependent weights $Q(\omega)$ and $R(\omega)$. This enables the application of loop-shaping techniques, since the $\mathcal{H}_2$-norms of suitable error signals in the frequency domain can be shaped as functions of their frequency. This approach requires the original system to be extended at the input and the output using suitable filters introducing additional dynamics, similar to the system extension used in the $\mathcal{H}_\infty$ approach. The controller and observer must then be designed for the extended system. Interested readers are referred to [1] and [18] for more theoretical background and illustrative examples.

In the scope of this text, frequency shaping LQR design techniques are not discussed in more detail. The main message here is to stress the disadvantage of the LQG/LTR procedure: Even though it allows for a frequency-dependent design, only the $\mathcal{H}_2$-norm of suitable error signals can be minimized. However, in order to *guarantee* robustness of a control loop by design, the $\mathcal{H}_\infty$-norm, i.e., the maximum singular value over all frequencies of certain transfer functions, must be kept within limits as discussed in detail in Chapter 3.

The limitation of the maximum singular values of suitable transfer functions can be achieved using $\mathcal{H}_\infty$ controller design methods which are introduced in Chapter 11.

10

Glover-McFarlane Controller

The Glover-McFarlane approach represents a bridge between the SISO and time-domain control system design methods, and the fully MIMO and frequency-domain design methods. This chapter introduces this approach because it is a relatively straightforward extension of the ideas introduces so far. The intention is to facilitate the transition to the more advanced $\mathcal{H}_2$ approach that is presented below, as it shows how some of the key ideas of SISO design approaches can be carried over to the MIMO world. For more information on this approach see [10] .

In a nutshell, the Glover-McFarlane method consists of the following preliminary steps:

1 A model $P(s) = C \cdot (sI - A)^{-1} \cdot B$ of the $m \times m$ MIMO plant is the starting point. The RGA method introduced in Chapter 2 is used to obtain the best possible input/output pairing.

2 The specifications are formulated by choosing a crossover frequency ω_c at which all singular values of the open-loop frequency response $L(j\,\omega)$ have to be approximately 1.[1]

3 A first controller $K_0(s)$ is designed such that the loop has the desired basic frequency domain characteristics: high (infinite) gain at low (zero) frequencies, moderate (-20 db/dec) roll-off around crossover, rapid roll-off at high frequencies. Typically this controller has the form

$$K_0(s) = \mathrm{diag}\left(k_{\mathrm{p,l}} \cdot \left(1 + \frac{1}{T_{\mathrm{i,l}} \cdot s}\right) \cdot \frac{1}{\tau_l \cdot s + 1}\right), \quad l = 1, \ldots m \qquad (10.1)$$

4 Two real constant $m \times m$ matrices K_1 and K_3 are used to further modify the loop gain such that the desired crossover frequency, a better decoupling

[1] This corresponds to requiring that all channels have approximately the same bandwidth. If there is a large separation of the bandwidths, several SISO loops designed following the cascaded-control paradigm are possible too.

of the control channels and a narrow singular value band at crossover are attained. The resulting transfer function of the extended plant

$$\widetilde{P}(s) = K_3 \cdot P(s) \cdot K_0(s) \cdot K_1, \tag{10.2}$$

which is realized using the matrices $\{\widetilde{A}, \widetilde{B}, \widetilde{C}\}$, forms the basis for the subsequent Glover-McFarlane method.

The core of the Glover-McFarlane approach is quite similar to the standard LQG design method, i.e., two Riccati equations must be solved, and the controller uses an observer-based state feedback. However, the method includes an additional tuning parameter α that can be used to choose a desired trade-off between performance and robustness.

To be more specific, a controller $K_2(s)$ is computed solving the following set of equations

$$\begin{aligned} \Phi \cdot \widetilde{B} \cdot \widetilde{B}^{\mathrm{T}} \cdot \Phi - \Phi \cdot \widetilde{A} - \widetilde{A}^{\mathrm{T}} \cdot \Phi - \widetilde{C}^{\mathrm{T}} \cdot \widetilde{C} = 0 \\ \Psi \cdot \widetilde{C}^{\mathrm{T}} \cdot \widetilde{C} \cdot \Psi - \widetilde{A} \cdot \Psi - \Psi \cdot \widetilde{A}^{\mathrm{T}} - \widetilde{B} \cdot \widetilde{B}^{\mathrm{T}} = 0 \end{aligned} \tag{10.3}$$

Two symmetric and positive definite solutions Φ and Ψ to these two Riccati equations exist under the usual conditions. The real positive scalar $\lambda_{\max}$, which is the largest eigenvalue of the matrix $\Phi \cdot \Psi$, is used to form a second real positive scalar

$$\gamma = \sqrt{1 + \lambda_{\max}} \cdot \alpha \tag{10.4}$$

where the influence of the design parameter $\alpha \in (1, \infty)$ will become clear shortly. Using the parameter γ the matrix

$$G = I - \frac{1}{\gamma^2}(I + \Psi \cdot \Phi) \tag{10.5}$$

is formed yielding the state feedback gain

$$\widetilde{K} = \widetilde{B}^{\mathrm{T}} \cdot \Phi \tag{10.6}$$

and the observation error feedback gain

$$\widetilde{L} = G^{-1} \cdot \Psi \cdot \widetilde{C}^{\mathrm{T}} \tag{10.7}$$

All necessary information is now available to build the controller $K_2(s)$

$$K_2(s) = \widetilde{K} \cdot \left(sI - (\widetilde{A} - \widetilde{B} \cdot \widetilde{K} - \widetilde{L} \cdot \widetilde{C}) \right)^{-1} \cdot \widetilde{L} \tag{10.8}$$

The final controller can now be formed using the equation

$$C(s) = K_0(s) \cdot K_1 \cdot K_2(s) \cdot K_3 \tag{10.9}$$

This controller is guaranteed to yield a stable closed-loop system (Separation Theorem). For $\alpha \to \infty$ the controller in Equation (10.8) simply represents the standard LQG controller obtained using Equation (5.11) with $R = I$ and $Q = \widetilde{C}^{\mathrm{T}} \cdot \widetilde{C}$, and using Equation (6.12) with $q = 1$. By decreasing α the robustness of the loop is increased. It can be shown that for $\alpha \to 1$ the ability of the loop to tolerate modeling errors is maximized [10]. Of course, this reduces the performance of the loop, i.e., the time constants of the closed-loop response become larger.

Experience has shown that a value of $\gamma \approx 2$ indicates a good robustness, whereas a value of $\gamma > 4$ is a sign of a rather fragile design, and further iterations on the compensators $K_0(s)$, K_1, and K_3 are recommended to decrease that value.

11

$\mathcal{H}_\infty$ Controller

11.1 Introduction to $\mathcal{H}_\infty$ Optimization

While the output feedback LQG controller introduced in Chapter 7 yields a stable control law, frequency domain specifications can only be imposed iteratively using an a-posteriori analysis. The $\mathcal{H}_\infty$ approach allows to account for frequency domain specifications already during the controller synthesis process. A few key properties of the $\mathcal{H}_\infty$ control design method are:

- The $\mathcal{H}_\infty$ control approach formulates the control system design as a mathematical optimization problem.
- The $\mathcal{H}_\infty$ method assures the stability of the closed loop system if the optimization problem can be solved.
- Loop shaping as well as robust control are combined in the optimization problem.
- The $\mathcal{H}_\infty$ controller can be used to minimize the effects of plant modeling errors on control system performance and robustness.
- The $\mathcal{H}_\infty$ approach is applicable to SISO systems as well as to MIMO systems with strong cross-couplings.
- The approach tries to minimize the maximal amplification, expressed by the infinity norm, of certain input signals. In this sense it is a worst-case analysis.
- In contrast to classical iterative loop shaping techniques, the $\mathcal{H}_\infty$ approach allows to impose specifications directly in the frequency domain as a part of the the controller design.

Although this method has several advantages, it also has its drawbacks. A higher level of mathematical understanding is necessary to apply the optimization successfully. Additionally, a good model of the plant uncertainty is

needed to find a reasonably good controller. Moreover, a proper formulation of several specifications in the frequency domain is very important because the controller obtained with this approach will only be optimal in the formulated problem setting.

Based on [19] this chapter gives a brief overview on the $\mathcal{H}_\infty$ controller synthesis method. First, the mixed sensitivity[1] approach is introduced which allows to synthesize controllers which satisfy the nominal performance and robust stability criteria introduced in [11]. The mixed sensitivity approach results in an augmented plant which can then be used within the general $\mathcal{H}_\infty$ framework. With those preparations, the solution to the general $\mathcal{H}_\infty$ problem is presented. The chapter finishes with a preview on the tools available in Matlab.

11.2 Mixed Sensitivity Synthesis

As mentioned in the introduction, the $\mathcal{H}_\infty$ approach allows to account for frequency domain specifications already during the controller synthesis process. The most important frequency domain characteristics of a closed-loop control system are the sensitivity $S(s)$ and complementary sensitivity $T(s)$. In [11] useful specifications on $S(s)$ and $T(s)$ are introduced which are shown to be good measures for performance and robustness.

The characteristics of the sensitivity $S(s)$ describe the performance properties of the closed-loop control system. A small sensitivity $S(s)$ guarantees good disturbance rejection and reference tracking behavior. A small complementary sensitivity $T(s)$ ensures good noise rejection behavior as well as robustness against modeling errors.

According to [11] the performance and robustness specifications on a closed-loop control system can be summarized in terms of the *robust performance* condition

$$\xi(C(j\,\omega)) = |W_1(j\,\omega) \cdot S(j\,\omega)| + |W_2(j\,\omega) \cdot T(j\,\omega)| < 1 \tag{11.1}$$

In Equation (11.1), the transfer functions $W_1(s)$ and $W_2(s)$ are the designer-specified weighting functions for the sensitivity $S(s)$ and the complementary sensitivity $T(s)$, respectively.

Unfortunately, there exists no known procedure that allows to find an optimal controller $C(s)$ that minimizes the scalar ξ for general plants $P(s)$ and weighting functions $W_1(s)$ and $W_2(s)$. However, using the $\mathcal{H}_\infty$ mixed

[1] The mixed sensitivity approach is sometimes also referred to as the S/KS/T-weighting scheme.

sensitivity approach allows to solve a slightly relaxed problem. The relaxed problem splits Equation (11.1) into a condition for *nominal performance*

$$||W_1(s) \cdot S(s)||_\infty < 1 \tag{11.2}$$

and a condition for *robust stability*

$$||W_2(s) \cdot T(s)||_\infty < 1 \tag{11.3}$$

The solution of the relaxed problem is the most common approach to synthesize $\mathcal{H}_\infty$ controllers.

By designing a controller which satisfies condition Equation (11.2) the weighting function $W_1(s)$ can be shaped in a way such that certain desired performance properties of the closed-loop control system are ensured. On the other hand, the transfer function $W_2(s)$ can be used to account for plant uncertainties if Equation (11.3) is satisfied (see [11] for more details). Hence, a reasonable choice of $W_2(s)$ allows to guarantee a desired robustness of the synthesized closed-loop control system.

Since by the definition of the sensitivity and the complementary sensitivity the equation $T(s)+S(s) = I$ is always satisfied, only one of these two transfer functions can be much smaller than I at a specific frequency s^*. Hence, $W_1(s)$ and $W_2(s)$ cannot be chosen arbitrarily. On the one hand, it is reasonable to choose $W_1(s)$ as a lag element. This choice enforces the sensitivity $S(s)$ to be small at low frequencies to suppress low frequency disturbances and to reduce the steady-state error. Particularly, the minimum return difference $\mu_{\min} = \min_\omega |I + L(j\,\omega)| = \max_\omega |S(j\,\omega)|$ can be adjusted by an appropriate choice of the upper limit of $W_1^{-1}(s)$. On the other hand, the inverse weighting transfer function $W_2^{-1}(s)$ is chosen to be small at high frequencies to account for the increased model uncertainty and to attenuate the measurement noise amplification at these frequencies. Figure 11.1 shows the bode magnitude plots of $S(s)$ and $T(s)$ of an arbitrary closed-loop SISO control system (in a MIMO setting the singular value plots are used). The weighting functions $W_1(s)$ and $W_2(s)$ are chosen as lag/lead elements. Figure 11.1 shows the inverse weighting functions $W_1^{-1}(s)$ and $W_2^{-1}(s)$ to verify that for the chosen controller $C(s)$, the conditions in Equations (11.2) and (11.3) are satisfied.

Of course also higher-order choices of $W_1(s)$ and $W_2(s)$ are possible to better account for steeper descents or ascents in the transition frequency band. The downside is an increased complexity of the subsequent controller design procedure. In addition to that the order of the resulting controller $C(s)$ will also be increased. In all cases, to obtain a feasible problem formulation, the transfer functions $W_1(s)$ and $W_2(s)$ must be proper and stable.

Once reasonable weighting transfer functions $W_1(s)$ and $W_2(s)$ are defined, a controller which fulfills Equations (11.2) and (11.3) needs to be found. The $\mathcal{H}_\infty$ approach allows to synthesize a controller that satisfies these conditions.

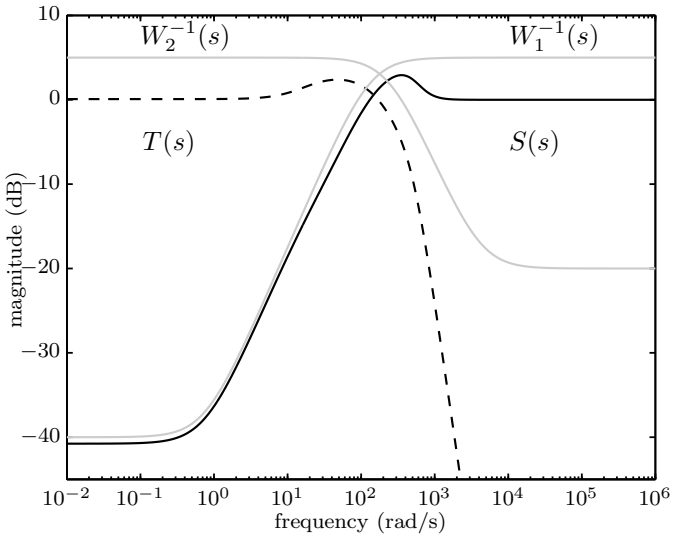

Figure 11.1: Exemplifying result of the mixed sensitivity approach that allows to shape the sensitivity $S(s)$ (solid) and the complementary sensitivity $T(s)$ (dashed) using the inverse weighting functions $W_1^{-1}(s)$ and $W_2^{-1}(s)$ (both gray).

The original plant $P(s)$ must be augmented such that it fits the standard $\mathcal{H}_\infty$ problem structure. Figure 11.2 shows the augmented plant $\Sigma(s)$. The augmented plant $\Sigma(s)$ has two inputs r and u and four outputs $z_{1,2,3}$ and e. The input r is the reference signal. The input u contains all signals that can be manipulated by the controller $C(s)$. The output e corresponds to the tracking error $e = r - y$ where y contains the measured signals. The loop is closed using the controller $C(s)$ whose input is the tracking error $e = r - y$ and whose output u is the control input of the plant $P(s)$.

The outputs $z_{1,2,3}$ are defined as follows. The transfer function from r to e corresponds to the sensitivity $S(s)$. The error signal e is fed through the weighting $W_1(s)$ to obtain the transfer function $W_1(s) \cdot S(s)$ from r to z_1 which is used in Equation (11.2). The transfer function from r to z_2 corresponds to the weighted complementary sensitivity $W_2(s) \cdot T(s)$ which is used in Equation (11.3). An additional third output z_3 is used to include the transfer function $W_3(s) \cdot C(s) \cdot S(s)$ from r to z_3, where $W_3(s)$ is a weighting that is used to limit the size of the control input u. Very often, $W_3(s)$ is chosen as a constant which results in a limitation of the gain of the controller $C(s)$.

With the augmented plant $\Sigma(s)$ at hand, the problem is in the standard form of the $\mathcal{H}_\infty$ approach.

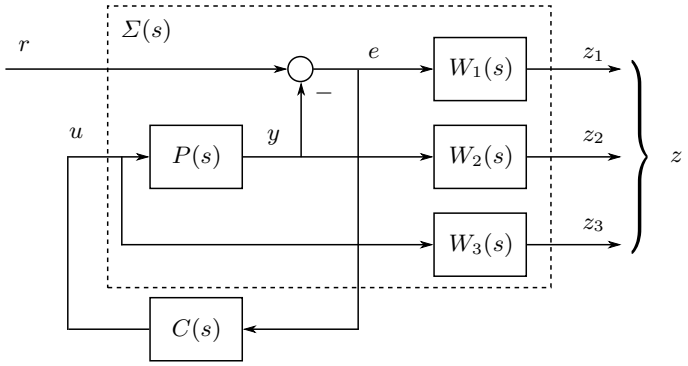

Figure 11.2: Plant augmentation used in the mixed sensitivity approach.

11.3 Solution to the $\mathcal{H}_\infty$ Problem

The mixed sensitivity problem description presented in Section 11.2 is a common starting point to synthesize $\mathcal{H}_\infty$ controllers. Several other ways to augment the plant are possible. Interested readers are referred to [19]. In this section the solution to the $\mathcal{H}_\infty$ control problem is presented for the mixed sensitivity approach.

The standard problem structure for the $\mathcal{H}_\infty$ controller synthesis is shown in Figure 11.3. The mixed sensitivity problem structure depicted in Figure 11.2 is in agreement with this setup.

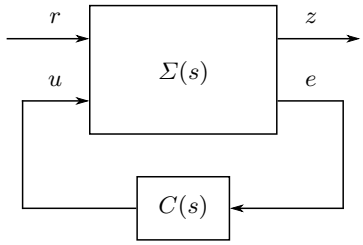

Figure 11.3: Standard configuration of the $\mathcal{H}_\infty$ control problem.

This standard problem structure of the augmented plant $\Sigma(s)$ can be expressed by the following system of transfer functions

$$\begin{bmatrix} Z(s) \\ E(s) \end{bmatrix} = \Sigma(s) \cdot \begin{bmatrix} R(s) \\ U(s) \end{bmatrix} = \begin{bmatrix} \Sigma_{11}(s) & \Sigma_{12}(s) \\ \Sigma_{21}(s) & \Sigma_{22}(s) \end{bmatrix} \cdot \begin{bmatrix} R(s) \\ U(s) \end{bmatrix} \tag{11.4}$$

$$U(s) = C(s) \cdot E(s) \tag{11.5}$$

where $\{R(s), U(s), Z(s), E(s)\}$ are the Laplace transformations of the signals $\{r, u, z, e\}$. Equation (11.4) can be written as

$$Z(s) = \Sigma_{11}(s) \cdot R(s) + \Sigma_{12}(s) \cdot U(s) \tag{11.6}$$

$$E(s) = \Sigma_{21}(s) \cdot R(s) + \Sigma_{22}(s) \cdot U(s) \tag{11.7}$$

The dependency of the output z on the input r is expressed as follows

$$\begin{aligned} Z(s) &= (\Sigma_{11}(s) + \Sigma_{12}(s) \cdot C(s) \cdot (I - \Sigma_{22}(s) \cdot C(s))^{-1} \cdot \Sigma_{21}(s)) \cdot R(s) \\ &= \mathcal{F}(\Sigma(s), C(s)) \cdot R(s) \end{aligned} \tag{11.8}$$

Quick Check 11.3.1: Derive Equation (11.8) using Equations (11.6) and (11.7). ⌟

The infinity norm of this transfer function is

$$\|\mathcal{F}(\Sigma(s), C(s))\|_\infty = \max_\omega \left(\max_i \sigma_i(\mathcal{F}(\Sigma(j\,\omega), C(j\,\omega))) \right) \tag{11.9}$$

The infinity norm can be interpreted as the maximum magnitude of the frequency response, which, in the MIMO case, is well approximated by the maximum singular value of the corresponding transfer function. Minimizing this maximum singular value, i.e., the infinity norm, is equivalent to minimize the worst-case amplification from r to z at any frequency.

If the plant $P(s)$ is augmented according to the mixed sensitivity approach presented in Section 11.2 the transfer function from r to z is

$$\mathcal{F}(\Sigma(s), C(s)) = \begin{bmatrix} W_1(s) \cdot S(s) \\ W_2(s) \cdot T(s) \\ W_3(s) \cdot C(s) \cdot S(s) \end{bmatrix} \tag{11.10}$$

If the controller $C(s)$ yields a stable closed-loop system that satisfies the condition

$$\|\mathcal{F}(\Sigma(s), C(s)\|_\infty < 1 \tag{11.11}$$

the conditions for nominal performance in Equation (11.2) and robust stability in Equation (11.3) are met.

For the mixed sensitivity approach but also for other plant augmentation schemes, Equation (11.11) can be generalized as an optimization problem

$$\min_{C(s)} \|\mathcal{F}(\Sigma(s), C(s))\|_\infty < \gamma \tag{11.12}$$

The generalization as an optimization problem introduces the scalar γ. This parameter represents a relaxation or restriction of the original condition in Equation (11.11). According to Equation (11.12), γ is the upper limit of the

infinity norm of the transfer function $\mathcal{F}(\Sigma(s), C(s))$ from r to z. By the definition of $\mathcal{F}(\Sigma(s), C(s))$ according to the mixed sensitivity approach one can think of this parameter γ as the upper limit of the disturbance rejection and robustness properties. The lower γ the better the disturbances are suppressed and the more robust is the closed-loop system.

If the solution of the optimization problem results in the optimum $\gamma^* \leq 1$, Equation (11.11) and hence also Equations (11.2) and (11.3) are fulfilled and the specifications expressed by $W_{1,2,3}(s)$ are satisfied by the controller $C(s)$. If the optimization returns $\gamma^* > 1$, Equation (11.11) is not satisfied and relaxed weights $W_{1,2,3}(s)$ must be accepted. On the other hand, if the optimization problem in Equation (11.12) returns a solution with $\gamma^* < 1$, more restricting $W_{1,2,3}(s)$ can be chosen. Therefore an iterative procedure of solving the optimization problem and restricting the weightings $W_{1,2,3}(s)$ can help to improve the properties of the control system.

The algorithm presented below returns a solution of the feasibility problem related to the optimization problem in Equation (11.12) for one specific γ^*. Applying this algorithm repeatedly while reducing γ (denoted by γ-iteration) leads to the solution of the optimization problem in Equation (11.12). Modern computer-aided control system design tools such as Matlab (see Section 11.5) allow to efficiently run this algorithm and also incorporate a γ-iteration.

The explicit solution of the optimization problem in Equation (11.12) for a fixed γ^* requires further manipulation. The augmented plant $\Sigma(s)$ has to be represented in state-space form. Since only the input-output behavior is of interest, any minimal-order realization which gives the same input-output behavior can be used. In that state-space description the augmented plant $\Sigma(s)$ is rewritten using the following set of matrices

$$\left(\begin{array}{c|cc} A_{\text{aug}} & B_1 & B_2 \\ \hline C_1 & D_{11} & D_{12} \\ C_2 & D_{21} & D_{22} \end{array}\right) \tag{11.13}$$

where B_1 denotes the gain matrix for the reference input r and B_2 the gain matrix for the control input u. The matrix A_{aug} is the system matrix of the augmented plant $\Sigma(s)$ after the transformation into the state-space. The matrices C_1, D_{11}, D_{12} are used to compute the signals z and the matrices C_2, D_{12}, D_{22} are used for the output e respectively. The dynamic equations can be written as

$$\frac{\mathrm{d}}{\mathrm{d}t}x(t) = A_{\text{aug}} \cdot x(t) + B_1 \cdot r(t) + B_2 \cdot u(t) \tag{11.14}$$

$$z(t) = C_1 \cdot x(t) + D_{11} \cdot r(t) + D_{12} \cdot u(t) \tag{11.15}$$

$$e(t) = C_2 \cdot x(t) + D_{21} \cdot r(t) + D_{22} \cdot u(t) \tag{11.16}$$

With the state-space description of the augmented plant $\Sigma(s)$ at hand, the optimization problem in Equation (11.12) can be solved. The explicit derivation

of the $\mathcal{H}_\infty$ controller equations is out of the scope of this course. Therefore, only the results are shown.

As mentioned above, the procedure involves essentially two iterations: one on the weights $W_{1,2,3}(s)$ and one on the parameter γ. A typical control system design process includes the following steps:

1. Fix a sufficiently large value for γ.
2. Find a quadratic real-valued matrix $X = X^T$ such that $X \geq 0$ is a solution to the algebraic Riccati equation

$$0 = XA_{\text{aug}} + A_{\text{aug}}^{\text{T}}X + C_1^{\text{T}}C_1 + X(\frac{1}{\gamma^2}B_1B_1^{\text{T}} - B_2B_2^{\text{T}})X \tag{11.17}$$

   and $\text{Re}\left[\lambda_i(A_{\text{aug}} + (\frac{1}{\gamma^2}B_1B_1^{\text{T}} - B_2B_2^{\text{T}})X)\right] < 0,\ \forall i.$[2]
3. Find a quadratic real-valued matrix $Y = Y^T$ such that $Y \geq 0$ is a solution to the algebraic Riccati equation

$$0 = A_{\text{aug}}Y + YA_{\text{aug}}^{\text{T}} + B_1B_1^{\text{T}} + Y(\frac{1}{\gamma^2}C_1^{\text{T}}C_1 - C_2^{\text{T}}C_2)Y \tag{11.18}$$

   and $\text{Re}\left[\lambda_i(A_{\text{aug}} + Y(\frac{1}{\gamma^2}C_1^{\text{T}}C_1 - C_2^{\text{T}}C_2)\right] < 0,\ \forall i.$
4. The spectral radius[3] ρ of the matrix product $X \cdot Y$ must satisfy the following inequality

$$\max_i |\lambda_i(X \cdot Y)| = \rho(X \cdot Y) \leq \gamma^2 \tag{11.19}$$

5. Reduce γ until no solution is found.[4]

If the resulting minimal γ^* is larger than 1, the feasibility conditions presented in Section 11.4 are violated. Relaxing the weighting functions $W_{1,2,3}(s)$ can make the problem feasible. If the resulting minimal γ^* is smaller than 1 the result can be accepted or the weighting functions $W_{1,2,3}(s)$ can be tightened.

Once a feasible solution is found, the resulting matrices X and Y can be used to calculate the $\mathcal{H}_\infty$ controller dynamics

$$\frac{\text{d}}{\text{d}t}\hat{x}(t) = A_\infty \cdot \hat{x}(t) - Z \cdot L \cdot y(t) \tag{11.20}$$

$$u(t) = F \cdot \hat{x}(t) \tag{11.21}$$

[2] The variable $\lambda_i(H)$ denotes the i-th eigenvalue of the matrix H.

[3] The spectral radius ρ of a matrix is the absolute value of its eigenvalue with the largest magnitude.

[4] Matlab uses a bisection algorithm; more details on that can be found below and in the case study in Appendix A.3

where

$$\begin{aligned} A_\infty &= A_{\text{aug}} + \frac{1}{\gamma^2} B_1 B_1^{\mathrm{T}} X + B_2 F + Z L C_2 \\ F &= -B_2^{\mathrm{T}} X \\ L &= -Y C_2^{\mathrm{T}} \\ Z &= (I - \gamma^{-2} Y X)^{-1} \end{aligned}$$

Equation (11.20) describes the state observer dynamics for the augmented plant in Equation (11.14). The state feedback law is given by Equation (11.21).

11.4 Feasibility Conditions

The method described in Section 11.3 works for a variety of linear time-invariant systems but there are certain conditions which always have to be fulfilled. Some of them are as simple as the controllability and the observability condition while others are slightly more complex. The following list shows all conditions which have to be fulfilled such that the $\mathcal{H}_\infty$ problem in Equation (11.12) has a stabilizing solution

- The controllability of the augmented plant $\Sigma(s)$ has to be verified. In case of any non-controllable states it has to be assured that these states remain bounded. So the pair (A_{aug}, B_2) must be stabilizable.
- The augmented plant $\Sigma(s)$ must be fully observable. If this is not the case, all non-observable states have to be stable. Hence, the pair (C_2, A_{aug}) must be detectable.
- Additionally, all four matrices D_{12}, D_{21}, $\begin{bmatrix} A_{\text{aug}} - j\,\omega\, I & B_2 \\ C_1 & D_{12} \end{bmatrix}$ and $\begin{bmatrix} A_{\text{aug}} - j\,\omega\, I & B_1 \\ C_2 & D_{21} \end{bmatrix}$ must have full rank for all ω.

11.5 Matlab Commands

There exist many computer-aided control system design tools that allow the efficient solution of the Riccati equations presented in Section 11.3. In Matlab the command

```
hinfsyn
```

can be used to find an $\mathcal{H}_\infty$ controller for the augmented plant $\Sigma(s)$. As described in the Matlab `help` this algorithm performs a γ-iteration to find the optimal γ^*. The algorithm is initialized with a high and a low estimate of the parameter γ with $\gamma_{\text{high}} \gg 1$ and $\gamma_{\text{low}} \ll 1$, respectively. A bisection algorithm solves Equations (11.17) and (11.18) for both values of γ and iterates on both γ_{low} by increasing it and on γ_{high} by reducing it. The algorithm terminates when the relative difference between the last value γ_{low} that does not satisfy Equation (11.19) and the last value γ_{high} that fulfills condition Equation (11.19) is less than a given tolerance. The Matlab `help` provides further information on how to use this function. The command[5]

```
Sigma = augw(P,W1,W2,W3)
```

is useful when applying the mixed sensitivity approach to augment the plant $P(s)$ as shown in Section 11.2. Details of how to do this will be given in the case study in Appendix A.3. In this case study the mixed sensitivity approach is applied to an unstable SISO plant.

[5] One should pay attention to the notation of the weighting functions $W_{1,2,3}(s)$ in Matlab which differs from the usage in this book.

Part IV

Appendix

A

Case Studies

A.1 Introduction

This chapter includes four case studies that illustrate some of the main points of the design methods introduced in the previous chapters:

- Appendix A.2: A SISO case study of an unstable plant is presented to illustrate all concepts introduced above and to help in the transition from SISO to MIMO design rules. The controller synthesis is done using the LQR/LQG approach with LTR.
- Appendix A.3: The same unstable SISO plant is used for the design of a $\mathcal{H}_\infty$ controller using the mixed sensitivity approach. The application of two different controller design approaches on the same plant allows for comparisons between the LQR/LQG and the $\mathcal{H}_\infty$ approach.
- Appendix A.4: A MIMO case study of a non-diagonally dominant plant is presented to exemplify the advantages a multivariable design approach can offer.
- Appendix A.5: A second MIMO case study is presented to show how the SISO loop-shaping ideas can be extended to MIMO systems.

A.2 Levitating Sphere (LQG/LTR)

In this case study, most of the ideas introduced in Part II are illustrated using a simple, yet interesting SISO plant. Since the plant is SISO, all results can be interpreted in an SISO framework (Bode and Nyquist plots, etc.). This should facilitate the transition from SISO to MIMO design methods and help develop an intuitive understanding of the MIMO ideas.

The plant analyzed in this case study is the *levitating sphere* system (see Figure A.1). The system is described by the following equations

$$\begin{aligned} \frac{\mathrm{d}}{\mathrm{d}t}x(t) &= \begin{bmatrix} 0 & 1 & 0 \\ 700 & 0 & -700 \\ 0 & 0 & -0.2 \end{bmatrix} \cdot x(t) + \begin{bmatrix} 0 \\ 0 \\ 1 \end{bmatrix} \cdot u(t) \\ y(t) &= \begin{bmatrix} 1 & 0 & 0 \end{bmatrix} \cdot x(t) \end{aligned} \tag{A.1}$$

The three state variables represent the position (x_1) and the velocity (x_2) of the sphere, and the current (x_3) in the electromagnet.[1] This system is unstable (one unstable eigenvalue $\lambda^+ \approx +26$ rad/s), but minimumphase and completely controllable and observable and, hence, well stabilizable.

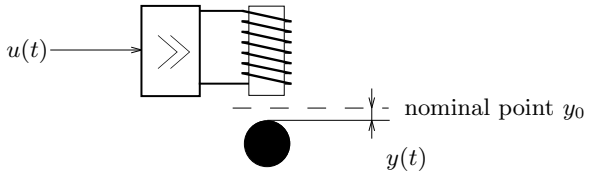

Figure A.1: Levitating sphere system: input $u(t)$ voltage at electromagnet; output $y(t)$ deviation of the sphere from its reference position.

The feedback controller in Equation (5.9) that minimizes the criterion in Equation (5.8) has the form

$$u(t) = -[k_1(r), k_2(r), k_3(r)] \cdot x(t)$$

The resulting trajectories of the closed-loop system for three different weights $r = \{1, 0.2, 0.01\}$ are shown in Figure A.2. As expected, decreasing r yields "faster" closed-loop systems, but requires larger control signals.

[1] These are the level variables of the three reservoirs potential energy, kinetic energy and magnetic energy.

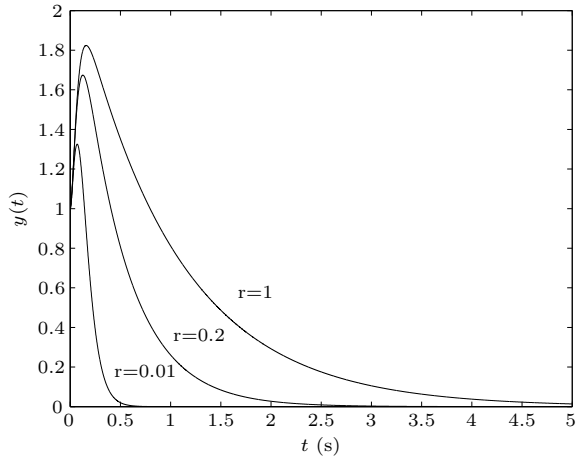

Figure A.2: Case study levitating sphere (LQR/LQG controller): closed-loop system behavior for three different weights r; regulator problem with $x(0) = [1, 0, 0]^{\mathrm{T}}$.

Table A.1 shows the resulting signal energies E_u and E_y defined in Equation (5.8). In general, the numerical values of r, E_u, and E_y have no physical meaning. In particular the weight r is simply a parameter with which the designer can influence the resulting controller bandwidth.

Table A.1: Output signal and control signal energies E_u and E_y defined in Equation (5.8) as functions of weight r.

$r = 1$	$E_u = 59$	$E_y = 2.17$
$r = 0.2$	$E_u = 62$	$E_y = 1.01$
$r = 0.01$	$E_u = 79$	$E_y = 0.27$

It is interesting to analyze two other system parameters: first the eigenvalues $\lambda_i(r)$ of the closed-loop system matrix $A - b \cdot k(r)$, i.e., the root locus, and second the Nyquist plot of the loop gain $L_{\mathrm{LQR}}(s, r) = k(r) \cdot (s\,I - A)^{-1} \cdot b$. Figure A.3 shows the root locus for $r \in [\infty, 0)$. The case $r = \infty$ corresponds to the open-loop case and one eigenvalue is in the right-hand plane.[2] For

[2] Note that for $r = \infty$, no valid LQR solution exists. A positive definite solution Φ to the equation $-\Phi A - A^{\mathrm{T}}\Phi - Q = 0$ only exists if A is Hurwitz, which is not the case in this example.

very large $r < \infty$ ("expensive control") the only unstable eigenvalue is mirrored into the left-hand plane, while the other two eigenvalues are not shifted. For decreasing r, i.e., for increasing feedback control action, the eigenvalues follow what is know as a Butterworth pattern: asymptotically, all eigenvalues approach straight lines which point to infinity ("cheap control"). For all weights $0 < r < \infty$ the eigenvalues stay in the left plane, i.e., the matrix $A - b \cdot k(r)$ is a Hurwitz matrix. Similarly to classical root-locus methods, complex conjugate eigenvalue pairs appear for sufficiently small weights r.

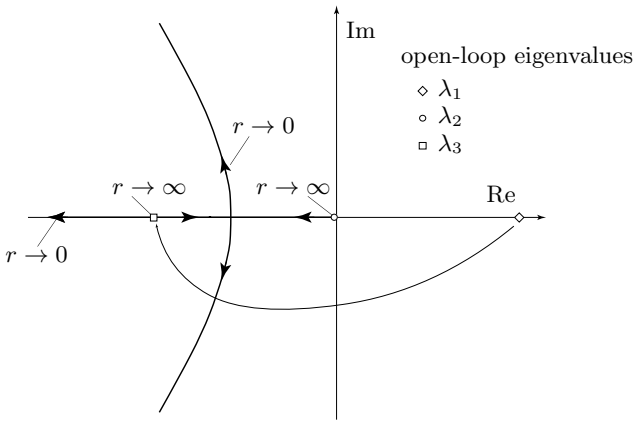

Figure A.3: Case study levitating sphere (LQR/LQG controller): eigenvalues $\lambda_i(r)$ of $A - b \cdot k(r)$ for $r \in (0, \infty)$.

In general, all elements k_i with $i = 1, \ldots n$ of the LQR gain k are non-zero real scalars. Accordingly, the relative degree of the LQR loop gain, in general, is 1. This is easy to see by writing the LQR loop gain as follows

$$L_{\mathrm{LQR}}(s) = k \cdot (s\,I - A)^{-1} \cdot b = \frac{k \cdot \mathrm{Adj}(s\,I - A) \cdot b}{\det(s\,I - A)} = \frac{b(s)}{a(s)} \tag{A.2}$$

The adjugate of $s\,I - A$, in general, is a polynomial matrix whose elements have as the highest order s^{n-1}. This follows from the definition of $\mathrm{Adj}(s\,I - A)$, whose elements are the determinants of matrices obtained by omitting one row and one column of $s\,I - A$. Since, in the general case, the vector k has non-zero elements only and since $a(s)$ is the determinant of the full matrix $s\,I - A$, the order of the numerator polynomial $b(s)$ is exactly 1 smaller than the order n of the denominator polynomial $a(s)$. Such systems have a relative degree 1, and their high-frequency behavior is characterized by a roll-off of -20 dB per frequency decade. Figure A.4 confirms that result for the example analyzed in this section.

The Nyquist plots of the LQR loop gains in Equation (5.25) are shown in Figure A.5. For $\omega = 0$ all curves start on the negative real axis and converge

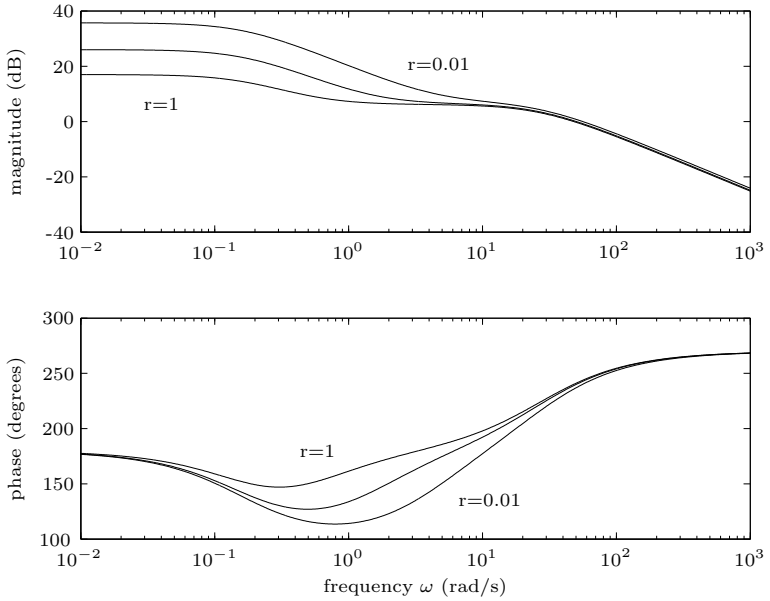

Figure A.4: Case study levitating sphere (LQR/LQG controller): Bode plots of the open-loop gain $L_{\mathrm{LQR}}(j\,\omega)$ for three different weights $r = \{0.01, 0.1, 1\}$.

to 0 for $\omega \to \infty$. The Nyquist criterion (one encirclement of the point -1 for $\omega \in [-\infty, +\infty]$) is satisfied for all weights r. The loop gain magnitude increases for decreasing r, which explains the faster closed-loop system behavior seen in Figure A.2.

Figure A.6 shows an enlarged view of the same loop gains as those shown in Figure A.5. As expected, the loop gains satisfy the inequality

$$|1 + L_{\mathrm{LQR}}(j\,\omega, r)| \geq 1, \quad \forall\ \omega \in \mathbb{R} \text{ and } r \in \mathbb{R}_+ \tag{A.3}$$

As mentioned in Section 5.4, this is one of the key properties of LQR controllers: the loop gains obtained with this approach have excellent robustness and can tolerate large modeling errors. The minimum return difference obtained with this design is

$$\mu_{\min \mathrm{LQR}} = \min_{\omega} \left(|1 + L_{\mathrm{LQR}}(j\,\omega, r)|\right) \geq 1 \tag{A.4}$$

The robustness margins of standard LQR design can be improved using the modified Riccati equation in Equation (5.31). Choosing a parameter $\beta > 1$ yields designs with loop gains similar to the one shown in Figure A.7 for the levitating sphere.

As mentioned in Chapter 7, the picture changes completely if only output feedback is possible. In this case, the loop gain $L_{\mathrm{LQG}}(j\,\omega)$ can pass arbitrarily

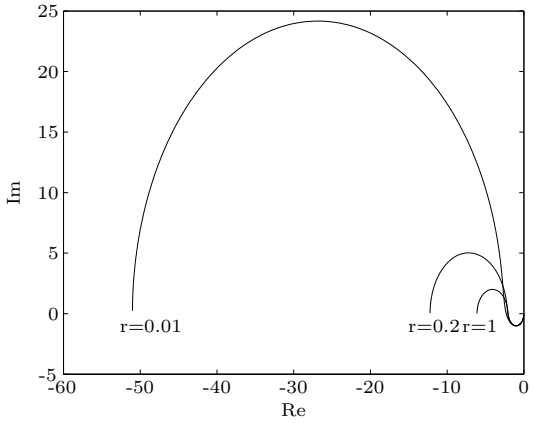

Figure A.5: Case study levitating sphere (LQR/LQG controller): Nyquist plots of the open-loop gain $L_{\mathrm{LQR}}(j\,\omega)$ for three different weights r; full picture.

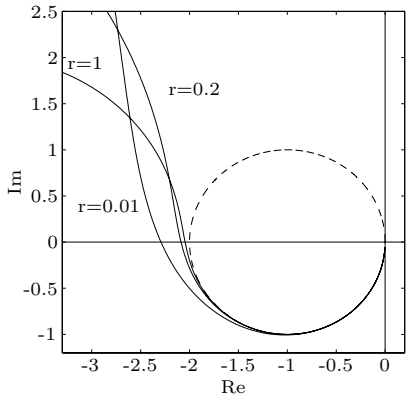

Figure A.6: Case study levitating sphere (LQR/LQG controller): Nyquist plots of the open-loop gain $L_{\mathrm{LQR}}(j\,\omega)$ for three different weights r; detail.

close to the critical point -1, and very small modeling errors can destabilize the closed-loop system. Figure A.8 shows the two loop gains for the levitating sphere example

$$L_{\mathrm{LQR}}(s) = k \cdot (s\,I - A)^{-1} \cdot b \tag{A.5}$$

$$L_{\mathrm{LQG}}(s) = k \cdot (s\,I - (A - b \cdot k - l \cdot c))^{-1} \cdot l \cdot c \cdot (s\,I - A)^{-1} \cdot b \tag{A.6}$$

where the gains k and l have been computed using the following weighting factors (in Matlab notation):

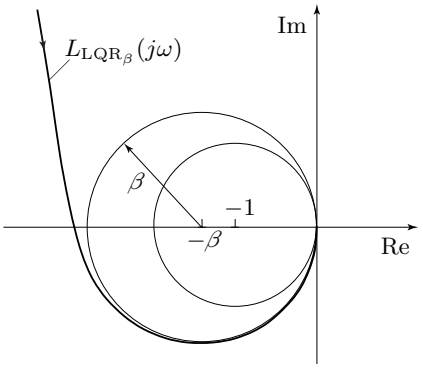

Figure A.7: Case study levitating sphere (LQR/LQG controller): Nyquist diagram of the open-loop gain transfer function $L_{LQR_\beta}(s) = k_\beta\,(s\,I - A)^{-1}b$, with k_β computed using Equation (5.31).

```
k=lqr(A,b,c'*c,0.1)

l=lqr(A',c',b'*b,0.001)'
```

Obviously, the LQG controller is stabilizing (correct number of encirclements of -1), but too fragile to be useful in practice. This example confirms that, in general, the excellent robustness properties of the state-feedback LQR design are lost when an output-feedback LQG approach is used. In particular, the minimum return difference

$$\mu_{\min,\mathrm{LQG}} = \min_{\omega}\left(|1 + L_{\mathrm{LQG}}(j\,\omega)|\right) \tag{A.7}$$

$$= \min_{\omega}\left(|1 + c\,(j\,\omega I - A)^{-1}b\,k\,(j\,\omega I - (A - b\,k - l\,c))^{-1}l|\right) \tag{A.8}$$

can be arbitrarily small, indicating that a very small model/plant mismatch can cause instability. As shown in Chapter 8, systematic iterative procedures exist, with which one can "recover" the desired robustness properties of LQR designs. Of course, hard limitations imposed by nonminimumphase zeros, delays, noise, etc., must be respected in these iterations.

Since the plant analyzed in this case study is SISO and minimumphase, the "naive" method introduced in Chapter 8 can be applied to improve the robustness of the loop. Using the controller in Equation (8.6) the loop gains shown in Figure A.9 are obtained. As expected, for larger τ the loop is unstable, i.e., the controller is too "slow" to compensate for the one unstable eigenvalue $\lambda^+ \approx +26$ rad/s. For smaller time constants τ the loop is stabilized and for $\tau \to 0$ the LQG loop gains approach the LQR loop gain with its excellent robustness properties. Of course this is only one side of the medal: smaller

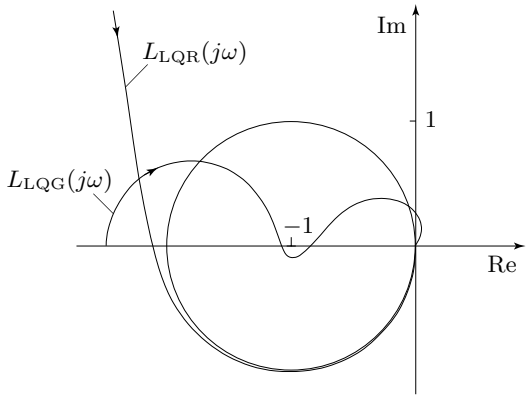

Figure A.8: Case study levitating sphere (LQR/LQG controller): loop gains of the LQR and the LQG designs.

values of τ increase the sensitivity of the loop to noise, which is an effect the designer must take into consideration when optimizing the parameter τ.

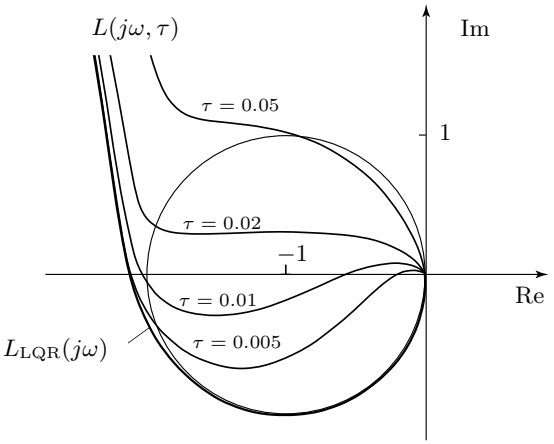

Figure A.9: Case study levitating sphere (LQR/LQG controller): "naive" LTR procedure, loop gains obtained with the controller in Equation (8.6) for different time constants τ.

The regular LTR procedure avoids the potential stability problem that the "naive" approach has. With controllers designed using the regular LTR approach, a sequence of designs result that all satisfy the stability requirements (correct number of encirclements of the critical point -1) and which approach the LQR loop. Figure A.10 shows the results of such an iteration.

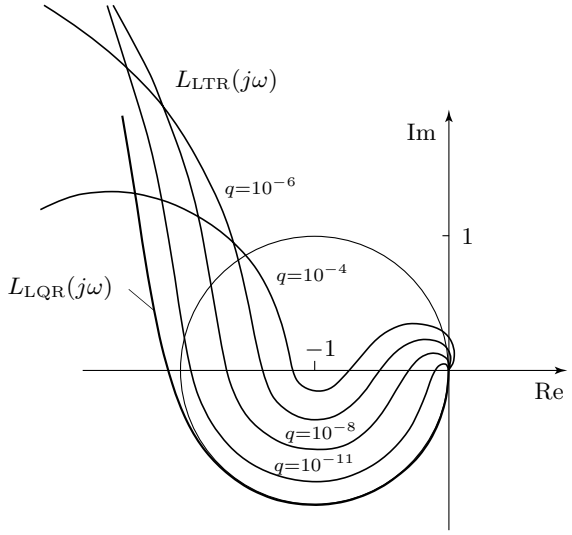

Figure A.10: Case study levitating sphere (LQR/LQG controller): regular LTR procedure, loop gains obtained for different LTR parameters q.

As mentioned above, increasing the LTR degree yields higher bandwidths and, therefore, higher noise amplifications. Figure A.11 shows the Bode magnitude plots of the LQR and the LQG-LTR designs. For higher LTR degrees the loop gains start to roll off at increasingly higher frequencies. If substantial noise is present for frequencies higher than the frequency ω_n, the LTR iteration must be limited such that the roll-off part starts at frequencies (substantially) below ω_n.

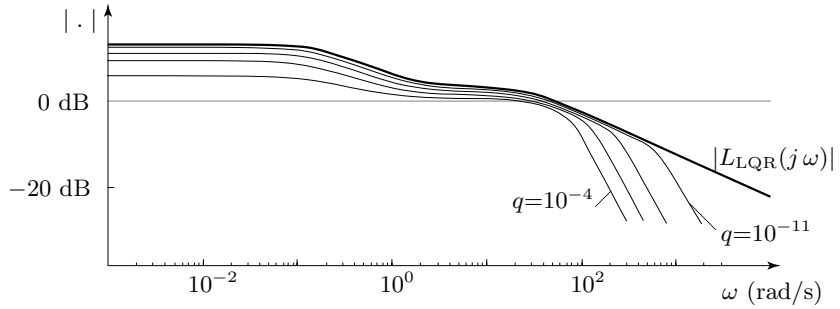

Figure A.11: Case study levitating sphere (LQR/LQG controller): regular LTR procedure, loop gains $|L_{\mathrm{LTR}}(j\,\omega)|$ obtained for different LTR parameters q.

A.3 Levitating Sphere ($\mathcal{H}_\infty$)

In this case study the same plant is analyzed as in the previous case study in Appendix A.2. Instead of an LQR/LQG-approach now the $\mathcal{H}_\infty$ mixed sensitivity approach as presented in Chapter 11 is used. The results of an LQG controller designed in the previous case study are shown for comparison.[3] The starting point for the $\mathcal{H}_\infty$ mixed sensitivity approach is the linearized model of the levitating sphere as shown in Equation (A.1).

The controller is to be designed such that the closed-loop system satisfies the following specifications:

- Disturbance attenuation above $3'000\,\mathrm{rad/s}$ by at least $-20\,\mathrm{dB}$ (noise suppression, robustness against modeling uncertainty, etc).
- Cross-over frequency at least a factor of 2 larger than the positive pole $\pi^+ = 26\,\mathrm{rad/s}$.
- Limitation of the control action of the input (to avoid actuator saturation).
- Disturbance attenuation at low frequencies of $-40\,\mathrm{dB}$.

According to the procedure described in Section 11.2 for both the weighting $W_1(s)$ of the sensitivity $S(s)$ and the weighting $W_2(s)$ of the complementary sensitivity $T(s)$ a lag/lead is chosen. Three different design cases are analyzed. One which aims at a robust design, one at an aggressive design and one at an intermediate ("moderate") design.

The three cases only differ in the choice of the weighting function $W_1(s)$. The inverse weighting function $W_2^{-1}(s)$ of the complementary sensitivity $T(s)$ is kept the same for all three design cases as

$$W_2^{-1}(s) = k \cdot \frac{T \cdot s + 1}{\alpha \cdot T \cdot s + 1} \tag{A.9}$$

with

$$\lim_{s \to 0} W_2^{-1}(s) = k = 1.7 = 5\,\mathrm{dB} \tag{A.10}$$

$$\lim_{s \to \infty} W_2^{-1}(s) = \frac{k}{\alpha} = 0.1 = -20\,\mathrm{dB} \tag{A.11}$$

$$\hat{\omega}_2 = (T \cdot \sqrt{\alpha})^{-1} = 2 \cdot \pi \cdot 500\,\mathrm{rad/s} \tag{A.12}$$

where $\hat{\omega}_2$ is the transition frequency of the lag element $W_2^{-1}(s)$. For the complementary sensitivity $T(s)$ this choice results in a maximum gain of 5 dB at low frequencies and -20 dB at high frequencies.

[3] An aggressive design with $r = 0.01$ and $q = 10^{-11}$ is chosen.

For the input weighting $W_3(s)$ a constant is chosen as it is often done to limit the control input. In the present case the input weighting is chosen to be $W_3(s) = 15 \cdot 10^4$.

Three designs with different robustness and performance properties are compared. For these designs the inverse sensitivity weighting function $W_1^{-1}(s)$ is chosen as a lead element

$$W_1^{-1}(s) = k \cdot \frac{T \cdot s + 1}{\alpha \cdot T \cdot s + 1} \tag{A.13}$$

according to Table A.2. The corresponding Bode magnitude plots of $W_1^{-1}(s)$ and $W_2^{-1}(s)$ for all three cases are shown in Figure A.13. The low frequency gain of the sensitivity $S(s)$ for all three cases is below $-40\,\mathrm{dB}$ which results in a steady state error of less than 1%. The high frequency gain k/α of the inverse weighting of the complementary sensitivity $W_1^{-1}(s)$ determines the lower limit of the minimum return difference $\mu_{\min} = \min_\omega |1 + L(j\,\omega)|$ of the resulting control system. Hence, it defines the robustness of the control system. The transition frequency $\hat{\omega}_1$ determines a lower bound on the cross-over frequency that the open-loop gain of the control system should have. The cross-over frequency is a good indicator of the performance of the control system (see [11] for more details). Due to the waterbed effect discussed in [11], the transition frequency must be adjusted in agreement with the high frequency gain k/α. More details on how to choose reasonable specifications such that the problem is well-posed can be found in [11].

Table A.2: The three inverse sensitivity weighting functions $W_1^{-1}(s)$ are chosen as lead elements. The corresponding high and low frequency gains and the transition frequencies are shown in the table.

	Robust	Moderate	Aggressive
k	-40 dB	-40 dB	-40 dB
k/α	2 dB	5 dB	10 dB
$\hat{\omega}_1 = (T \cdot \sqrt{\alpha})^{-1}$	$0.01\,{}^{\mathrm{rad}}/_{\mathrm{s}}$	${}^{5\,\mathrm{rad}}/_{\mathrm{s}}$	$20\,{}^{\mathrm{rad}}/_{\mathrm{s}}$

With the choice of the three weighting functions $W_1(s)$, $W_2(s)$ and $W_3(s)$ for each design case, all specifications are at hand to calculate the $\mathcal{H}_\infty$ controller using Matlab. In Matlab the command `augw(P,W1^-1,W3^-1,W2^-1)` augments the original plant $P(s)$ with the necessary outputs and weighting functions $W_{1,2,3}(s)$ such that the augmented plant $\Sigma(s)$ fits the mixed sensitivity structure as shown in Figure A.12. One should pay attention on the different numbering of the weighting functions $W_{1,2,3}(s)$ which is used in Matlab. The command `augw` also performs the conversion to the state-space description using canonical coordinates. The Matlab command `hinfsyn` can then be used to solve the Riccati equations stated in Section 11.3 and to

compute the controller $C(s)$. The function performs an iteration on the parameter γ to solve the optimization problem in Equation (11.12). For more information see the Matlab `help`. According to Section 11.4 the augmented plant $\Sigma(s)$ must be stabilizable and detectable. The Matlab function `hinfsyn` checks these conditions and returns an error if they are not fulfilled.

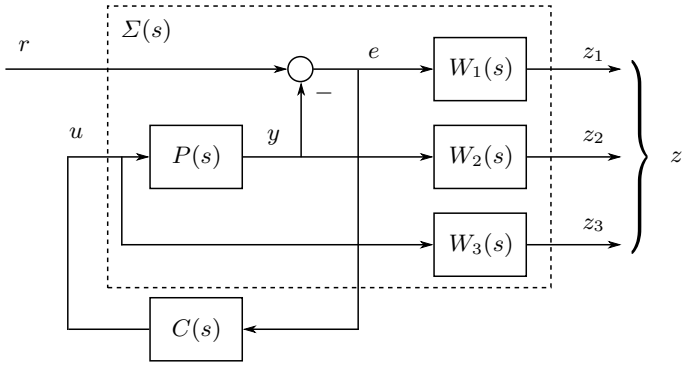

Figure A.12: Case study levitating sphere ($\mathcal{H}_\infty$ controller): $\mathcal{H}_\infty$ mixed sensitivity plant augmentation.

In contrast to the LQR/LQG-approach the command `hinfsyn` solves both the Riccati equation for the controller as well as the Riccati equation for the observer. Therefore no separate tuning of the state feedback controller and the state observer needs to be done.

The controller $C(s)$ is an output feedback controller which includes the state observer as shown in Equation (11.20) and the state feedback law in Equation (11.21). Since the state observer estimates the states of the augmented plant $\Sigma(s)$ its order is the sum of the order of the plant and the orders of the weighting functions $W_{1,2,3}(s)$. On the other hand, the state feedback law is a simple matrix multiplication which has no influence on the order of the controller $C(s)$. Therefore, choosing higher order weighting functions $W_{1,2,3}(s)$ also increases the order of the controller $C(s)$. In the present example, the plant has order 3 and the weightings $W_1(s)$ and $W_2(s)$ each have order 1 which results in a controller order of 5.

For the choices of $W_1^{-1}(s)$ made above, the resulting sensitivities $S(s)$ are shown in the top plot of Figure A.13 together with their corresponding inverse weighting functions $W_1^{-1}(s)$. It can be seen that all specifications are met. For inappropriate choices of the weighting functions $W_{1,2,3}(s)$ this is not necessarily the case, because there might be no solution of the optimization problem in Equation (11.12) that results in an optimum with $\gamma^* < 1$. In

this case, the specifications, i.e., the weighting functions $W_{1,2,3}(s)$, need to be relaxed.

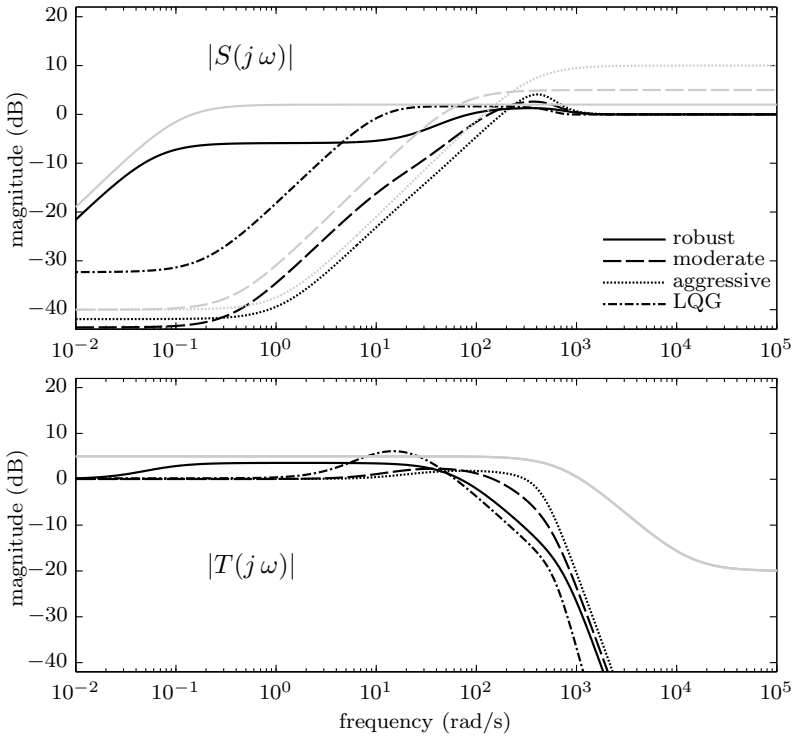

Figure A.13: Case study levitating sphere ($\mathcal{H}_\infty$ controller): Resulting sensitivities $S(s)$ (top plot) and complementary sensitivities $T(s)$ (bottom plot) for the three design cases and an LQG controller from the previous case study. The corresponding inverse weighting functions $W_1^{-1}(s)$ (top plot, three different weighting functions) and $W_2^{-1}(s)$ (bottom plot, only one weighting function) are shown with gray lines.

The second plot in Figure A.13 shows the complementary sensitivities $T(s)$ for the three design cases. Since the weighting $W_2(s)$ is the same for all cases, the shapes of the bode magnitude plots are very similar.

The chosen designs aimed at different robustness properties that can be visualized using the Nyquist plot of the open-loop transfer function $L(s)$ which is depicted in Figure A.14. As expected, the aggressive design has the smallest robustness margin. To better analyze the robustness of the three designs, Figure A.15 shows the return differences $\mu(s) = 1 + L(s)$. As expected, the aggressive design results in the smallest minimum return difference.

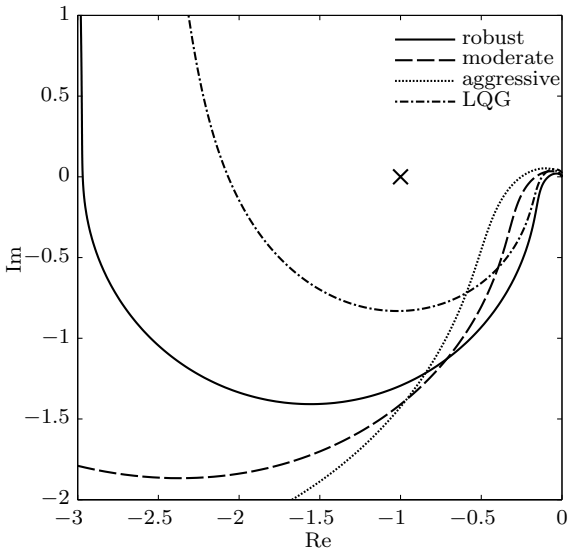

Figure A.14: Case study levitating sphere ($\mathcal{H}_\infty$ controller): Resulting open-loop Nyquist curves $L(s)$ for the three design cases and for an LQG controller from the previous case study.

In the introduction to this case study, the specification of the cross-over frequency ω_c was made with respect to the unstable pole of the plant which is at $\pi^+ = 26\,\mathrm{rad/s}$. The cross-over frequency must be significantly larger than the unstable pole to stabilize the system. A separation of at least a factor of 2 is a reasonable choice. Since the $\mathcal{H}_\infty$ controller synthesis as well as the LQR/LQG approach always yield a stabilizing controller both approaches will always satisfy the condition $\omega_c > \pi^+$ if the problem is feasible. Figure A.16 shows the bode magnitude plot of the open-loop transfer function $L(s)$ for the three different design cases and the LQG-controlled plant from the previous case study. As expected, all controllers yield a cross-over frequency at least a factor of 2 larger than the positive pole.

This is the case even for the robust design, where $W_1^{-1}(s)$ is parametrized such that its low transition frequency of $\hat{\omega}_1 = 0.01\,\mathrm{rad/s}$ does not enforce a priori the cross-over frequency of $L(s)$ to be larger than the positive pole. However, since the $\mathcal{H}_\infty$ approach always returns a stabilizing controller, a controller is synthesized which results in a cross-over frequency that is significantly larger than the positive pole π^+. This fact can be seen in Figure A.16 where the loop gain $|L(j\,\omega)|$ is kept above the 0 dB line up to a sufficiently high frequency such that $\omega_c \gg \pi^+$ holds.

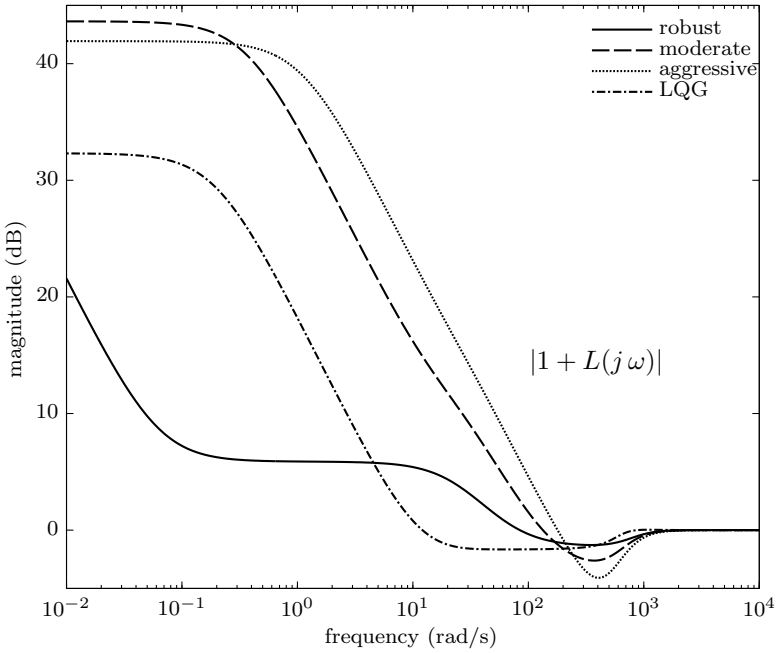

Figure A.15: Case study levitating sphere ($\mathcal{H}_\infty$ controller): Resulting return difference $\mu(s) = 1 + L(s)$ for the three design cases and for an LQG controller from the previous case study.

Finally, the time domain responses of the three design cases and an LQG controller from the previous case study are compared in Figure A.17. As expected, the aggressive controller with the highest cross-over frequency gives the best performance. It approaches the target position within the shortest time but has the largest undershoot. This behavior agrees with the frequency domain properties of the corresponding control system.

The presented case study is a simple SISO example for the $\mathcal{H}_\infty$ mixed sensitivity approach. It shows how frequency domain specifications can be used to tune the $\mathcal{H}_\infty$ controller in a straightforward way. Often the design specifications of a controller are given in the frequency domain, such as desired values for the sensitivities at different frequencies or a desired crossover frequency. If the specifications are given in the time domain, frequency domain specifications can be derived from them. If the design specifications yield a well-posed problem, they can be used directly for the weighting functions for the $\mathcal{H}_\infty$ controller and the $\mathcal{H}_\infty$ synthesis will find a solution with $\gamma^* < 1$. If classical loop shaping is used instead, the parameters of the controller will have to

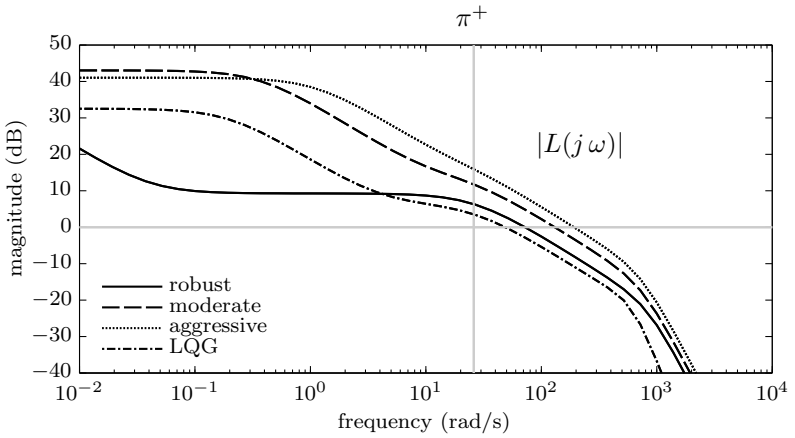

Figure A.16: Case study levitating sphere ($\mathcal{H}_\infty$ controller): Resulting open-loop gain $L(s)$ for the three design cases and an LQG controller from the previous case study. The location of the positive pole π^+ of the plant is also indicated.

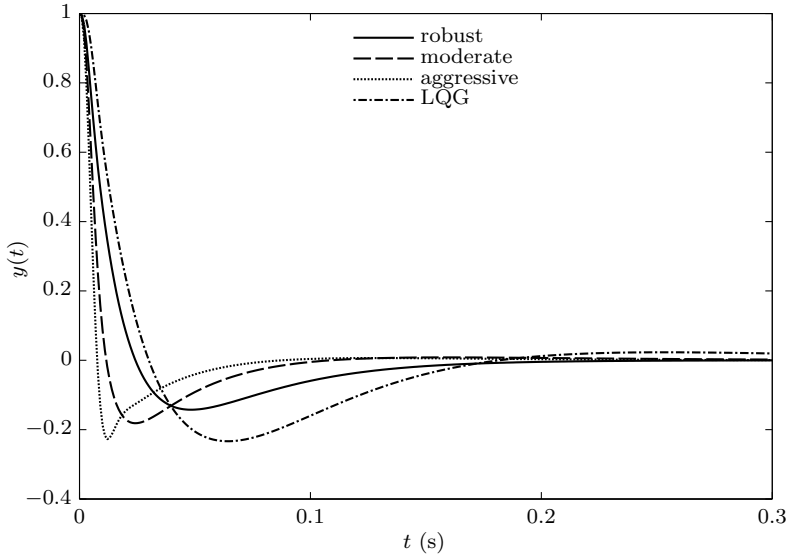

Figure A.17: Case study levitating sphere ($\mathcal{H}_\infty$ controller): Time domain response of the levitating sphere control system with three different $\mathcal{H}_\infty$ controllers and an LQG controller from the previous case study. The simulation is started with a deviation in the initial condition $y(0) = 1$.

be tuned iteratively. This is time consuming because the influence that the controller parameters have on closed-loop transfer functions (e.g. sensitivity $S(s)$) is not straightforward. The advantage of the $\mathcal{H}_\infty$ approach is that frequency domain specifications are used to determine frequency domain based controller parameters.

In the present case study, a SISO control problem was chosen for simplicity. This allowed to analyze the frequency domain properties using the standard SISO tools such as the Bode and Nyquist plots. However, as mentioned in the introduction to Chapter 11, the $\mathcal{H}_\infty$ technique can also be applied to MIMO systems. In the MIMO case, the frequency domain specifications are used to limit the maximum or minimum singular values of the corresponding MIMO transfer functions.

A.4 Geostationary Satellite (LQG/LTR)

Geostationary satellites play an important role in global communication systems (TV, data links, SAR, etc.). Such satellites are placed on an equatorial circular orbit at $r_0 \approx 4.217 \cdot 10^7$ m distance from the center of the earth and rotate with the sidereal angular velocity $\omega_0 \approx 7.292 \cdot 10^{-5}$ rad/s around the earth such that their position relative to earth is constant, see Figure A.18.

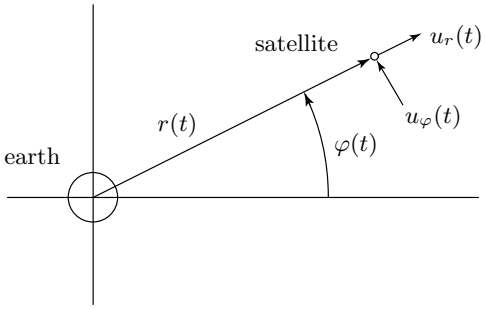

Figure A.18: Case study geostationary satellite: the input signals u_r and u_φ are the accelerations in radial and azimuthal direction; the output signals y_r and y_φ are the normed radius and the azimuth of the satellite.

The simplified and linearized dynamics of such a satellite are defined by[4]

$$\frac{\mathrm{d}}{\mathrm{d}t}x(t) = \begin{bmatrix} 0 & 1 & 0 & 0 \\ 3\,\omega_0^2 & 0 & 0 & 2\,r_0 \cdot \omega_0 \\ 0 & 0 & 0 & 1 \\ 0 & -2\,\omega_0/r_0 & 0 & 0 \end{bmatrix} \cdot x(t) + \begin{bmatrix} 0 & 0 \\ 1 & 0 \\ 0 & 0 \\ 0 & 1/r_0 \end{bmatrix} \cdot u(t) \quad \text{(A.14)}$$

and

$$y(t) = \begin{bmatrix} 1/r_0 & 0 & 0 & 0 \\ 0 & 0 & 1 & 0 \end{bmatrix} \cdot x(t) \quad \text{(A.15)}$$

The system is unstable (two eigenvalues $\lambda_i = 0$ in series configuration), but completely controllable and observable, hence stabilizable. Moreover, the MIMO system has no finite zeros such that, in principle, a perfect LTR is possible. The matrix C is not arbitrary: dividing the measured radius $r(t)$ by its nominal value r_0 yields a much better balanced system behavior. In particular at the crossover frequency the maximum and minimum singular values are much closer with this choice.

The transfer function of this 2×2 system is defined by

$$P(s) = \begin{bmatrix} \dfrac{1}{r_0 \cdot (s^2 + \omega_0^2)} & \dfrac{2\,\omega_0}{r_0 \cdot s \cdot (s^2 + \omega_0^2)} \\ \dfrac{-2\,\omega_0}{r_0 \cdot s \cdot (s^2 + \omega_0^2)} & \dfrac{s^2 - 3\,\omega_0^2}{r_0 \cdot s^2 \cdot (s^2 + \omega_0^2)} \end{bmatrix}$$

and the inverse of this polynomial matrix is

$$P^{-1}(s) = \begin{bmatrix} r_0 \cdot (s^2 - 3\,\omega_0^2) & -2\,\omega_0 \cdot r_0 \cdot s \\ 2\,\omega_0 \cdot r_0 \cdot s & r_0 \cdot s^2 \end{bmatrix}$$

Therefore, the RGA matrix of the satellite system has the following form

$$\mathrm{RGA}(s) = \begin{bmatrix} \dfrac{s^2 - 3\,\omega_0^2}{s^2 + \omega_0^2} & \dfrac{4\,\omega_0^2}{s^2 + \omega_0^2} \\ \dfrac{4\,\omega_0^2}{s^2 + \omega_0^2} & \dfrac{s^2 - 3\,\omega_0^2}{s^2 + \omega_0^2} \end{bmatrix}$$

[4] The modeling of this system is discussed in the class "Systems Modeling" in the fifth semester of the Bachelor's curriculum in mechanical engineering at ETH Zurich.

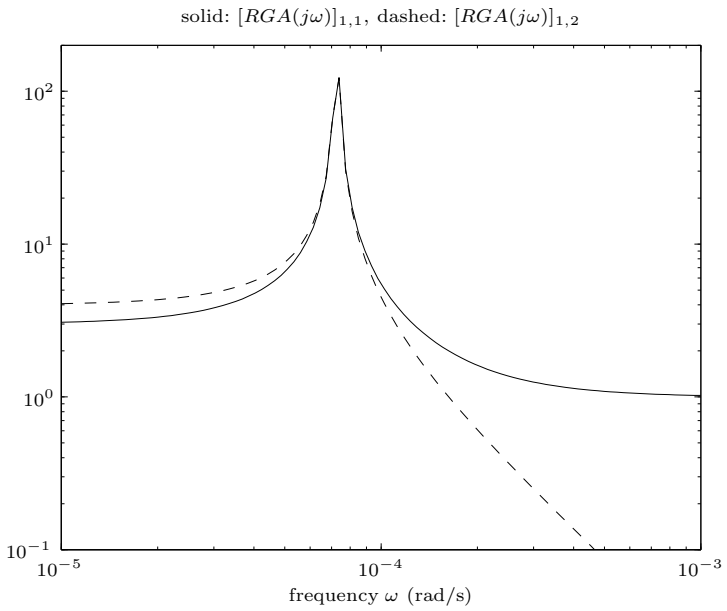

Figure A.19: Case study geostationary satellite: RGA matrix for $s = j\,\omega$.

Figure A.19 shows the elements $[\mathrm{RGA}(s)]_{1,1}$ and $[\mathrm{RGA}(s)]_{1,2}$ for $s = j\,\omega$ (after transients have decayed).[5] For very low frequencies, the cross couplings between the two channels are substantial, but not excessive. Close to the resonant frequency $\omega_0 \approx 7.3 \cdot 10^{-5}$ rad/s the interaction becomes very high. At frequencies $\omega \gg \omega_0$ the matrix $\mathrm{RGA}(s)$ converges to the identity matrix, and hence the cross couplings disappear.

Since the satellite is unstable, a stabilizing feedback control system is necessary. No measurable disturbances are present and the satellite reference position is not assumed to change. The problem to be solved is, therefore, a simple regulator problem. The expected disturbances are either impulses (impact of meteorites) or zero-mean periodic disturbances of low frequency (gravitational influence of the moon and the sun). Accordingly, no integral action is needed. Thruster efficiency and other system parameters are not very well known and can vary. Accordingly, the control system must be very robust against modeling errors. The RGA analysis shows that on one side the crossover frequency ω_c should be substantially larger than 10^{-4} rad/sec to avoid the severe cross couplings around ω_0. On the other side, ω_c should not be too large to avoid large control signals and thus large thruster fuel consumption.

[5] Remember that $[\mathrm{RGA}(s)]_{2,2} = [\mathrm{RGA}(s)]_{1,1}$ and $[\mathrm{RGA}(s)]_{2,1} = [\mathrm{RGA}(s)]_{1,2}$.

The following quantitative specifications for the design of the control system formalize these requirements:

- The system must be stabilized robustly, i.e., $\mu_{\min \mathrm{LQG}} \geq 0.7$ must be satisfied, where $\mu_{\min \mathrm{LQG}}$ is defined in in Equation (7.8).
- The crossover frequency must satisfy the bounds $0.05 \leq \omega_\mathrm{c} \leq 0.1$ rad/s.
- All disturbances up to $10 \cdot \omega_0$ must be attenuated by at least -40 dB.
- The disturbance amplification may not be larger than 3 dB at any frequency.
- The noise attenuation must be better than -40 dB for all frequencies higher than 10 rad/s.

The design follows the LQG/LTR procedure. Only two scalar design parameters are used, first the scalar r in the LQR step

```
K = lqr(A,B,C'*C,r*eye(2,2));
```

and second the scalar q in the observer-design step

```
L = lqr(A',C',B*B',q*eye(2,2))';
```

After several iterations the following two values were found

$$r = 4 \cdot 10^{-10}, \quad q = 1 \cdot 10^{-13}$$

Figure A.20 shows the open-loop gains when applying LQR and LQG control. As recommended above, LTR is not pushed too far to avoid high-frequency noise amplification. The crossover frequency is in the order of $7 \cdot 10^{-2}$ rad/s and the roll-off starts around $3 \cdot 10^{-1}$ rad/s. Notice that the minimum and maximum singular values are very close at ω_c. This is desired as such loops have an "almost-SISO" behavior around that important frequency. Scaling the individual control channels helps achieving this objective.

Figure A.21 shows the singular values of the transfer functions $T(s)$ and $S(s)$. The bounds chosen in the specifications (dashdotted lines) are marked in that figure as well. Obviously, the design meets these specifications. It must be stressed that the LQG/LTR approach is not able to directly enforce these specifications. The scalars $\{r, q\}$ indirectly influence the shape of the curves $\sigma\left(L(j\omega)\right)$, $\sigma\left(T(j\omega)\right)$, and $\sigma\left(S(j\omega)\right)$. However, working on these "tuning knobs" and observing the changes in the corresponding frequency-domain objects, an experienced designer can often meet reasonable specifications.

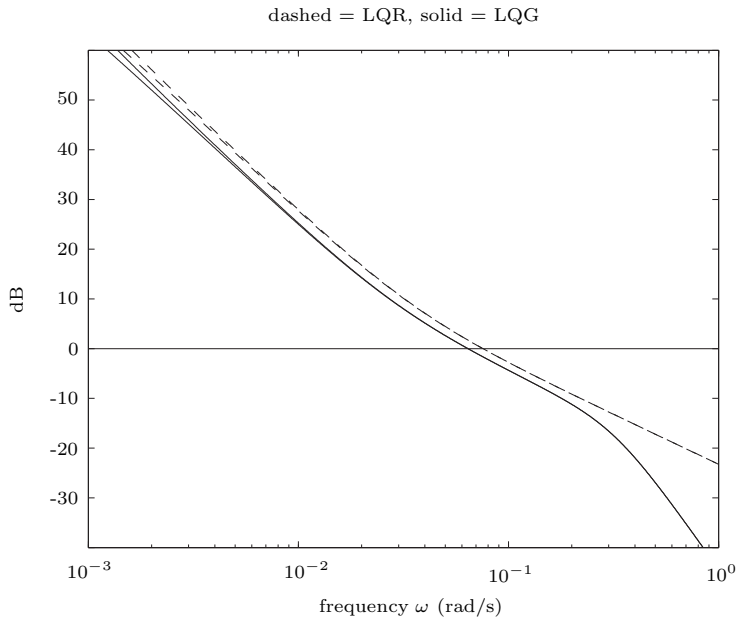

Figure A.20: Case study geostationary satellite: singular values of the open-loop gains $L(j\,\omega)$ of the satellite control system.

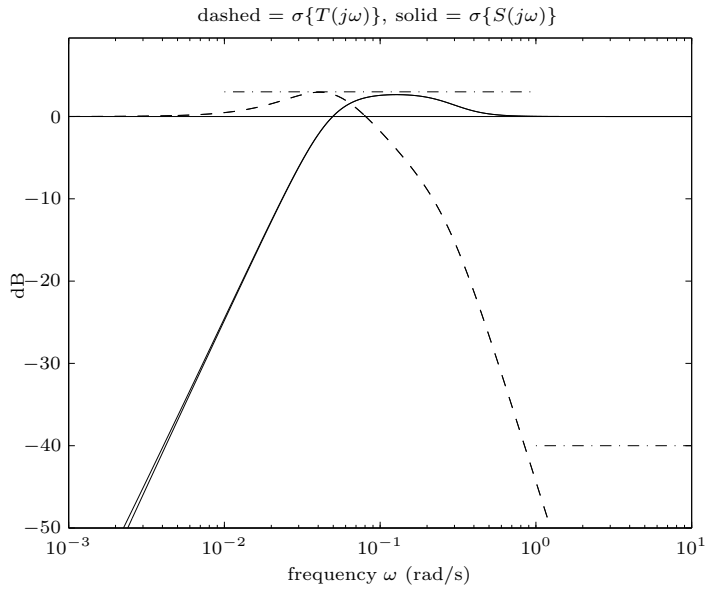

Figure A.21: Case study geostationary satellite: singular values of the closed-loop LQG sensitivity and complementary sensitivity.

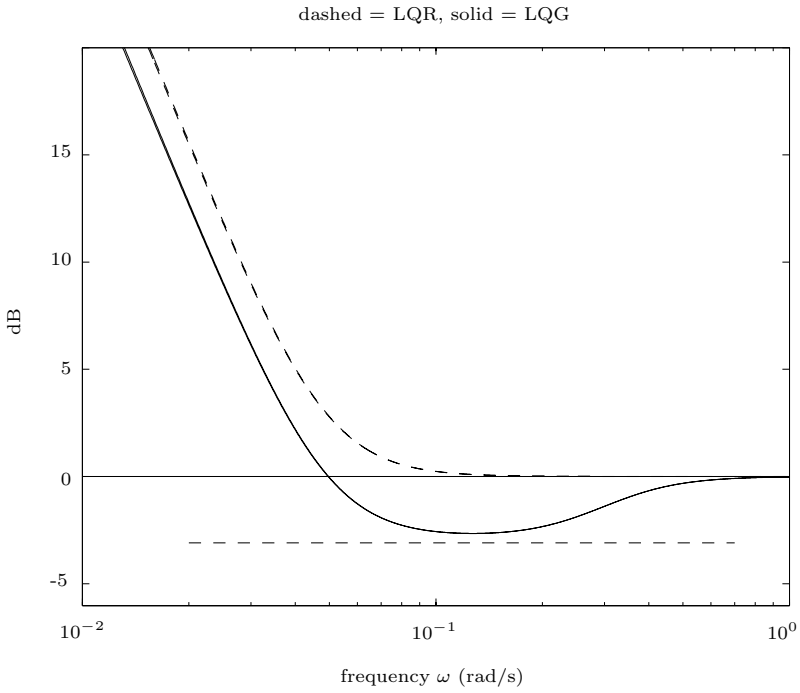

Figure A.22: Case study geostationary satellite: singular values of the return difference of the LQR and the LQG control systems.

The robustness of the design is analyzed using the minimum return difference $\mu_{\min \mathrm{LQG}}$ in Equation (7.8). As Figure A.22 shows, $\mu_{\min \mathrm{LQR}} = 1$ as expected. The LTR procedure is achieving a $\mu_{\min \mathrm{LQG}} \geq 0.7 \approx -3$ dB that is required by the specifications.

Figure A.23 shows a simulation in which the nonlinear satellite model is controlled using the LQG control system designed above. In these simulations, it is assumed that a meteorite of 0.1 g mass impacts the satellite, whose mass is 1000 kg, in negative radial direction with a speed of 36000 km/h (10^4 m/s). This impact causes the initial condition of the radial speed $x_2(0)$ to deviate from its nominal value of 0 to -0.001 m/s (all other variables are at their reference value, i.e., $x_1(0) = r_0$, $x_3(0) = 0$, and $x_4(0) = \omega_0$).

Caused by the impact, the satellite is pushed away from its desired orbit. As Figure A.23 shows, in this specific case the radius deviates no more than 0.014 m (left plot) and the azimuth no more than $7 \cdot 10^{-13}$ rad (right plot). These deviations are corrected by the feedback control system approximately

after 100 s. The maximum force that the radial thruster must deliver during this corrective action is approximately 0.06 N.[6]

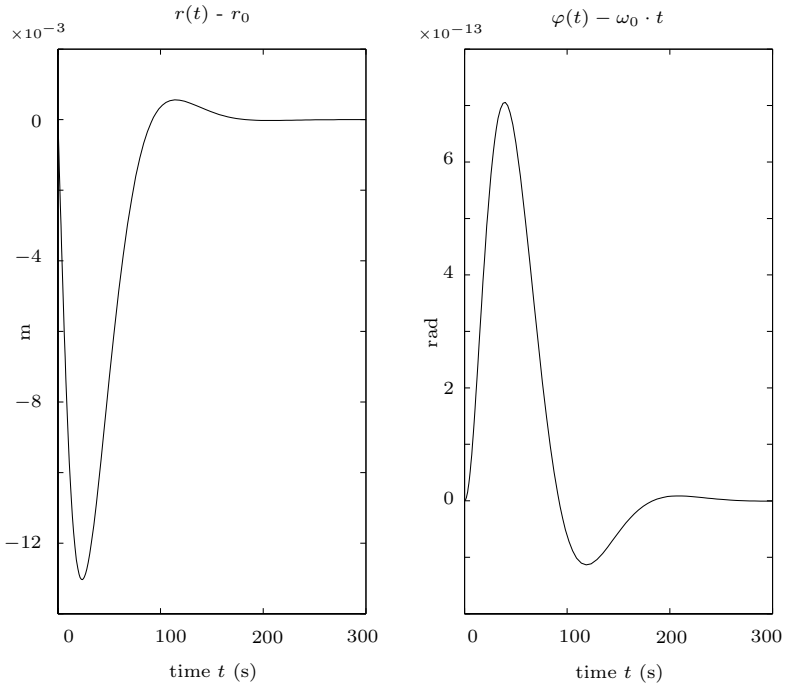

Figure A.23: Case study geostationary satellite: simulation of the nonlinear satellite model with LQG control active, transient caused by the impact of a meteorite.

Remark: Of course, this case study does not show a realistic satellite control system design. First of all, the attitude of the satellite must be controlled as well, and that problem is much more difficult to solve [12]. Second, the question of control signal magnitude and fuel consumption must be analyzed carefully to maximize the life span of the satellite. Third, questions such as fail-safe operation, computational burden, graceful degradation, etc. must be analyzed carefully in a real control system.

[6] The peak tangential thrust is substantially smaller in this case. Tangential impacts reverse the situation, but produce similar control signals for comparable impact energies.

A.5 Speed and Air/Fuel Ratio (Glover-McFarlane)

In this case study the Glover-McFarlane method is applied to the problem of simultaneously controlling the idle speed and the air/fuel ratio of a gasoline engine. The plant model is taken from [9]. The plant is a 2×2 system with engine speed and air/fuel ratio as outputs and throttle valve opening and amount of fuel injected as inputs. This case study is *not* meant to show how to design a true idle-speed control system (too many simplifications are adopted below), but to illustrate the main steps of the Glover-McFarlane design procedure as introduced in Chapter 10.

The system is of order four with the four state variables

$$x = \begin{bmatrix} x_1 \\ x_2 \\ x_3 \\ x_4 \end{bmatrix} = \begin{bmatrix} \text{throttle valve position} & (1 = 1^\circ) \\ \text{intake manifold pressure} & (1 = 0.05 \text{ bar}) \\ \text{engine speed} & (1 = 200 \text{ rpm}) \\ \text{air/fuel ratio} & (1 = 0.05) \end{bmatrix} \tag{A.16}$$

The deviations from the desired equilibrium point (engine idling speed 900 rpm, air-fuel ratio 1, i.e., stoichiometric) are normalized such that the physical interpretation shown in brackets can be given to each state variable. The input variables are

$$u = \begin{bmatrix} u_1 \\ u_2 \end{bmatrix} = \begin{bmatrix} \text{throttle valve command} & (1 = 1^\circ) \\ \text{air/fuel ratio command} & (1 = 0.05) \end{bmatrix} \tag{A.17}$$

and the output variables are

$$y = \begin{bmatrix} y_1 \\ y_2 \end{bmatrix} = \begin{bmatrix} \text{engine speed} & (1 = 200 \text{ rpm}) \\ \text{air/fuel ratio} & (1 = 0.05) \end{bmatrix} \tag{A.18}$$

Linearizing the plant around the desired equilibrium point yields the system matrices

$$\begin{bmatrix} A & B \\ C & D \end{bmatrix} = \left[\begin{array}{rrrr|rr} -25.00 & 0 & 0 & 0 & 25.00 & 0 \\ 5.22 & -4.00 & -8.24 & 0 & 0 & 0 \\ 3.09 & 1.91 & -3.07 & 0 & 0 & 0.85 \\ -7.68 & 5.89 & 12.10 & -2.10 & 0 & -2.10 \\ \hline 0 & 0 & 1 & 0 & 0 & 0 \\ 0 & 0 & 0 & 1 & 0 & 0 \end{array}\right]$$

The only relevant external disturbance is the load torque $w(t)$ (1 = 40 Nm) that acts on the engine's crank shaft. This disturbance can be modeled as an additional system input

$$\frac{\mathrm{d}}{\mathrm{d}t}x(t) = A \cdot x(t) + B \cdot u(t) + b_w \cdot w(t) \tag{A.19}$$

with

$$b_w = \begin{bmatrix} 0 \\ 0 \\ -7.6 \\ 0 \end{bmatrix} \tag{A.20}$$

Figure A.24 shows the singular values of the plant's frequency response and Figure A.25 the two relevant components of the plant's RGA($j\omega$) matrix. The plant has finite gain at low frequencies (type-zero system) and it is rather well decoupled up to a frequency of approximately 1 rad/s. This frequency is chosen as the desired crossover frequency, yielding expected settling times of the closed-loop system in the order of slightly below 2 s.

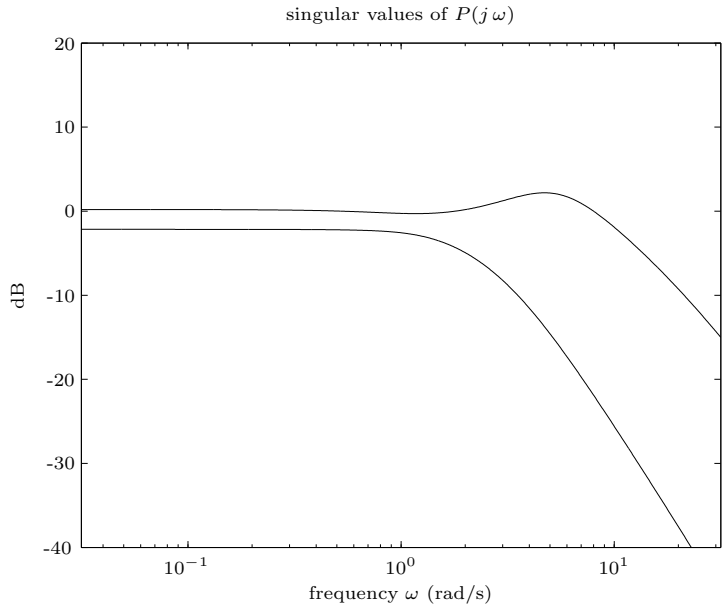

Figure A.24: Case study engine control: singular values plot of the plant's frequency response.

According to the Glover-McFarlane procedure, in the first step the plant is connected to a compensator $K_0(s)$ that is described in the state-space by

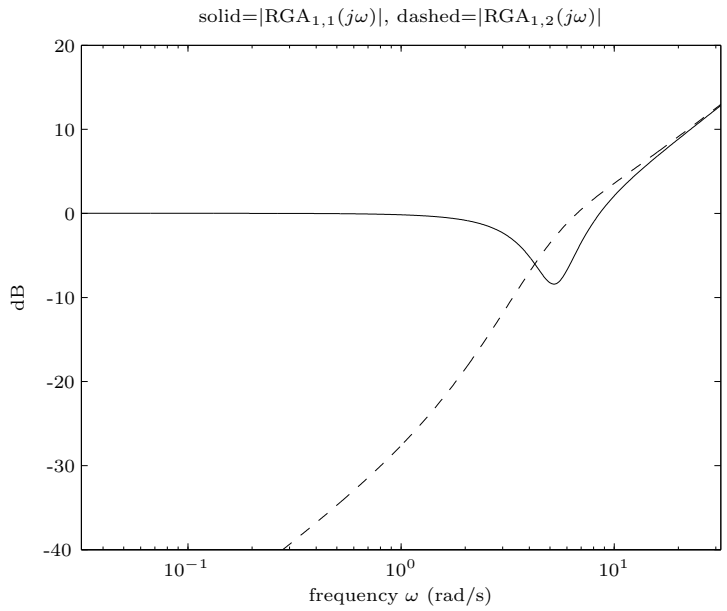

Figure A.25: Case study engine control: plot of the magnitude of the two relevant components of the RGA($j\omega$) matrix.

$$\frac{\mathrm{d}}{\mathrm{d}t}x_K(t) = A_K \cdot x(t) + B_K \cdot u_K(t), \tag{A.21}$$

$$u(t) = C_K \cdot x_K(t) + D_K \cdot e(t) \tag{A.22}$$

with the objective to shape the open loop according to the specification. In this example a PI element is used in each channel to obtain the desired high gains at low frequencies

$$\left[\begin{array}{cc} A_K & B_K \\ C_K & D_K \end{array}\right] = \left[\begin{array}{cc|cc} 0 & 0 & \frac{k_{p,1}}{T_{i,1}} & 0 \\ 0 & 0 & 0 & \frac{k_{p,2}}{T_{i,2}} \\ \hline 1 & 0 & k_{p,1} & 0 \\ 0 & 1 & 0 & k_{p,2} \end{array}\right] \tag{A.23}$$

After some iterations, the following parameters have been chosen

$$k_{p,1} = k_{p,2} = 0.5, \quad T_{i,1} = T_{i,2} = 0.15 \text{ s}$$

Of course, these parameters are not the best possible choice. However, they yield reasonable results as shown below.

In addition to this compensator, the Glover-McFarlane procedure uses two constant matrices K_1 and K_3 to narrow the singular-value distribution around the crossover frequency. In this case study the choice $K_1 = K_3 = I$ is made because the distribution is considered to be satisfactory without any additional correcting terms.

The next step in the Glover-McFarlane procedure is to solve the Equations Equations (10.3) to (10.7) for the augmented system in Equation (10.2). The solution is the controller $K_2(s)$ in Equation (10.8), which in this case study has the order 6. The design parameter α is chosen to be 1.01, i.e., the design is pushed towards maximum robustness. The resulting gain γ is approximately 2.07, i.e., a very good result is achieved. This can also be seen in Figure A.26, which shows that the minimum singular value of the return difference $I + L(s)$ is always larger than -2.5 dB (≈ 0.75).

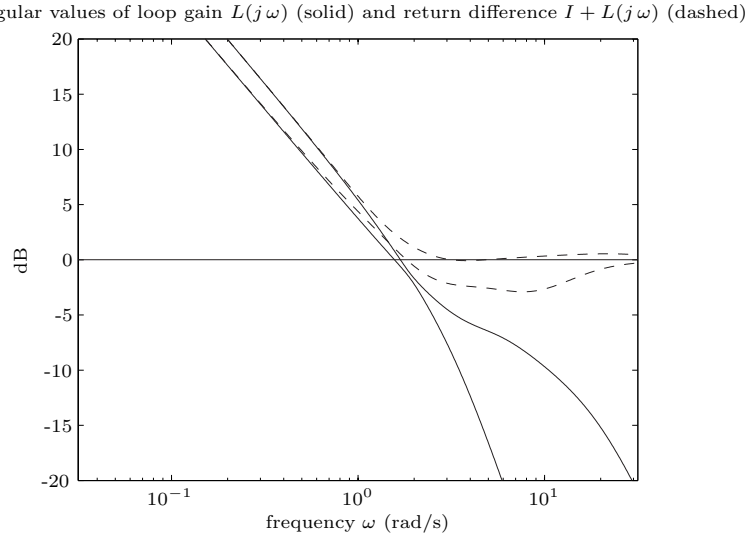

Figure A.26: Case study engine control: singular values plot.

Finally, Figure A.27 shows the closed-loop time-domain behavior of the proposed control system. Steps in the load torque and steps in the reference values of the engine speed and the air/fuel ratio are handled well in the expected time frame of 2 s. The cross-couplings are weak and the transients are well damped such that the design can be accepted.

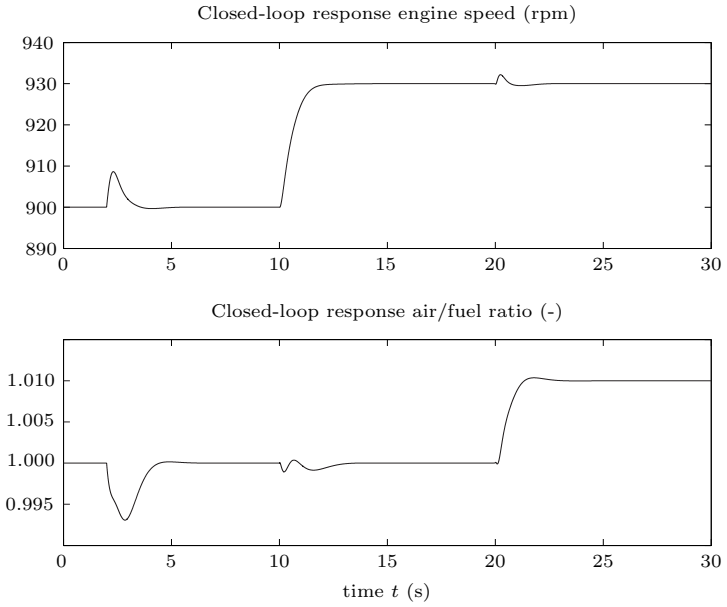

Figure A.27: Case study engine control: closed-loop time-domain responses of the engine case study; input disturbance $w(t) = -20 \cdot h(t-2)$ N m, reference values $r_1(t) = 30 \cdot h(t-10)$ rpm, $r_2(t) = 0.01 \cdot h(t-20)$.

B

Basic Mathematical Concepts

B.1 Numerical Solution of Ordinary Differential Equations

There are various methods to solve numerically ordinary nonlinear differential equations . The goal is to approximate the solution of the equation

$$\frac{\mathrm{d}}{\mathrm{d}t}x(t) = f(x(t), t) \tag{B.1}$$

Below, only the Euler forward and backward methods will be discussed in some detail.[1] If the initial condition $x_0 = x(t_a)$ is known, either Euler method is applicable with a positive time step h. If the final condition is $x(t_b)$ is given and the trajectory $x(t)$, where $t \leq t_b$, should be derived, both Euler methods can be used with a negative time step $h < 0$.

B.1.1 Forward Euler Method

The differential $\frac{\mathrm{d}}{\mathrm{d}t}x(t)$ can be approximated by the difference

$$\frac{\mathrm{d}}{\mathrm{d}t}x(t) \approx \frac{x(t+h) - x(t)}{h},\ h \to 0 \tag{B.2}$$

Rearranging (B.2) yields

$$x(t+h) \approx x(t) + h \cdot \frac{\mathrm{d}}{\mathrm{d}t}x(t) \tag{B.3}$$

and after inserting (B.1)

[1] Matlab provides more sophisticated solvers for differential equations. A short description of the corresponding commands is given in Appendix B.1.3

$$x(t+h) \approx x(t) + h \cdot f(x(t), t) \tag{B.4}$$

The Euler method uses this formula in the following way: First a step size $h > 0$ needs to be chosen. With the initial conditions $x_0 = x(t_a)$ and $t = t_a$, the following algorithm can then be used

$$x_n = x_{n-1} + h \cdot f(x_{n-1}, t_{n-1}),\ t_n = t_{n-1} + h \tag{B.5}$$

This iteration is repeated until $t = t_b$ is reached. Neglecting numerical issues, the smaller h is chosen, the more accurate the approximation of (B.1) will be.

B.1.2 Backward Euler Method

The forward Euler method shown above can become numerically unstable if the time step is not chosen sufficiently small. This problem is avoided by the backwards Euler method. However, the resulting algorithm requires an implicit equation to be solved, which, in general, is difficult. In the linear case a solution is always possible, but requires a larger numerical effort.

The starting point is the following slight modification of Equation (B.2)

$$\frac{\mathrm{d}}{\mathrm{d}t}x(t) \approx \frac{x(t) - x(t-h)}{h},\ h \to 0 \tag{B.6}$$

Again, rearranging yields

$$x(t) \approx x(t-h) + h \cdot \frac{\mathrm{d}}{\mathrm{d}t}x(t) \tag{B.7}$$

and with (B.1)

$$x(t) \approx x(t-h) + h \cdot f(x(t), t) \tag{B.8}$$

The resulting algorithm has now the form (note that the order of the operations is important)

$$t_n = t_{n-1} + h,\ x_n = x_{n-1} + h \cdot f(x_n, t_n) \tag{B.9}$$

This is an implicit equation for x_n, which must be solved in each time step. As mentioned above, in a general nonlinear case this is not trivial. If the system equations (B.1) are linear

$$\frac{\mathrm{d}}{\mathrm{d}t}x(t) = A \cdot x(t) + B \cdot u(t),\ x(t_a) = x_0 \tag{B.10}$$

with $u(t)$ and x_0 known then the implicit equation (B.9) can be solved yielding

$$t_n = t_{n-1} + h,\ x_n = (I - h \cdot A)^{-1} \cdot (x_{n-1} + h \cdot B \cdot u(t_n)) \tag{B.11}$$

Obviously, the matrix $I - h \cdot A$ will always be regular for sufficiently small time steps h.

B.1.3 Solving Differential Equations in Matlab

Matlab provides several algorithms to solve ordinary differential equations, e.g. `ode23` or `ode45`. The syntax to call these solvers is

```
[T,X] = ode45(odefun,tspan,x0)
```

where `odefun` is a function handle[2] to the right hand side of the differential equation, i.e., $f(x(t), t)$ in Equation (B.1). The variable `tspan` defines the time interval of integration. To integrate from $t = t_a$ to $t = t_b$, set `tspan = [t_a, t_b]`. The variable `x0` is the initial condition at $t = t_a$. The output `T` is a vector of time points and `X` contains the corresponding values of the state vector $x(t)$.

In some cases not the initial condition but the terminal condition is known, e.g., when solving the matrix differential equation in Equation (5.64) for the finite horizon LQR problem, only the final condition in Equation (5.65) is known. In this case, the Matlab ODE solvers can also be used. Set the time interval to `tspan = [t_b, t_a]` and `x0 = P`. As `t_b > t_a`, the solver will integrate backwards.

B.2 Proof of Parseval's Theorem

Only the scalar case will be discussed below, the generalization to the vector case is straightforward (use the inner product norm $|x| = x^* \cdot x = \bar{x}^{\mathrm{T}} \cdot x$).

Recall that the Fourier transform of a signal $x(t) \in \mathbb{R}$ with $x(t) = 0$ for $t < 0$ is defined as

$$X(\omega) = \int_0^\infty x(t) \cdot e^{-j\omega t} \, \mathrm{d}t \tag{B.12}$$

while the inverse Fourier transform is defined as

$$x(t) = \frac{1}{2\pi} \int_{-\infty}^\infty X(\omega) \cdot e^{j\omega t} \, \mathrm{d}\omega \tag{B.13}$$

With these results a proof of Parseval's theorem is possible. The squared magnitude of the signal $x(t)$ is equal to the product of its complex conjugate transposed (Hermitian) $x^*(t)$ and the signal itself

$$\int_0^\infty |x(t)|^2 \, \mathrm{d}t = \int_0^\infty x^*(t) \cdot x(t) \, \mathrm{d}t \tag{B.14}$$

[2] Function handles are well explained in the Matlab help.

The signal $x(t)$ can be replaced with inverse Fourier transform of its frequency counterpart $X(\omega)$ yielding

$$\int_0^\infty |x(t)|^2 \, \mathrm{d}t = \int_0^\infty x^*(t) \cdot \left(\frac{1}{2\pi} \int_{-\infty}^\infty X(\omega) \cdot e^{j\omega t} \, \mathrm{d}\omega \right) \mathrm{d}t \tag{B.15}$$

Interchanging the order of the integrations and a repositioning the complex conjugate operator, the following equation can be derived

$$\int_0^\infty |x(t)|^2 \, \mathrm{d}t = \frac{1}{2\pi} \int_{-\infty}^\infty \left(\int_0^\infty x^*(t) \cdot e^{j\omega t} \, \mathrm{d}t \right) \cdot X(\omega) \, \mathrm{d}\omega \tag{B.16}$$

$$= \frac{1}{2\pi} \int_{-\infty}^\infty \left(\int_0^\infty x(t) \cdot e^{-j\omega t} \, \mathrm{d}t \right)^* \cdot X(\omega) \, \mathrm{d}\omega \tag{B.17}$$

The brackets contain the Fourier transpose of the signal $x(t)$ and therefore

$$\int_0^\infty |x(t)|^2 \, \mathrm{d}t = \frac{1}{2\pi} \int_{-\infty}^\infty X(\omega)^* \cdot X(\omega) \, \mathrm{d}\omega = \frac{1}{2\pi} \int_{-\infty}^\infty |X(\omega)|^2 \, \mathrm{d}\omega \tag{B.18}$$

which concludes the proof.

C

Solutions to Quick Checks

C.1 Solutions to Quick Checks of Chapter 1

Solution to Quick Check 1.1.1 (p. 8): In the first case, the two strands of the heat exchanger are decoupled, i.e., each strand acts individually as a simple first-order element. Since no heat is lost to the environment, in the steady case, which corresponds to $s \to 0$ in the frequency domain, the output temperatures must be the same as the input temperatures in each strand, hence $P(0) = I$.

In the other case, the heat exchange is very large ($k \to \infty$), which yields a $\sigma = 1$. To compute the matrix $P(0)$ use the fact that $\beta = 1 - \sigma$ and the rule of Hôpital

$$\lim_{\sigma \to 1} \frac{1-\sigma}{1-\sigma^2} = \lim_{\sigma \to 1} \frac{-1}{-2 \cdot \sigma} = 0.5$$

With the resulting matrix

$$P(0)_{\sigma=1} = \begin{bmatrix} 0.5 & 0.5 \\ 0.5 & 0.5 \end{bmatrix}$$

the outputs y_1 and y_2 at steady state are simply the average input temperatures, i.e., $y_1 = y_2 = 0.5 \cdot (u_1 + u_2)$.

Solution to Quick Check 1.2.1 (p. 16): For the MIMO system at hand, $m = 2$, $p = 3$, and $n = 4$. Hence the matrices have following dimensions:

- $\dim(A) = n \times n = 4 \times 4$
- $\dim(B) = n \times m = 4 \times 2$
- $\dim(C) = p \times n = 3 \times 4$
- $\dim(D) = p \times m = 3 \times 2$

- $\dim(P(s)) = p \times m = 3 \times 2$

Solution to Quick Check 1.4.1 (p. 18): The closed-loop interconnection of the plant and the controller is shown in Figure C.1.

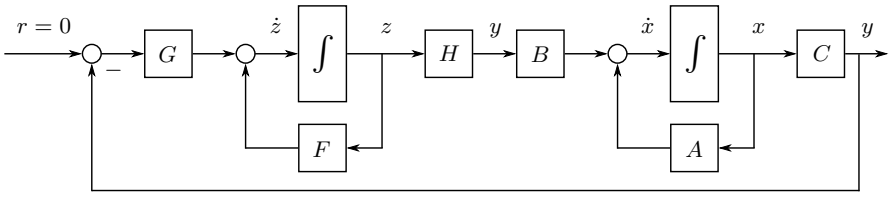

Figure C.1: Interconnection of the plant and the controller.

The resulting state-space equations are

$$\tilde{x}(t) = \begin{bmatrix} x(t) \\ z(t) \end{bmatrix} \tag{C.1}$$

$$\dot{\tilde{x}}(t) = \begin{bmatrix} \dot{x}(t) \\ \dot{z}(t) \end{bmatrix} = \begin{bmatrix} A & BH \\ -GC & F \end{bmatrix} \cdot \begin{bmatrix} x(t) \\ z(t) \end{bmatrix} \tag{C.2}$$

Solution to Quick Check 1.5.1 (p. 22): The directions $\delta_{\pi,i}^{\text{in, out}}$ associated with the pole π_i are defined by

$$P(s)|_{s=\pi_i} \cdot \delta_{\pi,i}^{\text{in}} = \infty \cdot \delta_{\pi,i}^{\text{out}} \tag{C.3}$$

where $\delta_{\pi,i}^{\text{in}}$ is the input and $\delta_{\pi,i}^{\text{out}}$ the output pole direction.

Similarly, the directions $\delta_{\zeta,i}^{\text{in, out}}$ associated with the zero ζ_i are defined by

$$P(s)|_{s=\zeta_i} \cdot \delta_{\zeta,i}^{\text{in}} = 0 \cdot \delta_{\zeta,i}^{\text{out}} \tag{C.4}$$

where $\delta_{\zeta,i}^{\text{in}}$ is the input and $\delta_{\zeta,i}^{\text{out}}$ the output zero direction.

In this example, the transfer function is

$$P(s) = \begin{bmatrix} \dfrac{s+2}{s+1} & 0 \\ 0 & \dfrac{s+1}{s+2} \end{bmatrix} \tag{C.5}$$

We are interested in the pole and zero $\pi = \zeta = -1$. Therefore we take the limit $s \to -1$ and get

$$P(s)|_{s\to -1} = \begin{bmatrix} \infty & 0 \\ 0 & 0 \end{bmatrix} \tag{C.6}$$

We can see that the pole directions are

$$\delta_\pi^{in} = \begin{bmatrix} \alpha \\ \beta \end{bmatrix},\ \delta_\pi^{out} = \begin{bmatrix} \gamma \\ 0 \end{bmatrix},\ \alpha \in \mathbb{R},\ \beta \in \mathbb{R},\ \gamma \in \mathbb{R},\ \alpha \cdot \gamma > 0 \tag{C.7}$$

because

$$\begin{bmatrix} \infty & 0 \\ 0 & 0 \end{bmatrix} \cdot \begin{bmatrix} \alpha \\ \beta \end{bmatrix} = \infty \cdot \begin{bmatrix} \gamma \\ 0 \end{bmatrix} \tag{C.8}$$

Similarly, we see that the zero directions are

$$\delta_\zeta^{in} = \begin{bmatrix} 0 \\ \epsilon \end{bmatrix}, \epsilon \in \mathbb{R} \qquad \delta_\zeta^{out} = \begin{bmatrix} \eta \\ \theta \end{bmatrix}, \eta, \theta \in \mathbb{R} \tag{C.9}$$

because

$$\begin{bmatrix} \infty & 0 \\ 0 & 0 \end{bmatrix} \cdot \begin{bmatrix} 0 \\ \epsilon \end{bmatrix} = 0 \cdot \begin{bmatrix} \eta \\ \theta \end{bmatrix} \tag{C.10}$$

Obviously the input direction of the pole δ_π^{in} and the input direction of the zero δ_ζ^{in} differ and, therefore, no pole/zero cancellation takes place.

C.2 Solutions to Quick Checks of Chapter 2

Solution to Quick Check 2.2.1 (p. 25): The output y_1 can be written as following

$$y_1 = P_{11}u_1 - P_{12}C_{21}y_1 \tag{C.11}$$

which can be rearranged to

$$y_1 = \frac{P_{11}}{1 + P_{12}C_{21}}u_1 \tag{C.12}$$

The output y_2 is

$$y_2 = P_{21}u_1 - P_{22}C_{21}y_1 = \frac{P_{21}(1 + P_{12}C_{21}) - P_{11}P_{22}C_{21}}{1 + P_{12}C_{21}}u_1 \tag{C.13}$$

For the case that $C_{21} = 0$, the output y_2 is

$$y_2 = P_{21}u_1 \tag{C.14}$$

and for the case that $C_{21} \gg 1$

$$y_2 = \frac{P_{21}P_{12} - P_{11}P_{22}}{P_{12}} u_1. \tag{C.15}$$

The RGA-element $[\mathrm{RGA}]_{21}$ is the ratio of these transfer functions

$$[\mathrm{RGA}]_{21} = \frac{\mathrm{P}_{21}\mathrm{P}_{12}}{\mathrm{P}_{21}\mathrm{P}_{12} - \mathrm{P}_{11}\mathrm{P}_{22}} \tag{C.16}$$

Solution to Quick Check 2.2.2 (p. 25): By interchanging the outputs y_1 and y_2, this RGA matrix will be the identity matrix. Accordingly, the corresponding system can be controlled well using two separate SISO controllers.

Solution to Quick Check 2.3.1 (p. 27): A matrix $Q \in \mathbb{R}^{n,n}$ is positive semi-definite if for all $x \in \mathbb{R}^n$

$$x^{\mathrm{T}} \cdot Q \cdot x \geq 0 \tag{C.17}$$

For the matrix $M^{\mathrm{T}} \cdot M$ this means that

$$x^{\mathrm{T}} \cdot M^{\mathrm{T}} \cdot M \cdot x \geq 0 \tag{C.18}$$

By substituting $M \cdot x = y$ we have

$$x^{\mathrm{T}} \cdot M^{\mathrm{T}} \cdot M \cdot x = y^{\mathrm{T}} \cdot y = ||y||^2 \geq 0 \tag{C.19}$$

Therefore, $M^{\mathrm{T}} \cdot M$ is positive semi-definite.

Solution to Quick Check 2.3.2 (p. 28): We know that x is an n-dimensional vector, so we can write

$$x = \begin{bmatrix} x_1 & x_2 & \dots & x_n \end{bmatrix}^{\mathrm{T}} \tag{C.20}$$

The derivative of a scalar $f \in \mathbb{R}$ with respect to the vector x is defined as

$$\frac{\partial f}{\partial x} = \begin{bmatrix} \frac{\partial f}{\partial x_1} & \frac{\partial f}{\partial x_2} & \dots & \frac{\partial f}{\partial x_n} \end{bmatrix} \tag{C.21}$$

With these definitions, we can analyze the derivative

$$\frac{\partial}{\partial x}(c \cdot x) = \frac{\partial}{\partial x}(c_1 \cdot x_1 + c_2 \cdot x_2 + \ldots + c_n \cdot x_n) = \begin{bmatrix} c_1 & c_2 & \dots & c_n \end{bmatrix} = c \tag{C.22}$$

Next, we will analyze the derivative

$$\frac{\partial}{\partial x}(x^{\mathrm{T}} \cdot Q \cdot x) \tag{C.23}$$

Recalling the product rule, we can write

$$\frac{\partial}{\partial x}(x^{\mathrm{T}} \cdot Q \cdot x) = \frac{\partial}{\partial x_1}(x_1^{\mathrm{T}} \cdot Q \cdot x_2) + \frac{\partial}{\partial x_2}(x_1^{\mathrm{T}} \cdot Q \cdot x_2) \tag{C.24}$$

Remark: x_1 and x_2 are both in $\mathbb{R}^n$ and represent the same vector as x. The second addend has the same structure as (C.22) and thus can be evaluated easily. The first addend is a scalar, so we do not change the expression by taking the transpose:

$$\frac{\partial}{\partial x_1}(x_1^{\mathrm{T}} \cdot Q \cdot x_2) + \frac{\partial}{\partial x_2}(x_1^{\mathrm{T}} \cdot Q \cdot x_2) = \frac{\partial}{\partial x_1}(x_2^{\mathrm{T}} \cdot Q^{\mathrm{T}} \cdot x_1) + x_1^{\mathrm{T}} \cdot Q \tag{C.25}$$

Again, we use (C.22) and the fact that $Q = Q^{\mathrm{T}}$ and get

$$\frac{\partial}{\partial x_1}(x_2^{\mathrm{T}} \cdot Q^{\mathrm{T}} \cdot x_1) + x_1^{\mathrm{T}} \cdot Q = x_2^{\mathrm{T}} \cdot Q^{\mathrm{T}} + x_1^{\mathrm{T}} \cdot Q \tag{C.26}$$

$$= x^{\mathrm{T}} \cdot Q^{\mathrm{T}} + x^{\mathrm{T}} \cdot Q \tag{C.27}$$

$$= 2 \cdot x^{\mathrm{T}} \cdot Q \tag{C.28}$$

Solution to Quick Check 2.3.3 (p. 30): The eigenvalues of the mapping M are

$$\lambda_{1,2} = \pm\sqrt{\varepsilon} \tag{C.29}$$

which seem to indicate that the transformation $y = M \cdot x$ is mapping *all* vectors x with $||x|| = 1$ to vectors y with very small norm $||y|| \ll 1$. However, this is not true, as the simple example $x = [0,\, 1]^T$ shows. The singular values of the matrix M

$$\sigma_1(M) = 1,\ \sigma_2(M) = \varepsilon \tag{C.30}$$

are better indicators of the "gain" of the mapping M: Any vector x with $||x|| = 1$ will be mapped to a vector y with a norm $||y||$ between ε and 1.

C.3 Solutions to Quick Checks of Chapter 3

Solution to Quick Check 3.2.1 (p. 32): The four cases are shown in Figure C.2. Changing μ_1 or μ_2 stretches or squeezes the phasors in the corresponding direction, see Figure C.2. The depiction of the phasor does not change for different frequencies ω.

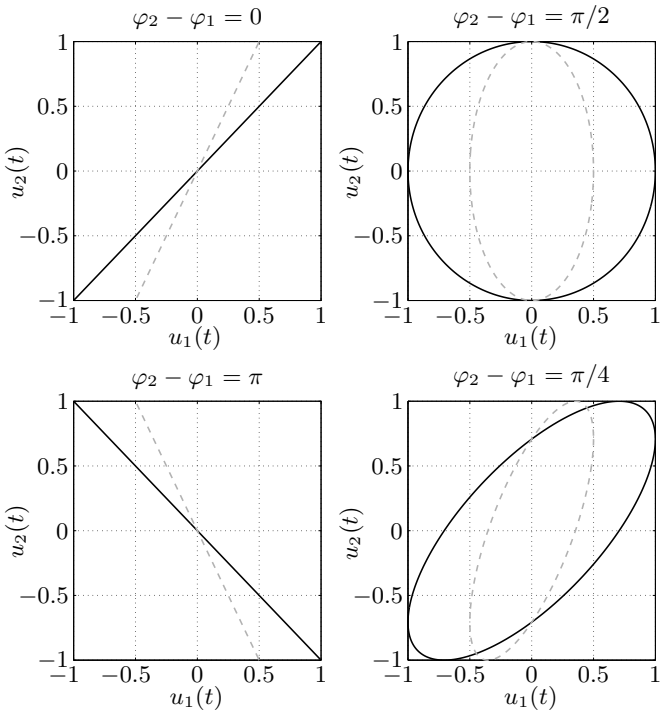

Figure C.2: Phasors for four different phase shifts. Solid lines: $\mu_1 = \mu_2 = 1$, Dashed lines: $\mu_1 = 0.5, \mu_2 = 1$.

Solution to Quick Check 3.2.2 (p. 33): One element of the vector $u(t)$ can be rewritten as

$$u_i(t) = \mu_i \cdot \cos(\omega\ t + \varphi_i) \cdot h(t) = \mu_i \cdot h(t) \cdot \cos\left(\omega \cdot \left(t + \frac{\varphi_i}{\omega}\right)\right) \tag{C.31}$$

Using the linearity and the shift property of Laplace transformations and

$$\mathcal{L}\left\{h(t) \cdot \cos(\omega \cdot t)\right\} = \frac{s}{s^2 + \omega^2} \tag{C.32}$$

we get

$$\mathcal{L}\{u_i(t)\} = U_i(s) = \mu_i \cdot \frac{s}{s^2+\omega^2} \cdot e^{\frac{\varphi_i}{\omega}\cdot s} \tag{C.33}$$

The complete input vector $U(s)$ is

$$U(s) = \begin{bmatrix} \mu_1 \cdot \frac{s}{s^2+\omega^2} \cdot e^{\frac{\varphi_1}{\omega}\cdot s} \\ \mu_2 \cdot \frac{s}{s^2+\omega^2} \cdot e^{\frac{\varphi_2}{\omega}\cdot s} \\ \cdots \\ \mu_m \cdot \frac{s}{s^2+\omega^2} \cdot e^{\frac{\varphi_m}{\omega}\cdot s} \end{bmatrix} \tag{C.34}$$

$$= \operatorname{diag}\left(e^{\frac{\varphi_i}{\omega}\cdot s}\right) \cdot \mu \cdot \frac{s}{s^2+\omega^2} \tag{C.35}$$

$$= e^{\Phi\cdot s/\omega} \cdot \mu \cdot \frac{s}{s^2+\omega^2} \tag{C.36}$$

Solution to Quick Check 3.3.1 (p. 42): We know that $(A \cdot B)^{-1} = B^{-1} \cdot A^{-1}$. Therefore

$$(A \cdot B \cdot C)^{-1} = (B \cdot C)^{-1} \cdot A^{-1} = C^{-1} \cdot B^{-1} \cdot A^{-1} \tag{C.37}$$

With this we can show that

$$\begin{aligned} T_1(s) &= P(s) \cdot C(s) \cdot (I + P(s) \cdot C(s))^{-1} \\ &= \Big((I + P(s) \cdot C(s)) \cdot (P(s) \cdot C(s))^{-1}\Big)^{-1} \\ &= \Big((P(s) \cdot C(s))^{-1} + I\Big)^{-1} \\ &= \big(C(s)^{-1} \cdot P(s)^{-1} + I\big)^{-1} \\ &= \big(C(s)^{-1} \cdot \big(P(s)^{-1} + C(s)\big)\big)^{-1} \\ &= \big(C(s)^{-1} \cdot (I + C(s) \cdot P(s)) \cdot P(s)^{-1}\big)^{-1} \\ &= P(s) \cdot (I + C(s) \cdot P(s))^{-1} \cdot C(s) \\ &= T_2(s) \end{aligned}$$

C.4 Solutions to Quick Checks of Chapter 4

No QC yet.

C.5 Solutions to Quick Checks of Chapter 5

Solution to Quick Check 5.2.1 (p. 51): In the limit $r = 0$ ("cheap control") the control energy E_u is not penalized at all (see Equation (5.8)) and, therefore, an infinitely large amount of it would be acceptable to reduce the output signal energy E_y to the smallest possible value (in the limit case $E_y = 0$). This situation corresponds to infinitely large control signal magnitudes $|u(t)|$ and no actuators could handle that in practice.

In the inverse case where $r = \infty$ no control action at all would be taken, i.e., $E_u = 0$ would be optimal. However, such a solution yields large E_y in the case that the plant is asymptotically stable, and $E_y = \infty$ in all other situations (provided that the pair $\{A, c\}$ forms an observable system).

Solution to Quick Check 5.4.1 (p. 59): The answer is "yes" because the matrix $A-B\cdot K$ is known to be Hurwitz, i.e., to have only eigenvalues $\lambda_i(A-B\cdot K) = \sigma_i + j\,\omega_i$ with $\sigma_i < 0$. This guarantees that all of these eigenvalues $\lambda_i \neq 0$. Using the well-known result that

$$\det(A - B \cdot K) = \prod_{i=1}^{n} \lambda_i(A - B \cdot K)$$

shows that $\det(A - B \cdot K) \neq 0$.

Solution to Quick Check 5.5.1 (p. 61): A second-order system in controllability canonical form with two eigenvalues in the origin is defined by

$$A = \begin{bmatrix} 0 & 1 \\ 0 & 0 \end{bmatrix}, \quad b = \begin{bmatrix} 0 \\ 1 \end{bmatrix}$$

Two cases have to be discussed, first the case $u_\infty = 0$, and then the case $u_\infty \neq 0$. In the first case, all vectors x_∞ that are in the kernel of A are admissible. This kernel is defined by

$$\ker\{A\} = \begin{bmatrix} 1 \\ 0 \end{bmatrix} \cdot \mu, \quad \mu \in \mathbb{R}$$

In the second case, there must be an intersection between the range space of A and the range space of b. The range space of A is the one-dimensional subspace of $\mathbb{R}^2$ defined by

$$\begin{bmatrix} 1 \\ 0 \end{bmatrix} \cdot \mu, \quad \mu \in \mathbb{R}$$

and this subspace does not have an intersection with the subspace spanned by the vector b. Accordingly, there are no steady-state solutions with $u_\infty \neq 0$. A more intuitive explanation for this example can be given using a block diagram representation of the system as shown in Figure C.3. The only admissible $u_\infty = 0$, any nonzero constant input u_∞ would produce an increasing state $x_2(t) = u_\infty \cdot t$, i.e., not an equilibrium state. Similarly, it is clear that any nonzero constant $x_2(t) = x_{2,\infty}$ yields an increasing state $x_1(t) = x_{2,\infty} \cdot t$. The only admissible nonzero constant variable is $x_1(t) = x_{1,\infty}$ as found above using geometric arguments.

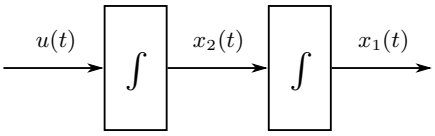

Figure C.3: Second-order system in controller canonical form with two eigenvalues in the origin.

Solution to Quick Check 5.5.2 (p. 62): The system depicted in Figure 5.7(b) represents the following set of differential equations

$$\frac{\mathrm{d}}{\mathrm{d}t}x(t) = (A - B \cdot K) \cdot x(t) + B \cdot (K \cdot x_\infty + u_\infty)$$

Since K is found solving an LQR problem the matrix $A - B \cdot K$ must be Hurwitz, i.e., $\lim_{t\to\infty} \frac{\mathrm{d}}{\mathrm{d}t}x(t) = 0$. Therefore

$$0 = (A - B \cdot K) \cdot x_\infty + B \cdot (K \cdot x_\infty + u_\infty) = A \cdot x_\infty + B \cdot u_\infty$$

which confirms Equation (5.38).

Solution to Quick Check 5.5.3 (p. 64): For a SISO plant the transfer function is

$$P(s) = c \cdot (s\,I - A)^{-1} \cdot b = \frac{c \cdot \mathrm{Adj}(s\,I - A) \cdot b}{\det(s\,I - A} = \frac{b(s)}{a(s)}$$

The zeros of $P(s)$ are those frequencies ζ_i where $P(\zeta_i) = 0$. If there is a $\zeta_i = 0$, i.e., if a zero is in the origin, then the DC gain (the gain at $\omega = 0$ in a Bode diagram) is zero. In other words, the system is a band-pass filter (not only very high, but also very low frequencies are not transmitted) and, therefore, it is not possible to impose a non-zero output at frequency $\omega = 0$. A typical example would be a loudspeaker that cannot transmit sound with frequencies below a lower threshold, say 20 Hz.

Solution to Quick Check 5.5.4 (p. 68): This is simply achieved by inspection.

C.6 Solutions to Quick Checks of Chapter 6

Solution to Quick Check 6.3.1 (p. 75): The plant is a physical system that must follow first laws that cannot be altered. For instance, if the plant is a mass m moving on a straight line, Newton's law says that the derivative of the velocity $v(t)$ is proportional to the applied force $u(t)$, but the derivative of the position $x(t)$ must be the velocity and that variable cannot be influenced by an exogenous input

$$\frac{\mathrm{d}}{\mathrm{d}t}v(t) = \frac{1}{m} \cdot u(t), \quad \frac{\mathrm{d}}{\mathrm{d}t}x(t) = v(t)$$

The observer, on the other hand, is an artificial dynamic system (a filter) that is realized, e.g., in a digital computer and that can be designed without being hampered by any physical constraints. This freedom can be utilized to realize the output injection shown in Figure 6.2.

C.7 Solutions to Quick Checks of Chapter 7

No QC yet.

C.8 Solutions to Quick Checks of Chapter 8

Solution to Quick Check 8.2.1 (p. 95): The "matrix" $s\,I - L \cdot C$ in Equation (8.15) is regular only for $n = 1$ when $L \to \infty$. In the case $n > 1$, the matrix $L \cdot C$ has, in general, only rank m as it is the outer product of two rank-m matrices. Accordingly, it cannot be inverted.

C.9 Solutions to Quick Checks of Chapter 10

No QC yet.

C.10 Solutions to Quick Checks of Chapter 11

Solution to Quick Check 11.3.1 (p. 110): Using the controller $U(s) = C(s) \cdot E(s)$, Equations (11.6) and (11.7) can be rewritten as

$$Z(s) = \Sigma_{11}(s) \cdot R(s) + \Sigma_{12}(s) \cdot C(s) \cdot E(s) \tag{C.38}$$

$$E(s) = \Sigma_{21}(s) \cdot R(s) + \Sigma_{22}(s) \cdot C(s) \cdot E(s) \tag{C.39}$$

Solving the Equation (C.39) for $E(s)$ yields

$$E(s) = (I - \Sigma_{22}(s) \cdot C(s))^{-1} \cdot \Sigma_{21}(s) \cdot R(s) \tag{C.40}$$

Inserting this expression into Equation (C.38), the dependency of the output $Z(s)$ on the input $R(s)$ is expressed as follows

$$Z(s) = (\Sigma_{11}(s) + \Sigma_{12}(s) \cdot C(s) \cdot (I - \Sigma_{22}(s) \cdot C(s))^{-1} \cdot \Sigma_{21}(s)) \cdot R(s) \tag{C.41}$$

$$= \mathcal{F}(\Sigma, C(s)) \cdot R(s) \tag{C.42}$$

D

List of English and German Control Engineering Terms

coupling	Kopplung
cross coupling	Kreuzkopplung
denominator	Zähler
feedforward	Vorsteuerung
iff – if and only if	dann und nur dann
induced norm	induzierte Norm
least common denominator	kleinster gemeinsamer Nenner
greatest common divisor	grösster gemeinsamer Teiler
linear transformation	lineare Abbildung
marginally stable	grenzstabil
multiplicity	Vielfachheit
numerator	Zähler
observer	Beobachter
polynomial	Polynom
reference tracking	Führungsfolge
separation principle	Separationstheorem
singular value	Singularwert
singular value decomposition	Singularwertzerlegung
step response	Sprungantwort
unitary matrix	unitäre Matrix
well-defined	eindeutig
white noise	weisses Rauschen

E

List of Symbols

Greek Letters

Γ	LQG feedforward gain matrix
$\phi_n(\omega)$	spectrum of a signal
λ_i	eigenvalue
Λ	LQG feedforward gain matrix
$\mu_{\min}$	minimum return difference
π_i	pole
ρ	density
$\sigma_i(M)$	singular value of a matrix M
$\sigma_{max}(M)$	maximum singular value of a matrix M
$\sigma_{min}(M)$	minimum value of a matrix M
τ	time constant
ϑ	temperature
ζ_i	zero
ω	frequency (all frequencies unit rad/s)
ω_c	crossover frequency
ω_n	lower frequency bound of the noise signal $n(t)$
ω_0	natural frequency

Latin Letters

c	specific heat capacity
$\mathbb{C}$	the set of complex scalars
$\mathbb{C}^n$	the set of n-dimensional complex vectors
$\mathbb{C}^{n\times p}$	the set of $n \times p$-dimensional real matrices
$\mathbb{C}_-$	the set of complex scalars with real parts strictly negative
$\mathbb{C}_+$	the set of complex scalars with real parts strictly positive
$d(t)$	output disturbance signal
$e(t)$	error signal
F	area
$h(t)$	step function
$\overset{*}{H}$	enthalpy flow
$J(p)$	objective function
k	heat transfer coefficient
K	state feedback gain matrix
K_I	integrator gain matrix
L	observer gain matrix
L_K	Kalman filter gain matrix
$L(s)$	loop gain transfer function
m	order of numerator polynomial
$\overset{*}{m}$	mass flow
n	order of denominator polynomial
n_+	number of poles with positive real part (Nyquist theorem)
n_0	number of poles on the imaginary axis (Nyquist theorem)
$n(t)$	noise signal
$n_u(t)$	input noise signal
$n_y(t)$	output noise signal
$\mathcal{O}_n$	finite-dimensional observability matrix
$P(s)$	plant transfer function (the system to be controlled)
$Q(s)$	return difference transfer function
$\overset{*}{Q}$	heat flow
$r(t)$	reference signal
$\mathcal{R}_n$	finite-dimensional reachability matrix
$\mathbb{R}$	the set of real scalars
$\mathbb{R}^n$	the set of n-dimensional real vectors

$\mathbb{R}^{n\times p}$	the set of $n \times p$-dimensional real matrices
s	complex frequency, Laplace variable
$S(s)$	sensitivity transfer function
$T(s)$	complementary sensitivity
$u(t)$	input signal(s)
U	internal energy
$U(s)$	Laplace transformed input signal $u(t)$
v_i	eigenvector
V	volume
$w(t)$	input disturbance signal
$x(t)$	state variable(s)
$x(0)$	initial condition
$\widehat{x}(t)$	state estimate
$\bar{x}(t)$	observation error
$y(t)$	output signal(s)
$y_o(t)$	measured output signal(s)
$\widehat{y}(t)$	output estimate
$Y(s)$	Laplace transformed output signal $y(t)$

Index

References

1. Anderson, B.D.O. and Moore, J.B. (1990) Optimal Control: Linear Quadratic Methods. Prentice Hall, Englewood Cliffs, NJ
2. Athans, M. and Falb, P.L. (1966) Optimal Control. McGraw-Hill, NY
3. Athans, M. A Tutorial on the LQG/LTR Method. (1986) IEEE American Control Conference, pp 1289–1296
4. Chui, C.K. and Chen, G. (1998) Kalman Filtering – With Real-Time Applications. Springer, Berlin
5. Doyle, J. and Stein, G. Multivariable Feedback Design: Concepts for a Classical/Modern Synthesis. (1981) IEEE T-AC, Vol. 26, No. 1, pp 4–16
6. Doyle J., Francis B. and Tannenbaum A. (1992) Feedback Control Theory. Macmillan Publishing Company, New York
7. Dullerud G. and Paganini F. (2000) A Course in Robust Control Theory. Springer Verlag, Berlin
8. Gantmacher F.R. (1977) Matrix Theory. Chelsea Publishing, New York
9. Geering H.P. (2003) Regelungstechnik. Springer Verlag, Berlin
10. Glad T. and Ljung L. (2000) Control Theory. Taylor & Francis, London
11. Guzzella L. (2007) Analysis and Synthesis of SISO Control Systems. vdf Verlag, Zürich
12. Isidori A., Marconi L., and Serrani A. (2003) Robust Autonomous Guidance. Springer Verlag, Berlin
13. Kailath T. (1980) Linear Systems. Prentice Hall, Englewood Cliffs, NJ
14. Khalil, H.K. Nonlinear Control. (2015) Pearson, London

15. Kwakernaak, H. and Sivan, R. (1972) Linear Optimal Control Systems. Wiley-Interscience, NY

16. Luenberger, D.G. An Introduction to Observers. (1971) IEEE T-AC, Vol. 16, No. 6, pp 596–602

17. Papoulis A. and Pillai S. U. (2002) Probability, Random Variables and Stochastic Processes. MacGraw Hill, New York

18. Preumont, A. (2018) Vibration Control of Active Structures: An Introduction. Springer International Publishing

19. Skogestad S. and Postlethwaite I. (2005) Multivariable Feedback Control. John Wiley & Sons, Chichester

20. Stein, G. and Athans, M. The LQG/LTR Procedure for Multivariable Feedback Control Design. (1987) IEEE T-AC, Vol. 32, No. 2, pp 105–114

21. Zhou K. and Doyle J. C. (1998) Essentials of Robust Control. Prentice Hall, Englewood Cliffs, NJ